République Algérienne Démocratique et Populaire
Ministère de l'Enseignement Supérieur et de la Recherche Scientifique

Université Batna 2 – Mostefa Ben Boulaïd
Faculté de Technologie
Département d'Electronique

Thèse

Présentée pour l'obtention du diplôme de :
Doctorat en Sciences en Electronique
Option : Micro-ondes

Sous le Thème :

Study and modeling of vibration sources and turbulence in telecommunications systems based on laser satellites.

Présentée par :

Al-Gobi Mohammed Senan Rageh

Devant le jury composé de :

M. FORTAKI Tarek	Prof.	Université de Batna 2	Président
M. BENATIA Djamel	Prof.	Université de Batna 2	Rapporteur
M. BOULAKROUNE M'Hamed	Prof.	ENP Constantine	Examinateur
M. BENABDELKADER Souad	MCA	Université de Batna 2	Examinateur
M. BENSLAMA Malek	Prof.	Université de Constantine 1	Examinateur
M. BEDRA Sami	MCA	Université de Khenchela	Examinateur

Mars 2020

شكر

بادئ ذي بدء ، أود أن أشكر الله العظيم الذي أعطاني الإرادة والصبر والصحة لانجاز هذا العمل.

أود أن أتقدم بالشكر لمشرفي البروفيسور جمال بن عطية على المساعدة والوقت الذي كرسه لي ، وبدونه لم تكن هذه الرسالة لترى النور أبداً.

أتوجه بالشكر الجزيل للبروفيسور طارق فرطاقي على الشرف الذي قدمه لي برئاسة لجنة المناقشة.

أود أن اشكر أيضا أعضاء لجنة المناقشة المتمثلة بكل من : البروفيسور بولقرون محمد من جامعة قسنطينة ، و البروفيسور بن سلامة مالك من جامعة قسنطينة 1 ، و بن عبد القادر سعاد أستاذ محاضر بجامعة باتنة 2 ، و بدرة سامي أستاذ محاضر بجامعة خنشلة لموافقتهم على تقييم هذا العمل.

أعرب عن فائق امتناني وتقديري لكل من ساعدني و ساهم في اخراج هذا العمل الى النور واخص بالذكر الأستاذ ناصر العابد أستاذ في قسم الإنجليزية بجامعة بسكرة والأستاذ بالي معاذ أستاذ في قسم الاعلام الالي بجامعة الوادي.

كما انتهز هذه الفرصة لاتقدم بالشكر الى اخوتي الأساتذة من اليمن واخص منهم الأستاذ عبدالله المتوكل دكتوراة اعلام الي بجامعة بسكرة والأستاذ إبراهيم الكبسي دكتوراة بقسم الميكانيك بجامعة باتنة والأستاذ كمال المعمار دكتوراة في الانشاءات بجامعة بسكرة لمساهمتهم الفعالة ودعمهم لي في احلك الظروف والصعاب. كما اعرب عن امتناني لجميع الاساتذة الذين لم يدخروا جهداً لتطويرنا وصقل مهاراتنا.

أخيرًا ، على الرغم من بعد المسافة احتفظ بمكانة خاصة لجميع أفراد عائلتي المقيمين في اليمن. أعرب عن عميق امتناني لهم لأنهم ساعدوني باستمرار ، بدعمهم المعنوي وتشجيعهم لاستكمال هذا العمل.

إهـــــداء

الى روح والدي العزيزين ،

الى زوجتي وطفلاي ،،

الى اخوتي واختي ،،،

الى وطني الجزائر فلم يعد لي وطن ،،،،

أهدي هذا العمل المتواضع

Table of contenants

List of Figures

General introduction

In the past, people looked at the sky and saw bright stars who could not imagine that they could fly. “Heavier-than-air flight”, this was a scientific principle mentioned by the English scientist William Thompson (also known as Lord Kelvin), who was a physicist and engineer, widely known for developing the Kelvin scale of absolute temperature. Until 1903 that principle was proven wrong by the Wright brothers who successfully built a powered plane, their engineering masterpiece inspired others, to develop and build flying machines "that were able to reach higher altitudes, and create one altitude record after another. The challenge got bigger when the idea came that we might one day send anything into space, let alone put men in an orbit.

The term "telecommunication" was used for the first time in 1904 by Edouard Estaunié [1], French novelist and engineer, in his practical treatise on electrical telecommunication. Edouard Estaunié, engineer at the Post and Telegraphs and director from 1901 to 1910 of the professional school of Post and Telegraphs, which then only considered electricity in its definition, wished to bring together under one discipline telegraphy, telephony and radio communications, taking into account technological developments compared to ordinary means of communication.

Nowadays, telecommunications characterized as follows: "the transmission, remote transmission and reception of information of all kinds by wire, radio electricity, optical or electromagnetic system" [2]. In other words, telecommunication is first and foremost an exchange of information in any given space. The specificity of telecommunications, unlike ordinary communication, is that information is conveyed using a medium (material or not), allowing it to be transmitted over long distances. Communications of all types have grown steadily. Television, much more than radio, symbolizes the transition from the industrial to the information age when it became a mass object in the late 1940s.

The idea of using satellites to communicate (on the ground and between each other) was brought up in 1928 by Austrian engineer Herman Potočnik [3], who specialized in rockets after studying electrical engineering at the Vienna University of Technology. His ideas must become

reality in 1957, when the Soviet Union launched its first satellite communication, "Sputnik 1 satellite; Americans launch their first satellite the following year [1].

The first satellites were initially passive; they simply reflected the signals from ground stations. The major drawback was that these signals were broadcast in all directions and could therefore be received anywhere in the world. The second types of satellites were then active. That is to say, they had their own reception and transmission systems [2],[4].

Communication systems by standard satellites used microwave radiation as a medium for transmitting information, but in the new generation of satellite networks, it was the laser (very narrow light beam and very concentrated in energy) that played the role of inter-satellite link and of a support in the communication between the satellites known today under the name of the laser satellites [4], [5].

The simplicity of implementing optical communications in free space, its low cost compared to fiber-optic links, as well as the significant capacities in terms of speed, contribute to the implementation of such communication systems. However, when the propagation distance increases, atmospheric turbulence deteriorates the quality of the link. Indeed, these reveal random movements of the laser beam, an enlargement and the scintillation which disrupt communications. Despite the advantages that optical links in free space can bring, the disturbances introduced by the atmosphere limit both propagation distances and flow. The difficulties of optical communications in terms of computing power of computers, delay the generalization of this principle of correction, which today equips the main world telescopes. The exploration of the solar system, as well as the ambitions of communication with spacecraft, motivated, the implementation of transmission systems between ground and space. Bandwidth, power and size are essential features of these systems. In the context of laser communications in free space, atmospheric turbulence has the notable effect of reducing the average flux received until the absence total signal and this with great temporal variability. This results in a much higher error rate than in the absence of turbulence, and which becomes incompatible with the conventional objectives of a link in terms of throughput, error rate and link permanence. These effects can be reduced by using the concept of adaptive optics (AO) which consists in measuring phase disturbances and compensating for them by means of a deformable mirror [6]. AO correction aims to concentrate and stabilize the flow at the receiving telescope. Fante [7] is one of the first to propose adaptive optics to solve this problem in the context of the transmission of information between ground and space.

In adaptive optics (AO), the most important element is the deformable mirror. Which controlled by the approximation algorithms [8]. There are many algorithms that can correct wave front sensor such as: the stochastic parallel gradient descent (SPGD), Simulated Annealing (SA), and genetic algorithm (GA) [9],[10]. This contribution provides a hybrid solution to correct wave front sensor. The provided solution consists of the combination of GA with AO solution. The hybrid solution gives significant results in correcting the wave front aberration in satellite laser communication.

In this work, we will treat the different sources that cause the vibrations of the emitted laser beam by a simulation tools called OOMAO and the different modulation schemes that ensure optimal performance.

We can summarize our work in four chapters:

• The first chapter concerns generalities on satellite transmission, constitution of the satellite, orbits, positions of satellites, etc ...

• The second chapter studies the different internal and external sources that cause the vibrations of the emitted laser beam and analyzes the standard structure of the optical communication system in laser satellite networks as well as the structure developed with its different communication schemes. We explain and focuses about the atmospheric turbulence, the effect of this turbulence for the laser satellite.

• The third chapter explains the adaptive optics systems, the wave front analysis, medialization and optimization of adaptive optics systems which make it possible to analyze and maximize the bandwidth of the communication system with variations in the amplitudes of the vibrations.

• The fourth chapter concerns the correction of wavefront sensor based on a satellite to ground laser communication links, we focused in this chapter to solve the problem of wavefront distortions and improve the proposed solution by new idea, the comparison between all used methods explain the satisfaction of the new solution, it includes the various concepts and improvements introduced in order to overcome the vibration effects and improve the quality of communication.

Finally, a conclusion will conclude this thesis summarizing the main tasks accomplished.

CHAPTER I:

General Overview of satellite communications

1 General Overview of satellite communications

1.1 Introduction

The development of the means of transmitting information, which is one of the main characteristics of our time, is the result, on the one hand, of a continuous increase in needs and, on the other hand, of the possibilities offered by technical progress.

One of the essential features of the evolution of our civilization is the constantly accelerating increase in the volume of information exchange (written, verbal or visual information). This increase in the volume of information transfers, their speed and the distances they cover profoundly controls the development of the major systems that characterize today's society: intercontinental transport, international industrial consortia, information agencies, forums for political confrontation between nations, weather forecasts, stock exchange exchanges, the dissemination of culture, etc.

The development of technology and its application to human needs has been carried out with unparalleled speed, which is characteristic of the acceleration of technical progress. At the forefront of this progress is satellite communications, which have taken a predominant place among the various means of transmitting information and which have made a major contribution to satisfying the immense needs. These satellite telecommunications systems have intrinsic qualities distinct from those of conventional terrestrial systems [5],[4].

This chapter begins with a general description of satellite telecommunications systems, focusing on the satellite itself (its make-up and the services that offers).

1.2 Description of satellite communication system

A satellite communication system is built around an earth sector (the earth stations), providing the connection to the ground networks, and a space sector (the satellite), providing the link between the stations.

Figure (1-1) shows the different components of a satellite communication system [11].

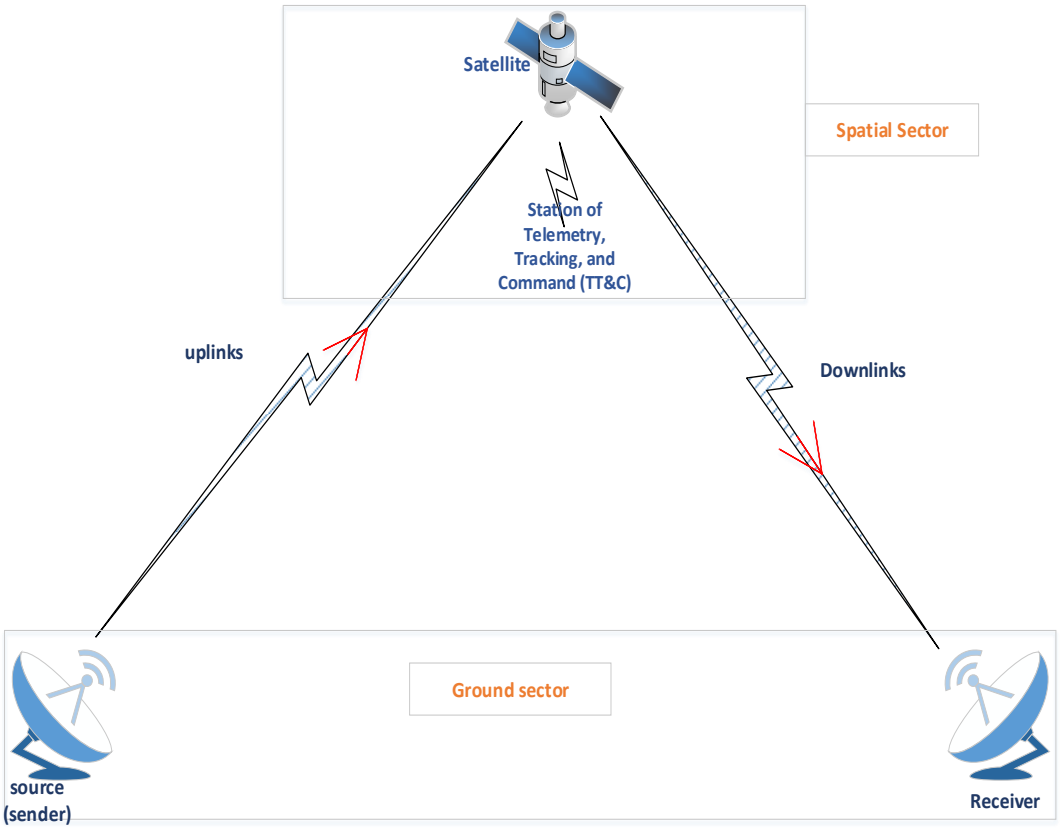

Figure 1-1: A component of satellite communication system.

1.2.1 Ground Sector

The ground sector is made up of all earth stations, most often connected to users' terminals by a terrestrial network or directly in the case of small stations (VSAT: very small aperture terminal) and mobile stations. The stations are distinguished by their size, which varies according to the type of traffic (telephone, television, and data. A distinction is also made between fixed stations, transportable stations and mobile stations. Some stations are both transmitting and receiving stations. Others are receive-only (RCVO: receive only): this is the case, for example, of the receiving station of a satellite broadcasting system, or of a television or data distribution system [12],[13]. The cost of earth stations can be a determining factor in a communication network for which security, availability and reliability of equipment are prime requirements.

1.2.2 Space Sector

The space sector comprises the satellite and all the ground-based control means, in other words all the tracking, telemetry, and command (TT&C) stations, as well as the satellite control

center where all the operations related to station-keeping are decided and the vital functions of the satellite are verified [12].

1.2.2.1 Definition of the communications satellite

The satellite is naturally the essential part of a satellite communications system. At the beginning of the 1960s, when various possibilities of space telecommunications were being tested [1, 2], the satellite was a purely passive object, a large reflecting sphere moving in the sky whose only function was to reflect the received energy, but the poor results obtained led to the abandonment of such a system.

The satellite is now of the active type: it behaves like a real radio relay in the sky. It receives emissions from the earth (uplink) and retransmits them back to earth (downlink) after frequency translation and amplification. There are many kinds of satellites [14],[15]:

- **Astronomical satellites:** they observe space as they are placed above the atmosphere, they can see the stars and black holes better because they are not hindered by the layer of air and pollution.
- **Navigation satellites:** they are used to track the position of ships and marine currents.
- **Meteorological satellites:** they are used to take pictures of the earth, the pictures allow to forecast the weather. They are either geostationary or in constant rotation around the earth.
- **Telecommunication satellites:** telecommunication satellites are used for telephone communications, television pictures and radio.
- **The military satellites:** there are two types of military satellites: telecommunication and surveillance (terrestrial and maritime reconnaissance) as soon as a satellite has accomplished its mission, there are two ways to get rid of it:

1. We let it rotate around the earth in a higher orbit.

2. It is allowed to fall back to earth: scientists calculate that it will fall back to an uninhabited area (often in the middle of the ocean). If it is small, when it reaches the atmosphere it disintegrates due to friction with the atmosphere.

1.2.2.2 Construction of a telecommunications satellite

The satellite is made up of a payload and a platform: **The platform** comprises all the subsystems that enable the payload to operate. We find:

- Power supply: all satellites need power to operate. The sun provides the energy needed for most satellites in orbit. This power supply system uses solar panels to convert light into electrical energy, batteries to store it, and a distribution system that transmits the electrical energy to each instrument.

- **The control system:** This system controls all of the satellite's functions. It is the satellite's brain. The heart of this system is called the Flight Computer. There's also an input/output processor that redirects all the control data that goes in and out of the Flight Computer.

- **Altitude and orbit control and propulsion equipment:** this system allows the satellite to remain stable and always be oriented in the right direction. The satellite has sensors that allow it to know its orientation. In addition, the satellite also needs to be able to move to correct its position, which is why it has a propulsion mechanism. The performance of the altitude control system depends on the use of the satellite. A satellite used to make scientific observations needs a more accurate control system than a communications satellite.

- **TT&C tracking, telemetry and remote control equipment:** this equipment consists of a transmitter system, a receiver system and various antennas to relay information between the Earth and the satellite. The ground control base uses this equipment to transmit new instructions to the satellite computer. This system also allows the transmission of images or other forms of recorded data to engineers on Earth.

- **Thermal control:** the system protects all satellite equipment from damage due to the space environment. In orbit, a satellite is exposed to sudden changes in

temperature (from -120° when the satellite is in darkness, to 180° when the satellite is exposed to the sun). Temperature control uses a heat distribution unit and a thermal blanket system to protect the satellite's electronic equipment from these sudden temperature changes.

The payload of a satellite represents all the equipment enabling the satellite to perform the function for which it is intended. For a communications satellite, the payload may represent the antennas reflecting the TV signal or the telephone signal. For an observation satellite, the payload consists of digital cameras and image sensors to take pictures of the Earth's surface. This payload consists of a set of channels, each channel being equipped with a transmit amplifier operating in a particular sub-band of the total band allocated to the satellite. This arrangement makes it possible to offer, in each channel, a power level commensurate with the state of technological development of the on-board microwave amplifiers, whereas the implementation of a single amplifier for the entire band would lead to a dissemination of the power of this amplifier.

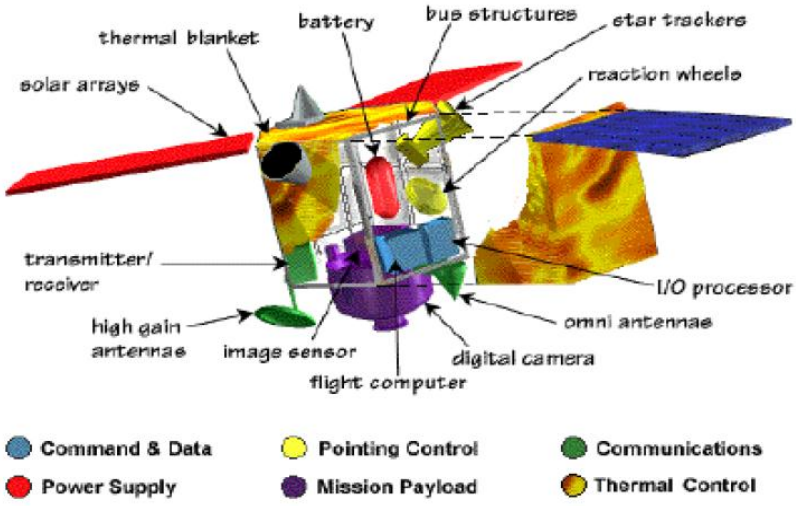

Figure 1-2: Satellite structure [12].

1.2.2.3 Service provided by satellite

There is a strong demand for personal and mobile services. Recently, the notion of multicast service, i.e. from one source to a specific group of users, has emerged. This definition is to be contrasted with broadcast, which floods an entire region with users without any distinction other than geographical. In any case, this desire to share information makes relays from space more attractive.

The distribution map between satellite networks and terrestrial networks is therefore changing radically in a synthetic way, the advantages of satellites are as follows:

- The covering of large geographical areas.
- The possibility to have multiple accesses and distinctions for the same Communication.
- The possibility of quick deployment of services.
- Adaptation to regions without telecommunications infrastructure.
- Observing the land, climate, plants and oceans.
- Transmit the waves: radio, television, telephone, and internet.

The waves they send out travel at 300,000 kilometers per second.

1.3 Orbits Tracked by Satellites

Satellites use the gravitational force of our planet in order to keep themselves at a certain position and distance from the earth. It is thus possible to define at any time what the characteristics of the satellite are in order to establish transmissions. We will see in this section what types of orbits are used and how they set certain limits or constraints in transmissions or equipment [16],[17].

- The orbit is the ideal trajectory that a satellite follows in the absence of disturbances.
- Orbits are usually classified according to their average altitudes and their synchronization with the earth or the sun.

Three different types of orbits can be distinguished: geostationary or geosynchronous orbit, medium-altitude or medium Earth orbit and low-altitude or low Earth orbit, each with different characteristics from the others [17].

We can also classify these orbits according to their shapes; in this case we distinguish two types: circular orbits and elliptical orbits.

1.3.1 Circular orbits

There are an infinite number of circular orbits, each corresponding to an inclination with respect to the orbital plane, but two kinds can be distinguished: the polar circular orbit and the inclined circular orbits [16].

1.3.1.1 Polar circular orbit:

The polar orbit is a circular orbit that passes over both poles of the earth. The main disadvantage for satellites in this type of trajectory is the slowness of their coverage, but this low speed still allows the satellite to cover a large part of the surface of the globe, or even the entire earth, given the rotation of the earth on itself. One example is the French observation satellite "Spot", located at an altitude of 800 km, which provides coverage of the entire surface of the globe in 21 days [18],[19].

1.3.1.2 Inclined circular orbit:

Inclined circular orbits also describe a circle around the earth, but each path is inclined at an angle to the equatorial plane. However, this inclination has a major disadvantage: since the highest latitude served by satellites with inclined orbits corresponds to the angular deviation from the equatorial plane, these satellites cannot cover the entire surface of the globe, but this orbit has an advantage: depending on the altitude of the satellite, it is possible to target areas of the globe, i.e. to serve parts of interest from the economic, military or other applications [16].

For example, the French project "Globalstar" plans to launch 48 satellites into a circular orbit inclined at 50° to the equator to provide mobile communications in most countries.

These two types of trajectories each have different characteristics, with different uses depending on the disadvantages and advantages. Nevertheless, they are used very little in comparison with the geostationary orbit, which currently has the most economic and practical advantages.

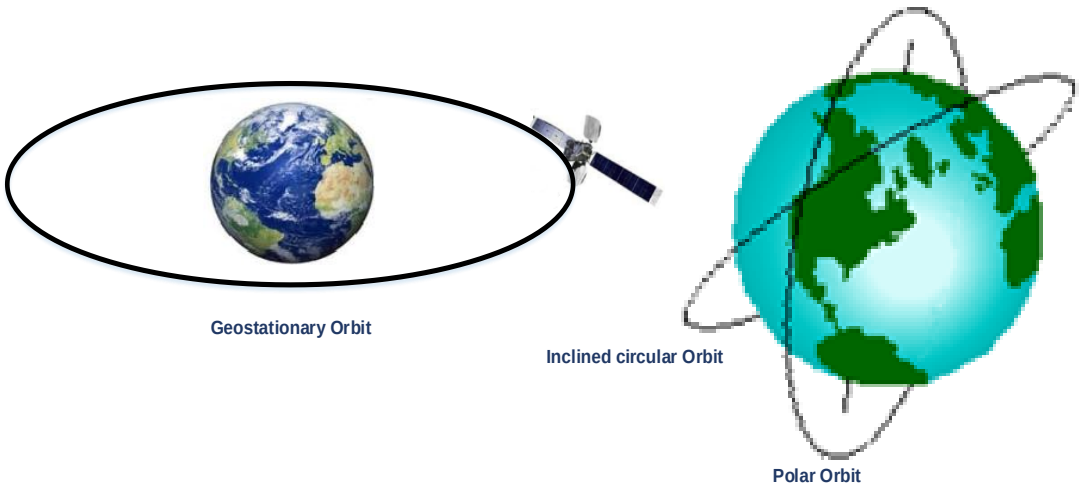

Figure 1-3: Circular orbits.

1.3.2 Elliptical orbit

As the name implies, a satellite placed in such an orbit describes an elliptical trajectory around the earth. The main characteristic of this type of orbit is the great variation in speed that the satellites undergo [17]. Indeed, the farther a satellite is from the earth, the lower its speed is because the speed "v" is inversely proportional to its altitude "h" according to the relation:

$$v^2 = G * m * (\frac{2}{h} - \frac{1}{a}) \quad (1\text{-}1)$$

Where G is the gravitational constant, m is the mass of the satellite and has the half-major axis of the orbit.

Figure 1-4: Elliptical orbit.

However, because the altitude varies greatly during its period and the trajectory describes an ellipse, the position of the satellite for a ground-based observer is not fixed. Therefore, the tracking of each satellite requires the equipment of transmitting and receiving stations with mobile antennas, which is considered a disadvantage from a financial and qualitative point of view. Nevertheless, satellites in elliptical orbits have the advantage of being able to serve areas far from the equator, which is not necessarily the case for circular and geostationary orbits. This is not necessarily the case for circular and geostationary orbits, since with a high inclination, it is possible to fly over territories on the periphery of the hemispheres. The atmospheric layer being narrower, the quality of the signals is therefore a little better [12].

For example, in the "Molnya" system used by Russia, 3 satellites whose orbits are inclined at 63° to the equatorial plane, cover Siberia completely because their slow parts correspond to two thirds of their period and they are then located vertically over the Siberian territory [12],[13].

Elliptical orbits have advantages, such as coverage of areas far from the equator, but also disadvantages such as the qualitative and financial aspects of mobile equipment on earth. For circular orbits, however, these disadvantages are almost non-existent.

1.4 Satellite constellations

A satellite constellation can be defined as several similar satellites of the same type having the same function and designed to be similar, complementary and orbiting for a common purpose under shared control [20],[21].

There are three types of constellation according to their orbital altitudes:

1.4.1 Low Earth Orbit Constellation

Satellites in low orbit describe elliptical or (more often) circular orbits within 2,000 kilometers of the earth. The orbital period at these altitudes is between 90 minutes and two hours. As for the radius of the coverage area, it is between 3000 and 4000 km [17].

A LEO satellite can remain visible for up to 20 minutes for an observer on earth.

A global transmission system using this type of orbit required a large number of satellites in a number of different orbital planes. When a satellite in charge of a given user is no longer

visible to that user (it passes below the visible horizon), the satellite must be able to transfer the services for which it was responsible to another satellite in orbit identical or adjacent: this is the management of the hand-over [12],[17].

LEO constellations in any case offer particularly low propagation delays, of the order of around 20 ms, which allow them to provide services of the same type as those of terrestrial wired fiber optic networks.

1.4.2 Medium Earth Orbit constellations

ICO or MEO (Intermediate Circular Orbits, Medium earth orbits) satellites describe circular orbits at an altitude of about 10,000 kilometers. The orbital period is about 6 hours and an earth observer can have a visibility of a satellite of a few hours [12],[22].

A global transmission system using this type of orbit requires a smaller number of satellites compared to the LEO constellations. Only 2 to 3 orbital planes are needed to achieve global coverage.

An MEO-type constellation works very similarly to LEO systems; however, by structure, there is obviously less need for a hand-over system.

The propagation delay is greater than in LEO constellations, but still much less than in GEO systems.

1.4.3 GEO Constellation

The most commonly used satellites for telecommunication purposes are geostationary satellites. The altitude of these equatorial satellites, such that their orbit period is synchronous with the earth, i.e. one rotation in 23h 56mn 4s, will be approximately 36,000km. Three satellites placed at 120° on the geostationary orbit allow to "seeing" almost the whole earth, except for a small polar zone located at the extremes (Fig. I.5). The propagation delay is greater than in the LEO and MEO constellations [12],[21].

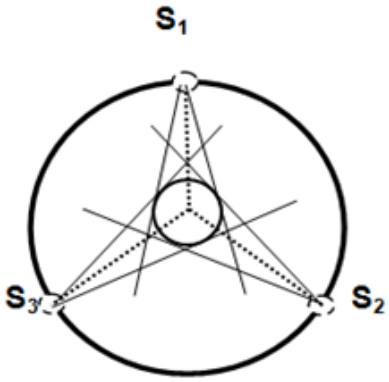

Figure 1-5: GEO constellation.

1.5 Geometry between earth and satellite

Each satellite is defined by its latitude and longitude relative to a reference point p [12].

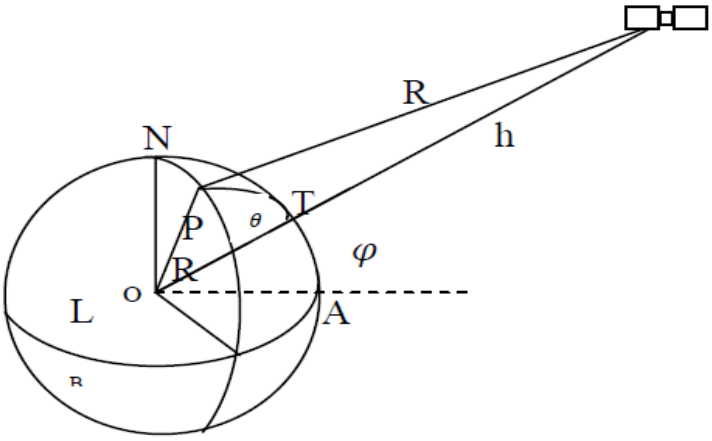

Figure 1-6: Geometry between earth and satellite.

Where: φ is a satellite latitude; λ: satellite longitude; l: latitude of a point of satellite longitude; θ: longitude of P; L= θ -λ: difference in longitude of satellite and point P; h: satellite altitude; RT=6378Km: earth radius; r=RT+h: distance between the centre of the earth and the satellite; $R = \sqrt{RT^2 + r^2 - 2R_T r cos\emptyset}$: Distance between the satellite and point P With $cos\varphi = cosL.cos\theta.cosl + sin\theta.sinl$

Two angles are used to locate the satellite from a point P on the earth's surface, usually the elevation angle and the azimuth [23].

- The elevation angle E_l is the angle between the horizon at the point in question and the satellite, measured in the plane containing the point in question, the satellite and the center of the earth.

- The azimuth angle A is the angle, measured in the horizontal plane at point P, between the direction of true north and the intersection of the plane containing the satellite and the center of the earth.

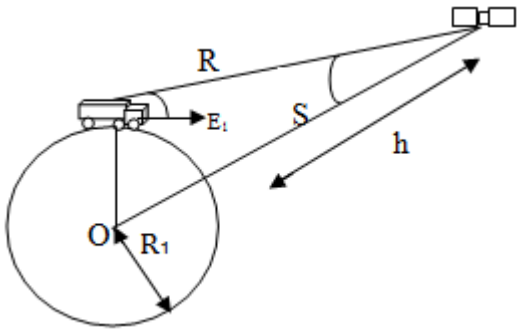

Figure 1-7: Nadir angle and elevation angle.

- Another useful angle is the nadir angle S. This is the angle at the satellite between the direction of the centre of the earth and the direction of the reference point P.

1.6 Basics of space mechanics

We consider the evolution of a mobile assimilated to a material point in the vicinity of a celestial body. It is assumed that [23]:

- The only forces taken into account are the Newtonian forces of attraction.

- The celestial body is assumed to be spherically symmetrical and of constant mass distribution.

Under these conditions, the study of the motion of the mobile can be assimilated as a first approximation to a 2-body problem: a particle of mass m attracted by a particle of mass M.

1.6.1 Kepler's laws

1.6.1.1 First Law or Law of Orbits

In the heliocentric frame of reference, the orbit of each planet is an ellipse with one of its foci occupied by the sun [16],[17].

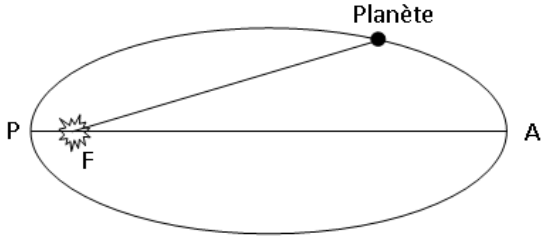

Figure 1-8: The ellipse.

In fact, the first law states that all orbits have the shape of an ellipse. This law does not prohibit circular orbits, in fact the latter are considered as ellipses whose two foci are confused.

1.6.1.2 Second Law or Area Law

The motion of each planet is such that the line segment connecting the sun and the planet sweeps equal areas for equal lengths of time [16].

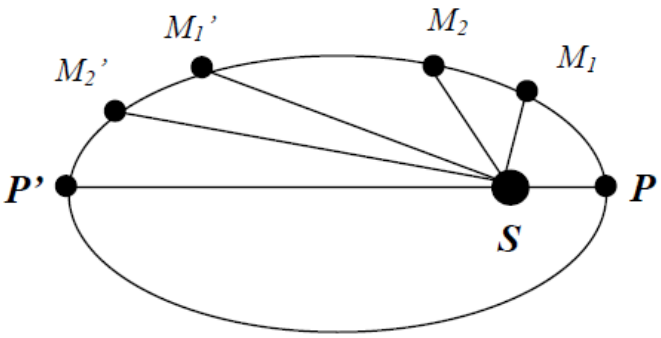

Figure 1-9: Law of areas.

1.6.1.3 Third Law or Law of Periods

For all the planets, the ratio between the cube of the trajectory's half-major axis (a) and the square of the period (T) is the same [12],[16].

$$\frac{T^2}{a^3} = cte \tag{1-2}$$

This means that the time it will take the satellite to complete one orbit (period) can be calculated from half the dimension of the half-major axis.

The law indicates that the satellite will have a slower speed at higher altitudes and conversely a faster speed at lower altitudes.

1.6.2 Orbital parameters

An elliptical trajectory is characterized by six orbital elements (corresponding to six degrees of freedom). Two define the shape of the ellipse: a and e which are respectively the semi-major axis and the eccentricity. Three orbital elements are used to orient the position of the ellipse in space: w, Ω, i, respectively the perigee argument, the right ascension of the ascending node and the inclination [12],[13].

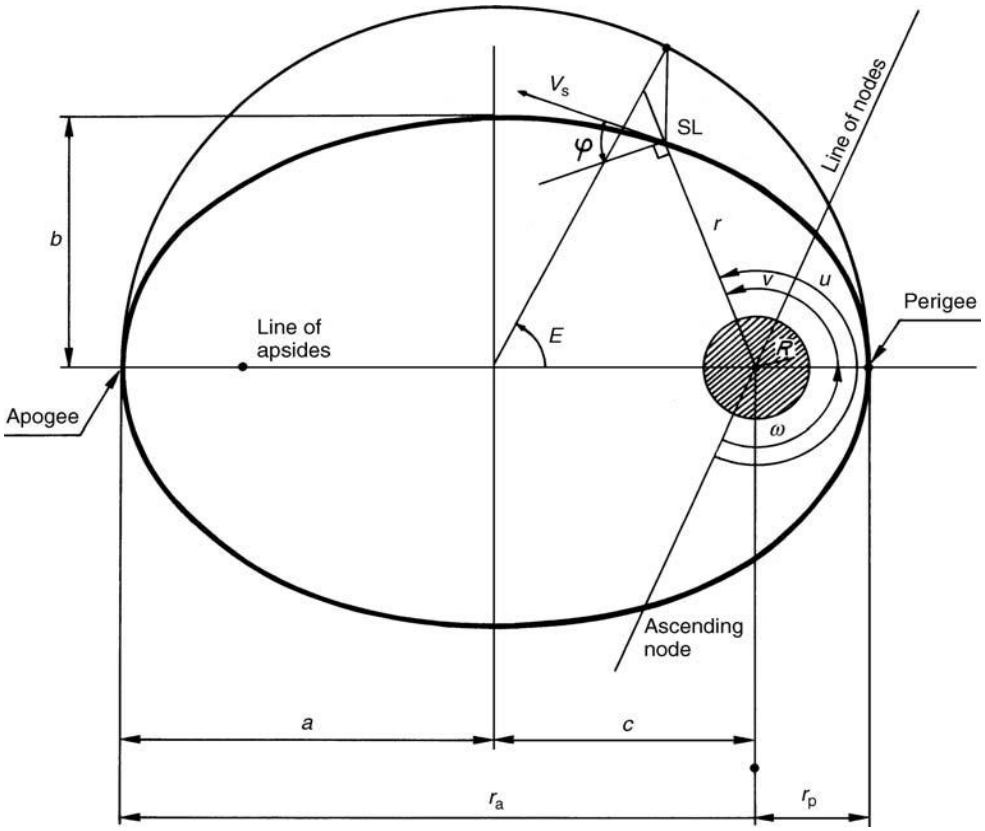

Figure 1-10: Two-body problem.

1.6.2.1 Reference axis

The satellite's orbit crosses the plane of the equator at two points called the descending node ND at the northern hemisphere to southern hemisphere crossing point, and the ascending node NA at the northern hemisphere crossing point. The line (NA, ND) is the line of nodes [16],[24].

1.6.2.2 Parameters defining the position of the orbit plane

We know by Kepler's first law that motion is plane and that the trajectory has the shape of an ellipse [12].

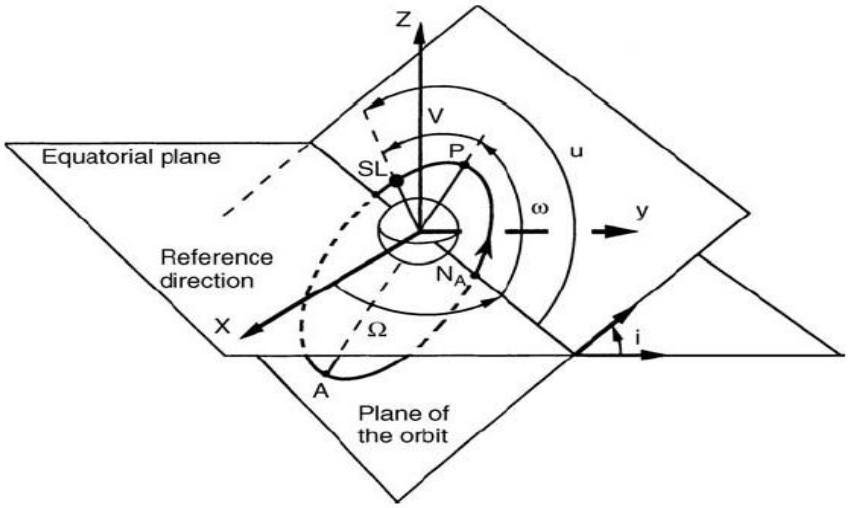

Figure 1-11: Position of the orbit plane.

We can therefore define 2 angles allowing to position the plane of the orbit with respect to an initial equatorial reference frame :

I= the inclination with respect to the equator.

Ω= the right ascension of the ascending node i.e. the angle between the X axis and the line of intersection of the plane of the orbit with the equator (longitude).

The node line (N_A, N_D) bisects the equatorial plane and the orbit plane.

- The angle I formed by the half-plane of the orbit containing the satellite's trajectory from N_A to N_D and the half-plane of the equator containing the trajectory of a point on the equator from N_A to N_D, is the inclination which ranges

from 0° to 180°. The orbit is said to be direct when i is less than 90° and retrograde when i is greater than 90°.

- The angle Ω which, in the plane of the equator, forms the node line and the direction of the vernal point, defines the orientation of the node line. It is the straight ascent of the ascending node which is measured from 0° to 360°, from the vernal point to the ascending node, in the direction of rotation of the earth or direct direction.

1.6.2.3 Orbital shape and position

In the plane of the orbit, the ellipse itself is characterized by two parameters:

a: the semi-major axis, b: the semi-small axis.

We very often replace b by the eccentricity e, knowing that

$$b^2 = a^2(1 - e^2) \tag{1-3}$$

Then defines an origin on the ellipse; conventionally, we are used to locate it at the perigee (the point closest to the earth) of the orbit.

The position of the major axis in the plane of the orbit is defined by the angle ω, formed by the line joining the center of the earth at perigee on the one hand and the line of the nodes on the other. It is the argument of the perigee ω, which is measured from 0° to 360°, from the ascending node to the perigee in the direction of the satellite's revolution.

1.6.2.4 Position of the satellite in orbit

Now we need to know exactly where the satellite is positioned on the ellipse [16].

The angle determining the position of the satellite relative to the perigee can be expressed in different ways:

V= the varying anomaly actually corresponds to a polar coordinate.

E=the eccentric anomaly by projecting the satellite on the main circle of the ellipse

M= the mean anomaly defined by Kepler's equation: $M = E - esinE$.

This fictitious angle M makes it possible to simply define the Keplerian motion as a function of time by:

$$M = M_0 + n(t - t_0) \tag{1-4}$$

Where n is the mean motion equal to:

$$n = \sqrt{\frac{\mu}{a^3}} \tag{1-5}$$

In addition, constant due to Kepler's third law. We thus obtained 6 orbital parameters: $a, e, i, \omega, \Omega, V\ or\ E\ or\ M$.

The main advantage of the Keplerian parameters is that, if the disturbances are not taken into account, the first five are constant over time while the sixth (V, E or M) varies linearly with time.

1.6.3 Orbital perturbations

There are a number of physical contributions that influence the trajectory of a body in Earth orbit. These are called perturbations and if it is not always possible to take them into account analytically in the calculation of the orbit, it is necessary to take them into account, for example, to make periodic corrections to the trajectory.

There are various numerical methods [13] to evaluate these disturbances

1.6.3.1 Perturbation of the third body

The presence of the sun and moon causes variations in all orbital elements, but the secular (long-term linear) effects are mainly on the right ascension ω and the perigee argument ω [1],[16].

For satellites with circular orbits and a higher attitude than a geostationary one, this disturbance predominates.

1.6.3.2 Disturbance due to the non-spherical earth

For satellites whose orbit is less than or equal to a geostationary orbit, it is the effect of the flattening of the earth at the poles that dominates, causing variations on the right ascension and the perigee argument [12].

1.6.3.3 Disturbances due to atmospheric friction

This is the main force of non-gravitational origin that affects satellites in Low Earth Orbit (LEO). This friction causes them to lose kinetic energy and therefore altitude. As a result they can end up re-entering the atmosphere if the trajectory is not compensated [5].

1.6.3.4 Solar radiation perturbations

At altitudes above 800 Km, another disturbance takes precedence over atmospheric friction: the pressure due to solar radiation which causes an acceleration, applied in the direction of the sun, equal to [5],[13]:

$$a = -4.5.\,10^{-8} A/m \qquad (1\text{-}6)$$

Where A is the surface exposed to the sun and m the mass of the satellite.

1.6.3.5 Intrinsic perturbations

There is a range of disturbances that depend directly on the construction of the satellite. Among them are the following [5],[12]:

- Uncertainties about the center of Les gravity.
- Uncertainties about propulsion.
- The vibration modes of the structure.

These intrinsic disturbances mainly concern the attitude (the angular position of the satellite and its variation with respect to time) of the satellite but can also indirectly influence the orbital trajectory.

1.6.4 Maintenance and survival in orbit

The earth contains strong magnetic fields, which affect its surroundings. Specifically, some areas beyond the earth's surface have radiation levels high enough to damage electronic components that pass through them [12],[25].

At high altitudes, the Earth's magnetic field is strongly distorted by the pressure of the solar wind, and at low altitude and (LEO), it is approximately that of a dipole tilted about 11.5 degrees from the Earth's rotation axis.

One of the most important effects of the Earth's magnetic field, in terms of engineering is due to Van Allen's belts, named after the American physicist who discovered them in 1958. They are two toric zones, where the electron concentration and of protons is very important because they have been trapped by the magnetic field [19]. The first belt is between 600 and 90000 Km of altitude for a latitude between +40° and -40°; the second is located at an altitude of about four times the Earth's radius and largely overlaps the first [12].

There are four main regions where satellites are put into orbit:

- The LEO (Low Earth Orbit) zone, between the end of the atmosphere and the first Van Allen belt, from 400Km to 1500 Km of altitude.
- The MEO zone (Medium Earth Orbit), between the two Van Allen belts, from 5000 Km to 13 000Km of altitude.
- The HEO (High Earth Orbit) zone, whose apogee is beyond the Van Allen belts, but which, within the framework of elliptical orbits, encompasses one or more of the previous zones.
- The GEO (Geostationary Earth Orbit) zone, which could be seen as a special case of HEO, for geostationary satellites, at an altitude of Seventy-five thousand miles.

It is not interesting to place a satellite with an elliptical orbit in the LEO area, given the small margin that one has (the main half-axis and the minor half-axis are both between 7 000 Km and 8 000 Km). There is still the possibility of placing them in orbit, or passing them through the Van Allen belts, which reduces the lifetime of the electronic components. In summary, the classification in figure (I-12) can be considered [12].

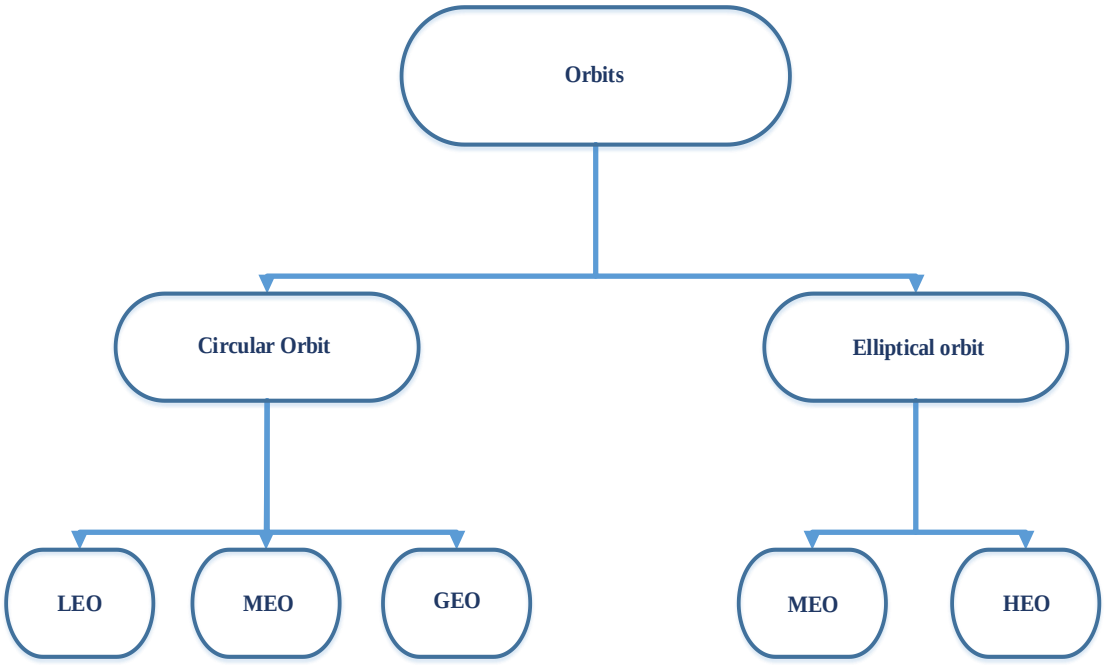

Figure 1-12: Classification of the different types of exploitable orbits.

1.7 Conclusion

In this chapter, we provided a comprehensive description of the communications by satellite. We also talked about the types of orbits in terms of form, which led us to address mentioning the types of satellite and the characteristics of each satellite, the appropriate orbit for each satellite and the minimum number of satellites to cover the globe also the distance of the satellite and the globe. In addition, we discussed geometry between satellite and Earth and some of the basics of space mechanics. Finally, we described how to maintain the satellite in orbit, and what is its expected lifetime.

In the next chapter, we will talk in detail about optical communications, especially lasers, their origin and stages of development, up to the application of their use in the satellite.

CHAPTER II:

Optical Telecommunications and the Effect of Atmosphere

2 Optical telecommunications and the effect of atmosphere

2.1 History of optical telecommunications

In this chapter, we will try to make a historical overview of the techniques that humans can set up to establish connections using optical signals. While focusing on some important technical advances as they reflect the principle of Atmospheric Optical Link (AOL).

The idea of using an optical signal to communicate is not new. The light spreads naturally and the eyes are already a powerful detector for this type of signal. In Antiquity, ancient Greeks used mirrors directed to target ships, or dangled their shields to communicate in battle. The succession of sent signals constituted a Morse coded message.

The main limitations are then the range and the flow of information transmitted reduced. Claude Chappe made a first progress in 1794 in terms of flow [26]. By observing with binoculars the position of the arms of a pantograph at the top of a tower, the operator is sent back to a number corresponding to an agreed-upon message (birth of telegraphy). However, the real precursory contribution of the AOL is the proposal of Maurat, taken by Mangin. It consists in improving the directivity, therefore the range, of the optical signal emitted by a set of mirrors and simple lenses collimating the beam (Figure 2-1). Thus, in 1873, with optics 30 cm in diameter, this device allowed to work on ranges of 36 km at a rate of the order of 200 words per hour.

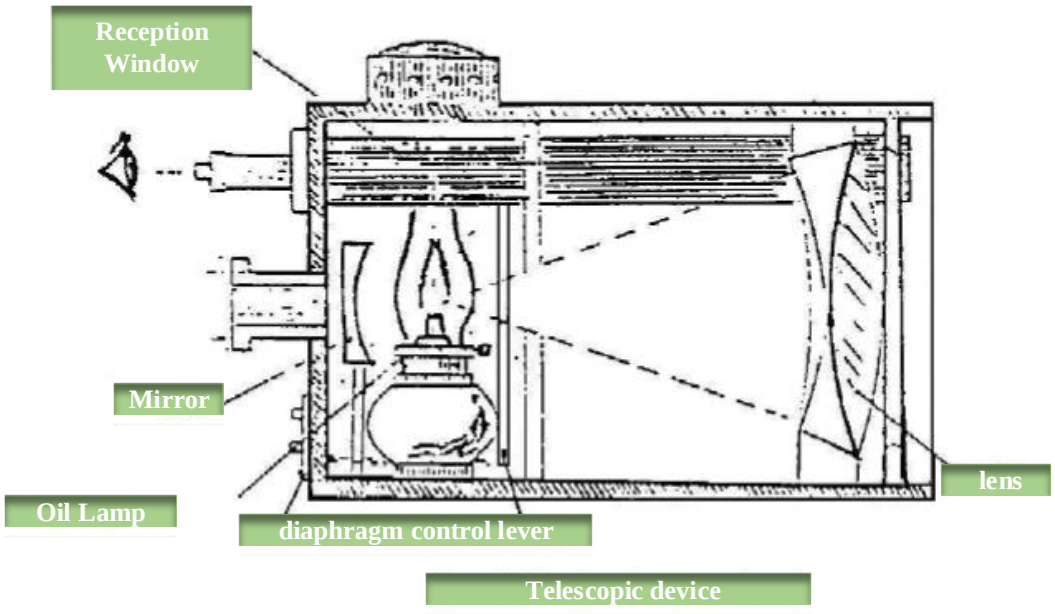

Figure 2-1 :Optical telegraph of Mangin [27].

With the invention of the photophone in 1880 (see figure 1.2), Graham Bell demonstrates the effectiveness of the use of an optical signal (here solar radiation) to transmit information, the voice [27], using the intensity modulation. The distance it establishes is 200m [28].The variability of the light source (the sun) and the short propagation distance limited by the low sensitivity of the detection system will be the reason for its invention.

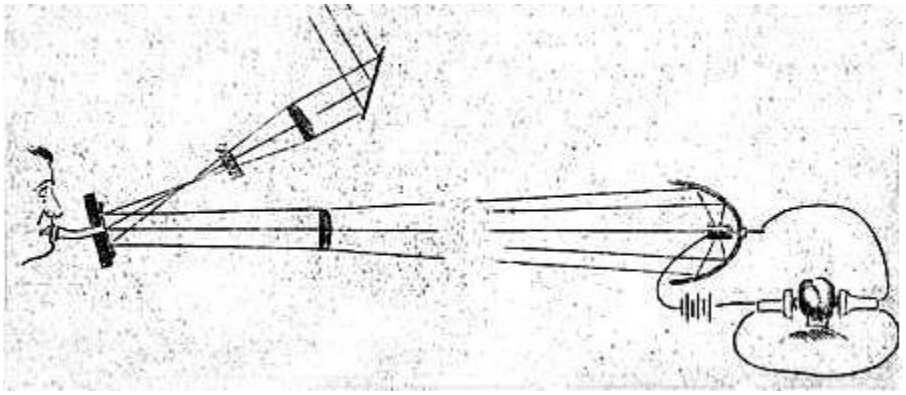

Figure 2-2: Schematic representation of Graham Bell's photo phone [27]. Under the influence of speech, the mirror deforms and modulates the intensity of the light coming from the sun as it reaches the receiver. The resistance of the selenium receiver varies according to the intensity of the light received and allows the information to be retrieved.

The telecoms initially abandoned the optics for the benefit of electronics. Indeed, the advent of electronics allows a modulation and demodulation of the signal much faster, telecommunications know their true revolution. The first wired networks date from the 19th century. They guide a message electrically and solve at once the problem of range and flow. First copper cables were thrown in 1850 into the Atlantic Ocean to allow telegraphic communications between Europe and America. This date corresponds to the control of the insulation of cables under water [29].

To overcome the wired network, it was again necessary to look into the free space propagation of an electromagnetic wave. The first breakthrough in this direction was achieved in the range of radio waves, the propagation of which is not altered by atmospheric turbulence. It will be seen later that this is not the case in the optical range.

Thus, in 1896, Marconi transmits and captures signals over a distance of 250m, having synthesized the inventions of Alexander Popov's antenna, the Branly electromagnetic wave detector and the principles of the established radio program by Tesla. Three years later, the latter made the first radio communication program between France and England [29].

The scientific community has been trying, since the 1960s and the invention of the laser, to set up free space communications using an optical signal to establish a direct line of sight link. The first applications are developed for links to satellites [30],[31]. Unfortunately, the limited lifetime of lasers, their size and insufficient light output cause the rapid decline in interest in this technology.

In the 1980s, the appearance of semiconductor lasers with long life span, low footprint and high efficiency, contributes to the emergence of laser communication programs from Europe and the United States. United States [32],[33]. Lasers, being high-power directive sources, make it possible to work with high signal-to-noise ratios (SNRs) when they are associated with modern detectors, which was lacking in Bell's photophone.

Again, the challenge is to achieve the same quality of telecommunication with free-space signal propagation. This is the purpose of AOLs. Under certain conditions, favorable in terms of atmospheric turbulence encountered, namely telecommunications in space or from space to the ground, AOLs have already appeared:

- In 2001, the first unidirectional satellite-satellite optical link (SILEX project) which enabled the transfer of data from the ARTEMIS satellite to SPOT 4 [22],

- In 2002, the first two-way ground-to-satellite optical link between the Optical Ground Station built at the Mount Teide Observatory (Canary Islands) and the ARTEMIS satellite (SILEX project) [34],

- In 2006, the first two-way satellite-to-satellite optical link between the ARTEMIS and OICETS satellites (Japan) [35],[36]

- In 2006, the first optical link between a satellite (ARTEMIS) and an aircraft (Mystery 20) of 50 Mbits / s (LOLA project) [37],

- In 2007, the first bidirectional ground-to-satellite optical link between the KIRARI satellite and a mobile telescope of 0.4 m diameter of the DLR [36].

However, outside the experimental setting, the transfer of data on the ground is still done by radio frequencies, with a much lower flow rate. For endo-atmospheric propagation, the use of radiofrequencies is all the more justified by the main limitation encountered by AOLs: propagation through the atmosphere.

2.2 Principle and characteristics of atmospheric optical links

Atmospheric optical links (AOLs) rely on the propagation of light in free space to transmit information between two points. These links are usually point-to-point, but there are also point-to-multipoint links. The different areas of AOL applications (air-to-air links, satellite-underwater, air-submarine, air-satellite, satellite-satellite, etc.) have a major impact on their characteristics and their locations. It is, therefore, difficult to have a general discourse encompassing all AOL systems. We only consider AOLs as part of an air-to-satellite line of sighting line. Figure 2-3 shows schematically an atmospheric optical link in the case of a point-to-point application between two urban sites. AOLs make it possible to overcome the disadvantages of a fiber-optic type connection, which is often long and expensive to set up. In addition, the absence of the license requirement, interference immunity as well as natural link security (directional beam) that can operate in full-duplex (Telecommunication system where the signal is transmitted in both directions simultaneously) and the possibility of reaching high transmission rates are additional advantages over conventional wireless communications.

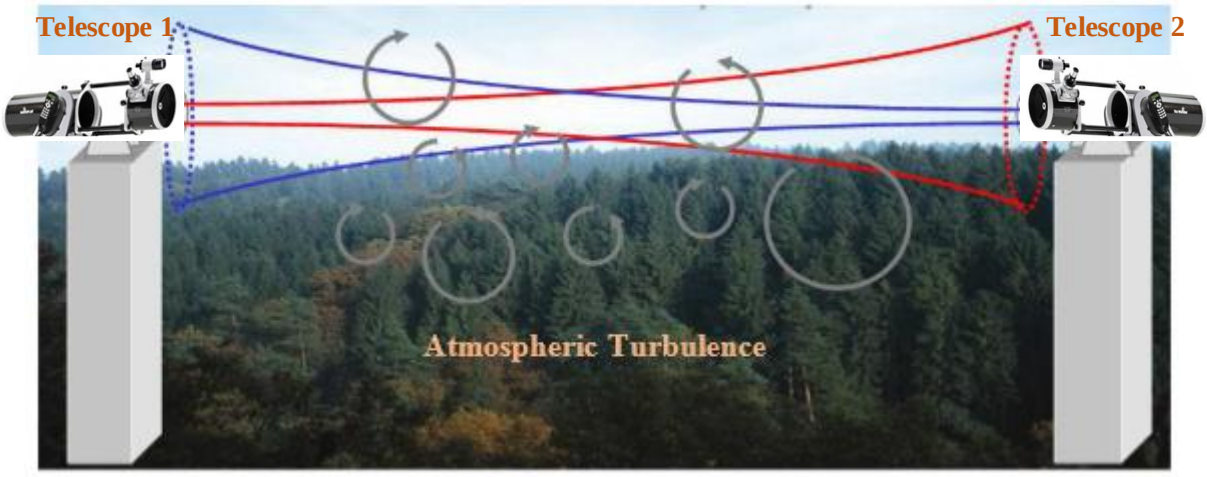

Figure 2-3: A modern optical telegraph

A modern optical telegraph, or AOL, consists of two distant telescopes facing each other, each with emission and laser detection. Each telescope simultaneously transmits and detects the stream emitted by the other, thus creating a bidirectional optical link in direct line of sight (Figure 2-3).

For a civilian use, this device must be reproduced identically to renew the range of the signal and thus grid a given territory. The telescopes should be placed at least 30 meters above the ground to avoid physical obstacles. This also has the advantage of avoiding the most turbulent air layer at ground level (see §2.3.1 The physical phenomenon of turbulence) [38].

2.2.1 Modulation of AOLs endo-atmospheric

Free space propagation can benefit from the same modulation and demodulation technologies as those developed for guided optics. Modulation techniques include On-Off Keying (OOK), which is simply based on modulating the amplitude of the source to encode binary information. However, there are also more subtle strategies, such as Pulse Position Modulation (PPM) [39], which requires less average energy than the OOK modulation for the same error rate on reception. On the other hand, PPM requires greater bandwidth and more difficult reception timing [40]. We limit ourselves in the following of the manuscript to the case of the modulation OOK.

2.2.2 Benefits of AOLs endo-atmospheric

Free space telecommunications are nowadays very common use in the terrestrial range. However, the optical range has much shorter wavelengths to modulate the signal much faster, and thus increase the rate. Thus, optical telecommunications allow considering rates well above the 10Gbit/s [41]. Moreover, with respect to a strongly diverging radio emission due to the diffraction (high wavelength), the laser emission is very directive. This gives him several advantages:

- The communication is more secure because difficult to intercept;
- There is no bandwidth to share because the environment is not drowned out signal;
- It is possible to reduce the transmission power.

It is possible to combine all these qualities with guided optics. However, the propagation in free space differs from a fiber network by the following aspects:

- Implementation of the immediate network;
- Portability;
- Lower installation cost;
- Mobile target tracking.

Thus, there are applications for which it is not possible to extend a cable and which may require a much higher rate than that offered by a microwave link. One can imagine for example the rapid implementation of an AOL on a disaster area by an earthquake that broke the existing fiber network. The AOL would provide for the speed and quality of on-site intervention. On the other hand, the saturation of an urban network following the organization of an exceptional event, which does not justify the permanent increase of the capacity of the network [42].

The AOLs can thus provide a high-speed telecom connection at a given moment, without investing the necessary sums for the installation of a new fiber network.

2.2.3 The limitations in atmospheric optical links

Optical communication has grown rapidly because it provides a stable propagation medium that limits the loss of flux during propagation. In the case of a AOL, the propagation medium is the ambient atmosphere that has two main limiting factors:

- Attenuation of the signal;
- Degradation of the optical quality of the laser beam.

Concerning attenuation, a drop in the received signal necessarily induces a decrease in the range of the system. In the visible range, the attenuation by the atmosphere is very dependent on the climatic conditions (fog, rain ...) [43],[44]. Apart from the choice of a transmission wavelength at a minimum of attenuation by the atmosphere, the increase of the flux is the only possible solution to bring [45].

The degradation of the quality of the laser beam during propagation has, for its part, other origins. The atmosphere being a turbulent medium, the inhomogeneity of the medium can deflect or even burst the beam, so that it is no longer detected by the target. As the impact of atmospheric turbulence increases with the volume of turbulence traversed, the system is limited in scope. However, one can imagine solutions such as the pre-compensation of the beam at the emission to mitigate the effects of the turbulence [46]. For example, in the case of deflection from the beam by the turbulence, the beam can be emitted in another direction of propagation so that the turbulence brings it back to the target. The study of signal propagation allows us to develop precompensation strategies to overcome the limitations introduced by turbulence [47].

2.3 Atmospheric turbulence

2.3.1 The physical phenomenon of turbulence

Theorists such as Poiseuille, Reynolds later followed by Taylor and Von Karman, gave the first definition of turbulence as “an irregular movement that appears in fluids when they encounter solid obstacles”. At the beginning of the 19th century, Claude Navier wrote the basic equations governing the temporal evolution of the flow of a fluid in turbulence [48].

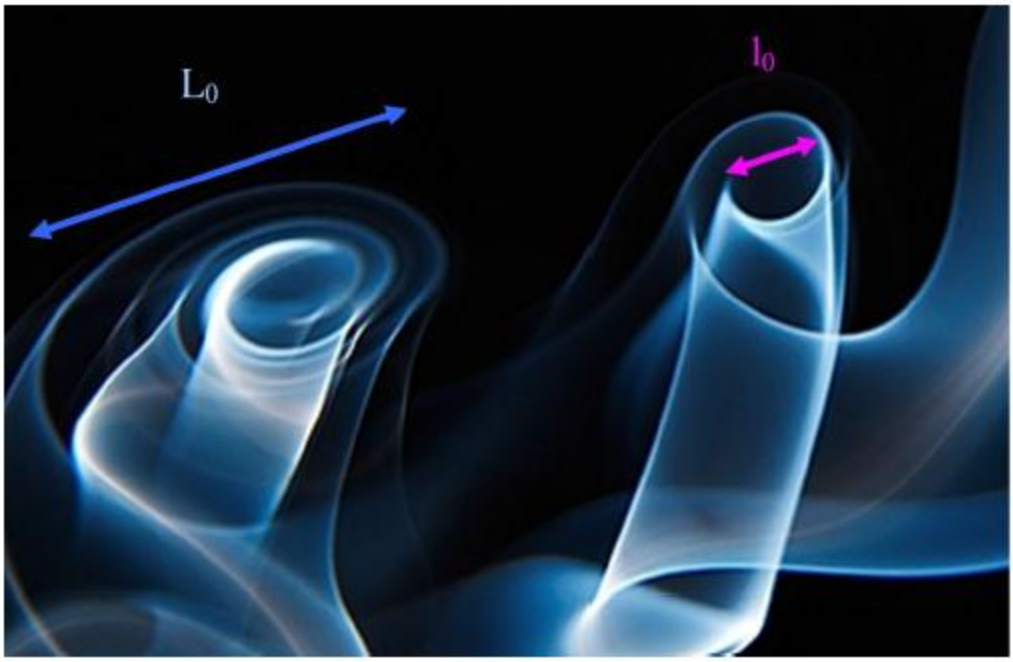

Figure 2-4:An overview of the principle of energy cascade in a fluid in turbulent flow where the transfer is from large to small scale [48].

The Earth's atmosphere is made up of a gas mixture in perpetual evolution. On the one hand, it is heated by solar radiation, and on the other hand, it undergoes radiative interactions with the ground. The temperature in the atmosphere is therefore highly inhomogeneous. This results in the formation of air masses of different densities. Under the effect of gravitation, these air masses are set in motion and interact constantly. A turbulent flow is created at their interface: it is the formation of turbulent layers. These layers are characterized by local variations in temperature, pressure, and humidity, which cause local variations in the refractive index of the air. These fluctuations cause a disturbance of the propagation of electromagnetic waves [49].

2.3.2 Theory of energy cascades

Kolmogorov [48] proposed a statistical description of the phenomenon of atmospheric turbulence, based on scale laws [50]. A turbulent flow leads to the formation of large vortices, the kinetic energy of which is transmitted to smaller and smaller vortices, in the form of a cascade of energy, until dissipation by viscous friction.

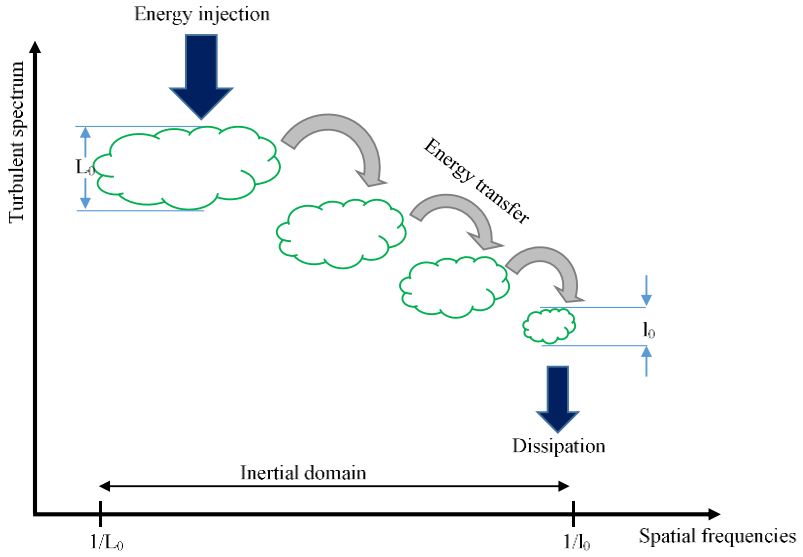

Figure 2-5: Schema of the energy cascade process and the division of turbulence cells in the atmosphere.

➢ **Inertial domain:** Spatial scales for which the turbulence is said to be fully developed and for which the Kolmogorov model applies define the inertial domain. It is bounded on the one hand by the size of the largest vortices, of the order of a few tens of meters, and on the other by the size of the smallest vortices, of the order of a few millimeters.

➢ **The external scale:** The external scale L_0 is the magnitude characterizing the spatial dimension of the largest eddies. Its size influences the amplitude at low spatial frequencies of phase disturbances due to turbulence. For future large telescopes, whose diameter will be several tens of meters, the influence of the external scale becomes significant, and one needs to access to its measurement. Several techniques nowadays make it possible to estimate L_0. The Generalized Seeing Monitor (GSM) uses fluctuations in the arrival angle of the wavefront [51],[52],[53]. The external scale can also be deduced from interferometric data[54], or data from adaptive optics [55]. Finally, the Monitor of Outer Scale Profile (MOSP) provides access to external scale profiles as a function of altitude [53],[54], from the correlations of wavefront arrival angle fluctuations measured on lunar edge images. The typical value of the external scale is generally of the order of a few tens of meters [56].

➢ **The internal scale:** The internal scale 10 corresponds to the spatial dimension of dissipation of the kinetic energy by viscosity. Studies offer techniques to access its value. Some use angle of arrival fluctuations [57],[58], others intensity fluctuations [59],[60]. It is also possible to estimate 10 from the scanning effect of a laser beam [57],[61]. Finally, there

are hybrid techniques that use both phase and intensity fluctuations [62]. The typical value of the internal scale is generally of the order of a few millimeters.

2.3.3 The refractive index of air

2.3.3.1 Fluctuations in the refractive index

Consider the difference between the value n (r) at a point r and the value n (r + ρ) at a point distant from a distance ρ. The vectors r and ρ respectively represent a position and a separation distance in a three-dimensional space.

For an established turbulent regime (temporally and spatially stationary), in the inertial domain, the variance of the difference of the refractive index at two points of space, or function of structure, is given by [63],[64]:

$$D_n(\rho) = \langle |n(r) - n(r+\rho)|^2 \rangle = C_n^2 . \rho^{2/3} \quad (2\text{-}1)$$

Where the brackets ⟨⟩ represent the overall mean. $D_n(\rho)$ is called the structure function of the refractive index and C_n^2 is the structure constant of the refractive index. C_n^2 is expressed in $m^{-2/3}$ and ρ = | ρ | is expressed in m.

Equation 2.1 is actually only a valid approximation as long as ρ is smaller than the external scale of turbulence. However, for the great distances ρ, the values n (r) and n (r + ρ) will become complementarily independent. According to equation 2-1, the fluctuations of the refractive index are then at infinity, which has no physical meaning. D_n (ρ) is only valid for $l_0 < \rho < L_0$.

2.3.3.2 Spectral density of index fluctuations

Obukhov and Yaglom [63],[64] have shown that the power spectra of temperature and humidity fluctuations follow the law in $f^{-11/3}$. A power law in $f^{-11/3}$ also describes the fluctuations of the air index, directly related to these two parameters.

Tatarski gives the expression of the spectrum of fluctuations of index $W_n(\vec{f})$ valid between l_0 and L_0 [65]:

$$W_n(\vec{f}) = 0.033(2\pi)^{-2/3}\ C_n^2 f^{-11/3} \quad (2\text{-}2)$$

Where f denotes the modulus of the spatial frequency expressed in m^{-1}. The Kolmogorov spectrum (equation 2-2) is theoretically valid only in the inertial domain: $1/L_0 < f < 1/l_0$. It assumes an external scale and an internal scale of turbulence respectively infinite and zero and diverges in f = 0.

To justify the use of a spectrum over all frequencies, parameters L_0 and l_0 are introduced into the Kolmogorov spectrum. The introduction of these parameters into the Kolmogorov spectrum gives rise to the modified von Karman spectrum which saturates for $f < L_0$ and cuts in $f = l_0$ whose expression is given by equation (2-3) [65]. This saturation guarantees a spectrum without singularity at the cost of using the L_0 parameter, which is currently unknown. Figure 2.2 shows the Von Karman spectrum for different values of the internal and external scales. All the results presented in this manuscript were obtained using the modified spectrum of von Karman.

$$W_n(f) = 0.033(2\pi)^{-2/3}\ C_n^2(f^2 + \frac{1}{L_0})^{-11/6} e^{-(\frac{2\pi l_0}{5.91} f^2)} \qquad (2\text{-}3)$$

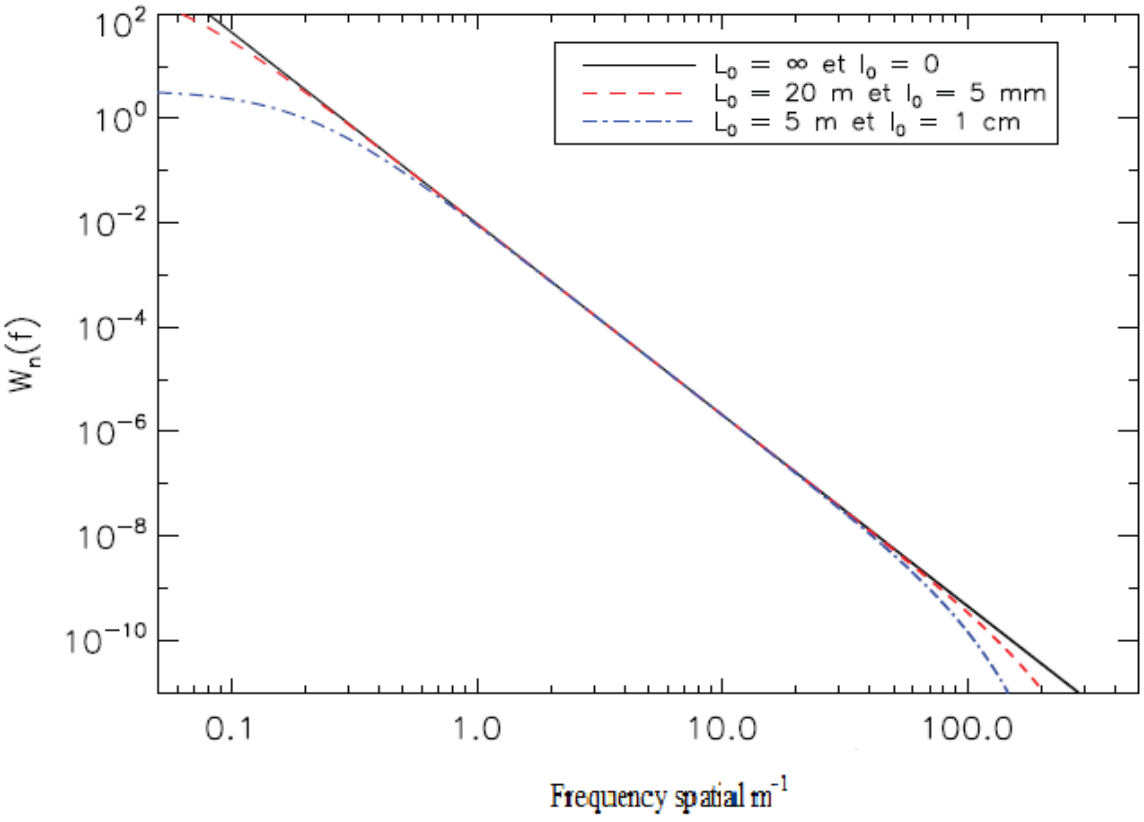

Figure 2-6: Power spectral density of refractive index fluctuations for $C_n^2(h) = 1$and different values of inner scale and outer scale [38].

2.4 Propagation of the Optical signal through the turbulence

When the optical propagation through atmospheric turbulences, the optical wave will fluctuate in amplitude and phase because of the refractive index variations. The description of these fluctuations relies on the analytic resolution of the Helmholtz propagation equation including paraxial approximation.

2.4.1 Helmholtz equation

The propagation of an electromagnetic field in a dielectric medium such as air obeys Maxwell's equations. In the visible or near infrared, the period τ of the wave is of the order of 10^{-15}s, much less than the time of evolution of turbulence of the order of a millisecond.

In addition, over a kilometer propagation distance, the wave propagation time is of the order of 10 μs, during which time the turbulence can again be considered as frozen. We therefore consider that n, the air index, is independent of time. We can then show that the electric field $\vec{E}$ obeys the propagation equation:

$$\nabla^2\vec{E}(\vec{r}) + k_0^2 n^2(\vec{r})\vec{E}(\vec{r}) + 2\nabla(\vec{E}(\vec{r}).\nabla(\log(n(\vec{r})))) = \vec{0} \quad (2\text{-}4)$$

In equation (2-4), $k_0 = 2\pi/\lambda$, where π denotes the wavelength of the electromagnetic wave.

The quantity $2\nabla(\vec{E}(\vec{r}).\nabla(\log(n(\vec{r}))))$ translates the polarization changes of the wave. The wavelength of an AOL is in the visible or near infrared; the working wavelength (of the order of 10^{-6}m) is therefore very small compared to the scale of evolution of the spatial fluctuations of the index (greater than 10^{-2}m according to Figure 2-6). This term therefore becomes negligible [66] in equation (2-4). We obtain the new equation:

$$\left(\nabla^2 + k_0^2 n^2(\vec{r})\right)\vec{E}(\vec{r}) = \vec{0} \quad (2\text{-}5)$$

It should be noted, however, that more recent studies retain the polarization term for the study of the propagation of Gaussian beams in free space [67], all the more since the expected performance in terms of data transmission error rate are very demanding.

2.4.2 Paraxial approximation

Consider the electromagnetic field $\vec{E}$ propagating in atmospheric turbulence in the direction $\vec{e}_z$ in an orthonormal reference frame. The absence of any coupling in equation (2-5) by deleting the term of polarization makes it possible to pass from a vectorial writing to a scalar writing of the field:

$$E(\vec{r}) = A_0 \Psi(\vec{r}) e^{ikz} \tag{2-6}$$

Where $\Psi(\vec{r})$ is the complex amplitude of the wave representing the deviation from the perfectly plane wave. By injecting equation (2-4) in equation (2-6) we obtain a new equation with $\Psi(\vec{r})$ as the unknown variable:

$$\nabla^2 \Psi(\vec{r}) + 2i\langle n(\vec{r})\rangle k_0 \frac{\partial \Psi(\vec{r})}{\partial z} + k_0\left((n(\vec{r})^2 - \langle n(\vec{r})\rangle^2)\Psi(\vec{r})\right) = 0 \tag{2-7}$$

We denote $\langle n(\vec{r},t)\rangle$ the temporal average of the refractive index characterizing the propagation medium. The paraxial approximation consists in assuming that the scale of spatial fluctuations of $\Psi(\vec{r})$ is small compared to the wavelength and we can consider that $\left|\frac{\partial^2 \Psi}{\partial z^2}\right| \ll \left|\frac{\partial \Psi}{\partial z}\right|$. This approximation remains true as long as the diffraction effects affecting $\Psi(\vec{r})$ vary slowly in propagation direction. In addition, the refraction index fluctuations can be written as $(\vec{r}, t) = \langle n(\vec{r},t)\rangle + N$ where N are fluctuations of refractive index around the mean value that we consider $N \ll 1$. Hence, we can write, according to Taylor

$$n(\vec{r})^2 \approx \langle n(\vec{r})\rangle^2 + 2N\langle n(\vec{r})\rangle \tag{2-8}$$

Finally, under all these condition, the (2-7) becomes:

$$\frac{\partial^2 \Psi(\vec{r})}{\partial x^2} + \frac{\partial^2 \Psi(\vec{r})}{\partial y^2} + 2i\langle n(\vec{r})\rangle k_0 \frac{\partial \Psi(\vec{r})}{\partial z} + 2k_0 \langle n(\vec{r})\rangle N\, \Psi(\vec{r}) = 0 \tag{2-9}$$

2.4.3 Weak fluctuations Rytov approximation

The propagation equation does not allow an analytical solution in the general case. Other simplifying assumptions are necessary. The weak disturbance hypothesis allowing a perturbative type resolution of the wave equation has thus made it possible to develop the Rytov approximation [65]. Rytov's approximation considers the disturbances as multiplicative with respect to the undisturbed field, which makes it possible to establish the main statistical expressions of the field in weak disturbances.

The amplitude of the field of a monochromatic optical wave can be written:

$$E(\vec{r}) = e^{\psi_0(\vec{r})} \tag{2-10}$$

During the atmospheric propagation, it is affected by random fluctuations of the refractive index and it can be written under Rytov approximation:

$$E(\vec{r}) = e^{\psi_0(\vec{r})+\psi(\vec{r})} \tag{2-11}$$

Where can be developed as: $\psi(\vec{r}) = \psi_0 + \psi_1(\vec{r}) + \psi_2(\vec{r}) + \cdots$ Applying this new amplitude field to the equation (2-7), we obtain

$$\nabla^2(\psi_0 + \psi_1(\vec{r}) + \psi_2(\vec{r}) + \cdots) + \left(\nabla(\psi_0 + \psi_1(\vec{r}) + \psi_2(\vec{r}) + \cdots)\right)^2 + k_0^2 n(\vec{r})^2 = 0 \tag{2-12}$$

In addition, the unperturbed field follows Helmholtz's equation

$$\nabla^2\psi_0(\vec{r}) + \left(\nabla\psi_0(\vec{r})\right)^2 + k_0^2\langle n(\vec{r})\rangle^2 = 0 \tag{2-13}$$

In the Rytov method, only the first order is taken into account and higher levels are neglected and we can write $\psi(\vec{r}) = \psi_0 + \psi_1(\vec{r})$. In order to simplify, we consider that $\langle n(\vec{r})\rangle = 1$ and we can express $\langle n(\vec{r})\rangle^2$ defined on the equation (2-7), at the first order, as $\langle n(\vec{r})\rangle^2 = 1 + 2N$. The equation (2-13) becomes:

$$\nabla^2\left(\psi_1(\vec{r})\right) + \nabla\psi_1(\vec{r})\left(\nabla\psi_1(\vec{r}) + 2\nabla\psi_0(\vec{r})\right) + 2Nk_0^2 n(\vec{r})^2 = 0 \tag{2-14}$$

In the weak turbulence condition, Rytov approximation assumes $|\nabla\psi 1(\vec{r})| \ll |\nabla\psi 0(\vec{r})|$ and the equation (2-14) becomes:

$$\nabla^2\left(\psi_1(\vec{r})\right) + 2\nabla\psi_1(\vec{r})\nabla\psi_0(\vec{r}) + 2Nk_0^2 = 0 \tag{2-15}$$

Which has a solution [46]:

$$\psi_1(\vec{r}) = \frac{k^2}{2\pi E_0(\vec{r})}\int d\vec{r}'\, N(\vec{r}')E_0(\vec{r})\frac{e^{ik|\vec{r}-\vec{r}'|}}{|\vec{r}-\vec{r}'|} \tag{2-16}$$

2.4.4 Statistic properties of the field

In the Rytov approximation framework, the perturbation $\psi_1(\vec{r})$ can be decomposed as:

$$\psi_1(\vec{r}) = \chi(\vec{r}) + i\varphi(\vec{r}) \tag{2-17}$$

Where ($\vec{r}$) and ($\vec{r}$) are respectively the log-amplitude and the phase of the field. By applying the paraxial approximation to the equation (2-14), ($\vec{r}$) and $\varphi(\vec{r})$ can be written as [46],[68] :

$$\chi = \frac{k^2}{2\pi}\int_0^L \frac{dh}{L-h}\int_{-\infty}^{+\infty} d\rho' n_1(\rho', h) cos\left(k\frac{|\rho-\rho'|^2}{2(L-h)}\right) \tag{2-18}$$

$$\varphi = \frac{k^2}{2\pi}\int_0^L \frac{dh}{L-h}\int_{-\infty}^{+\infty} d\rho' n_1(\rho', h) sin\left(k\frac{|\rho-\rho'|^2}{2(L-h)}\right) \tag{2-19}$$

2.4.5 Power spectral densities

According to the equation (2-13) and the phase-screens decomposition of turbulent volume given in [46], the power spectral densities of χ and φ are given for a propagation distance of L by:

$$W_\chi(f) = k^2 \int_0^L W_{\Delta n} sin^2(\pi h\lambda f^2) dh \tag{2-20}$$

$$W_\varphi(f) = k^2 \int_0^L W_{\Delta n} cos^2(\pi h\lambda f^2) dh \tag{2-21}$$

Where $W_{\Delta n}$ is Power spectra density of the refractive index given by equation (2-7) and h is the propagation distance between h = 0 and h = L.

2.4.6 Probability density function

In the weak atmospheric turbulence case, χ and φ is the sum of random independent and centered Gaussian variables. For φ, it obeys a Gaussian probability density function centered in 0 with a full width at half maximum of $2\sqrt{2\log(2\sigma_\varphi)}$ [69]. On the other hand, χ permits to calculate the optical wave irradiance (depending on the optical intensity) that is a parameter of greater interest in the regime of strong turbulence. It is be calculated as:

$$I = \Psi(\vec{r})\Psi(\vec{r})^* = I_0 e^{2\chi} \tag{2-22}$$

Therefore, the irradiance follows a log-normal probability law and the probability density of I is given by [69]:

$$P(I) = \frac{1}{\sqrt{2\pi I \sigma_\chi}} e^{-\left[\frac{\left(log\left(\frac{I}{I_0}\right) - 2\langle\chi\rangle\right)^2}{8\sigma_{\chi^2}}\right]}, I > 0 \quad (2\text{-}23)$$

The useful variable is the scintillation index noted σ_I^2 calculated as the normalized variance of the field intensity. It is related to the variance of the log-amplitude as follows:

$$\sigma_I^2 = \frac{\langle I^2 \rangle}{\langle I \rangle^2} - 1 = e^{4\sigma_\chi^2} - 1 \quad (2\text{-}24)$$

Being on the weak condition fluctuations and with an expansion on the first order of the intensity: $e^{2\chi} \approx 1 + 2\chi$. The probability density of the normalized intensity can be approximated by a normal distribution with:

$$\sigma_I^2 = e^{4\sigma_\chi^2} \quad (2\text{-}25)$$

To conclude the analytical study, the Rytov approximation leads to simplify the model characterization of the optical field propagation and simplifying its properties and deformations. For strong fluctuations condition, there is no analytic solution to the Helmholtz equation. We limited the presented work to plane wave but the same calculation can be done for spherical and Gaussian waves detailed in [46],[70]. However, it is important to understand that this analytic characterization includes many approximations that can be more difficult to take into account in practice and in strong condition of atmospheric turbulence.

2.5 Effects of turbulence on laser propagation

The use of a laser beam is essential for establishing a link with a high signal-to-noise ratio. The results presented so far do not take into account the spatial limitation of the field present in the AOL. We study the effects of turbulence on a spatially limited electromagnetic wave.

2.5.1 Atmospheric turbulence on the Gaussian beam waves

The Gaussian optical beam have a characteristic radial intensity profile that expands laterally during their propagation. Gaussian beams are one of solutions to the electromagnetic wave equation under paraxial condition, as we used previously to describe the atmospheric effects.

The free space propagation of a single mode laser beam can be modeled as the lowest order Gaussian beam wave noted TEM_{00}.

Assuming that the optical source is located at z = 0 and the wave is propagating in the vacuum along $\vec{z}$, the field distribution of this fundamental mode is given by [69]

$$E_0(r,z) = \frac{w_0}{w(z)} e^{-\left(\frac{\rho^2}{w(z)^2}\right)} e^{-\left(\frac{ik_0\rho^2}{2R(z)}\right)} e^{\left(ikz - i\tan^{-1}\left(\frac{z}{Z_R}\right)\right)} \quad (2\text{-}26)$$

For a beam propagating in a vacuum, its minimum size w_0 defines the beam waist. The wave surface is flat at the beam waist (infinite radius of curvature). L & z_0 denote the plane in which the waist is located. The evolution of the beam size w_z = L as a function of the waist distance, z - z_0 and of the beam waist w_0 is governed by the equation:

$$w(z) = \sqrt{w_0^2\left(1 + \left(\frac{z-z_0}{Z_R}\right)^2\right)} \quad (2\text{-}27)$$

Where $Z_R = \frac{\pi w_0^2}{\lambda}$ represents the Rayleigh distance. The term $\tan^{-1}\left(\frac{z}{Z_R}\right)$ describes the phase shift for a z distance propagation (beam divergence) corresponding to the angle between the asymptotes and the propagation axis. For an optical wave, the divergence is typically small and the half angle divergence can be written as, $\theta_D = \frac{\lambda}{\pi w_0}$. For large propagation distances (z $\gg$ Z_R) we have the approximation: w (z) $\approx$ θ_Dz.

The evolution of the radius of curvature R (z) as a function of the propagation distance can be written:

$$R(z) = (z - z_0)\left(1 + \left(\frac{Z_R}{z-z_0}\right)^2\right) \quad (2\text{-}28)$$

Figure 2-7 an example of Gaussian beam, the evolution of the diameter at 1 / e in amplitude as a function of the propagation distance. The form of the fundamental Gaussian beam is uniquely determined once the minimum spot size and its location are specified.

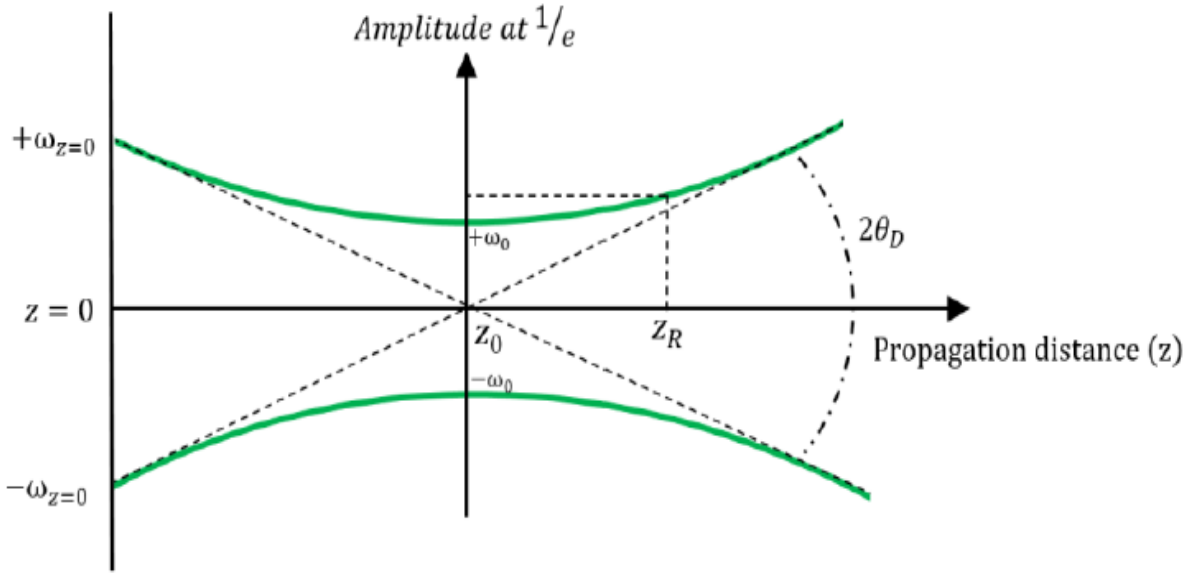

Figure 2-7: Propagation of a converging Gaussian beam (radius of curvature> 0 at the origin) in free space without turbulence.

2.5.2 Impact of Scintillation on propagation

The classical models used for describing the propagation of optical radiation are plane and spherical waves. The most important part of the scientific literature devoted to optical propagation in atmospheric turbulence has been focused on the scintillation phenomenon [71].

2.5.2.1 Beam wander and beam spreading

As we introduced previously, the optical beam suffers from atmospheric turbulences acting on the refractive index along the propagation path. These index variations have a significant impact on the detected irradiance. We focused on effects observed on a ground to satellite path (uplink) where most of atmospheric effects are located on first kilometers of propagation. In addition, the effects on the beam depends also on the turbulent size eddies and the optical beam properties such as the beam radius and beam divergence [72].

The main effects is the beam wander that it consists on the beam deviation from the original direction. It results from turbulent eddies that the size is larger than the beam radius. The optical beam is then refracted causing an important irradiance variations arriving to the satellite and the loss of ground to satellite communication link. This phenomena is most important for the long distance communication (ground-to-GEO) because the beam deviation

radius becomes important unlike to short distance. The Figure 2-8 illustrates the beam wander effect [71].

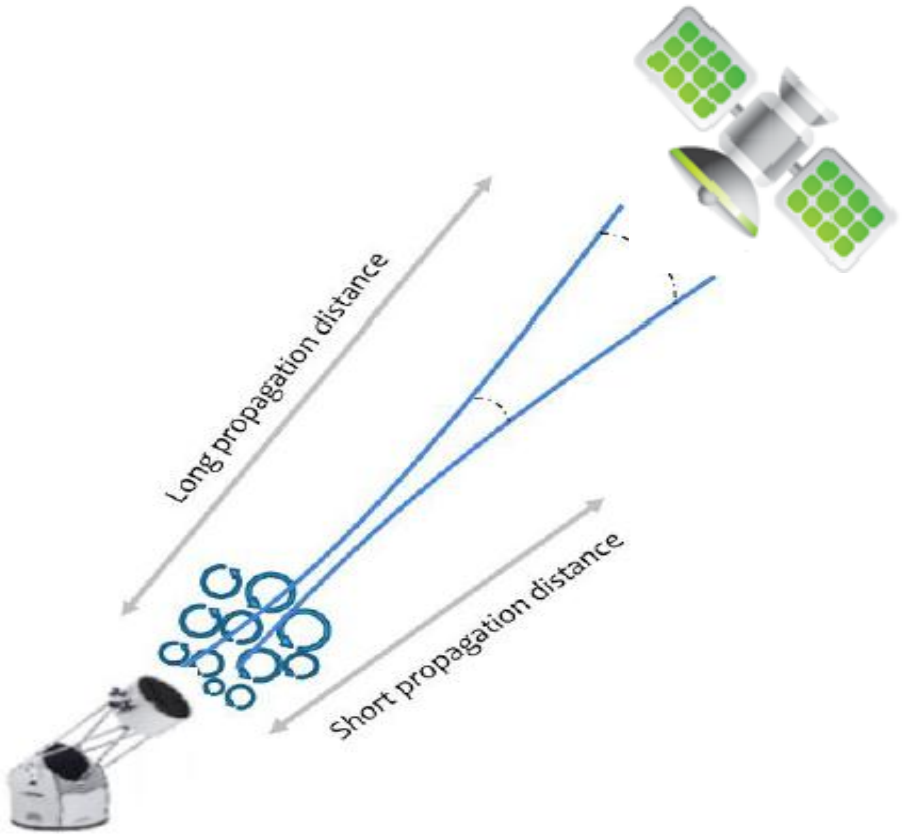

Figure 2-8: The beam wander effect

Another effect exists during these atmospheric propagation and it is called beam spreading that corresponds to an energy spreading. It consists on the widening of the beam size that is larger than atmospheric diffraction. In addition, the beam spreading appears when turbulent eddies are smaller than the beam size and it doesn't have any effect on the beam's direction. Fante [7] introduces three variables to describe irradiance fluctuations arriving to the satellite. The first one is the short-term beam radius noted rs corresponding to the radius of the beam spot observed with a very short exposure and caused by small eddies. The beam is then deflected by a distance of rc that is a measure of the beam displacement at satellite altitude due to the beam wander effects (large eddies). The last variable is a long-term beam radius rL corresponding to the beam radius with an exposure much large than time intervals between two deflections of the beam. The Figure 2-26 shows a comparison of these parameters in front the satellite. These three parameters can be linked by:

$$\langle \rho_L^2 \rangle = \langle \rho_s^2 \rangle + \langle \rho_c^2 \rangle \tag{2-29}$$

Analytical expressions have been given for the mean square of these variables. For ρ_L^2, it can be expressed by terms corresponding to the beam propagation through the vacuum and both of beam wander and beam spreading [71],[72].

$$\langle \rho_L^2 \rangle = \left(\frac{z\lambda}{\pi w_0}\right)^2 + w_0^2 + 8.8\left(\frac{z\lambda}{\pi \rho_0}\right)^2 \tag{2-30}$$

The beam wander is given by:

$$\langle \rho_c^2 \rangle = \frac{18.2z^2}{k_0^2 r_0^{\frac{5}{3}} w_0^{\frac{1}{3}}} \tag{2-31}$$

Finally, the short-term beam spread is given by subtracting $\langle rc2 \rangle$ from $\langle rL2 \rangle$.

$$\langle \rho_s^2 \rangle = \langle \rho_L^2 \rangle - \langle \rho_c^2 \rangle = \left(\frac{z\lambda}{\pi w_0}\right)^2 + w_0^2 + 8.8\left(\frac{z\lambda}{\pi \rho_0}\right)^2 - \frac{18.2z^2}{k_0^2 r_0^{\frac{5}{3}} w_0^{\frac{1}{3}}} \tag{2-32}$$

Depending on the size of waist at the emission, the atmospheric effects differ and three different regime can be shown in figure 2-9.

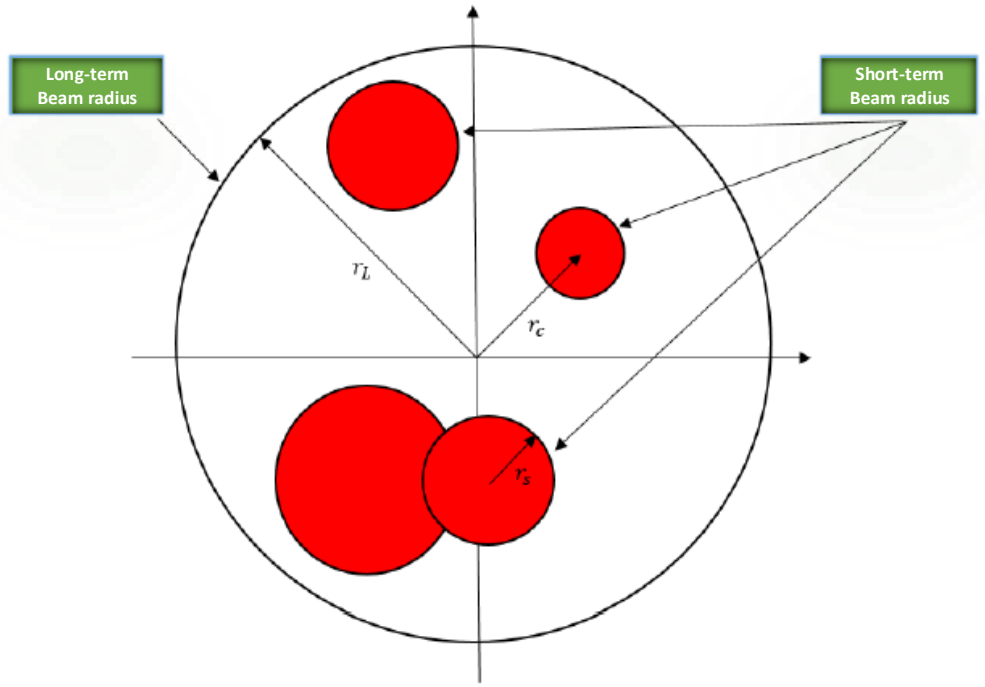

Figure 2-9: Illustration of the impact of atmospheric turbulence on laser propagation in the detection plane. Each footprint corresponds to an independent realization of turbulence.

The expressions for beam wander and beam spreading are obtained without approximating small disturbances. In addition, when the radius of curvature becomes small, we are then brought back to the case of the spherical wave.

2.5.2.2 Fluctuations of intensity and power in the bucket

1 Fluctuations of intensity

The effects we have presented are average effects of turbulence on the Gaussian beams. The scintillation will also modify the intensity collected after propagation. Due to the spatially limited Gaussian profile of the beams [73], we cannot assume spatial stationary. The average intensity changes radially as a function of the distance from the optical center. Similarly, the normalized variance of the log-amplitude will also change in the field. We note the variance of the log-amplitude:

$$\sigma_{\chi}^{2}(\rho) = \frac{Var[\chi(\rho)]}{\langle \chi(\rho) \rangle^{2}} \tag{2-33}$$

The variance $\sigma_{\chi}^{2}(\rho)$ generally grows with the distance ρ. This equation does not have a simple analytical solution, but can be evaluated by numerical simulation [74]. However, at low perturbations, Velluet [75] offer a simplified model for estimating these fluctuations. The fluctuations of χ can be explained by a combination of the effects of the beam wander and the small fluctuations (scintillation) of the log amplitude of the laser beam. When considering a Gaussian beam, χ is in the absence of disturbance $\chi_0 = -\rho^2/w$, where ρ is the distance to the axis and w the radius of the beam. The variance of χ induced by the displacement of the Gaussian beam (beam wander) can be written:

$$\sigma_{\chi,bw}^{2}(\rho) = 4\frac{\rho^{2}}{w}\langle \rho_{c}^{2} \rangle \tag{2-34}$$

An estimate of the variance in weak perturbations (equation 2.34), noted $\sigma_{\chi}^{2}(\rho)$, can be obtained by adding the term induced by the beam wander and the over-axis variance. The on-axis variance $\sigma_{\chi}^{2}(0)$ can be estimated by the Rytov variance for the case of a spherical wave.

$$\sigma_{\chi}^{2}(\rho) = \sigma_{\chi}^{2}(0) + \sigma_{\chi,bw}^{2}(\rho) \tag{2-35}$$

In strong disturbances, equation 2-35 is no longer valid. Indeed, the beam is strongly burst, increasing the fluctuations close to the axis.

2 Power-in-the-Bucket:

The first criterion for the performance of an optical link is the ratio of the quantity of flux received IR by the receiving telescope to the quantity of flux emitted IE by the transmitting telescope. This criterion is called in the Power-in-the-Bucket literature (PIB):

$$PIB(t) = \frac{I_R(t)}{I_E} = \frac{\int |\psi_R(\overrightarrow{r'},t)|^2 \mathcal{P}_R(\overrightarrow{r'}) d\overrightarrow{r'}}{\int |\psi_E(\vec{r})|^2 \mathcal{P}_E(\vec{r}) d\vec{r}} \quad (2\text{-}36)$$

Where P_E and P_R are the transmitting and receiving pupils respectively. In practice, I_E can be considered constant. I_R, and therefore PIB, are always a function of time (evolution of turbulence), or of the printing of phase screens considered in the context of a digital simulation (see 3.4)[38].

3 Bit-Error-Rate

In the telecommunications sector, the most widely used criterion for characterizing the quality of data transmission is called Bit-Error-Rate (BER). It represents the ratio of the number of errors (lost or erroneous bits) to the number of bits actually sent:

$$\langle BER \rangle = \frac{Number\ of\ errors}{Number\ of\ bits\ sent} \quad (2\text{-}37)$$

For links with a bandwidth of the order of GHz, the average BER tolerated is begin of the order 10^{-9}. In the case of modulation of the OOK signal, and of Gaussian detection noise, the average error rate is written [76]:

$$\langle BER \rangle = \frac{1}{2} \int_0^{\infty} erfc\left(\frac{I_R}{2\sqrt{2\sigma_D}}\right) P_{IR}(I_R) dI_R \quad (2\text{-}38)$$

Where P_{IR} is the probability density of I_R, and σ_D is the standard deviation of the detection noise. We define the average Signal to Noise Ratio (SNR):

$$\langle SNR \rangle = \frac{I_R}{\sigma_D} \quad (2\text{-}39)$$

2.6 Conclusion

In this chapter, we presented a little profile about the optical communication and different characteristics of optical links for satellite communications, we defined the atmospheric turbulence, and then we illustrate different mathematical descriptions of irradiance fluctuations

resulting from the atmospheric turbulence. We provided an analytical study for atmospheric propagation model based on Low Order Turbulence (LOT) is studied and described, by the Rytov approximation leads to simplify the model characterization of the optical field propagation and simplifying its properties and deformations. However, it is important to understand that this analytic characterization includes many approximations that can be more difficult to take into account in practice and in strong condition of atmospheric turbulence. That description will be used for simulation communication link and will be developed in the next chapter.

CHAPTER III:
Adaptive Optics for Laser Satellite-To-Ground Communications

3 Adaptive Optics for Laser Satellite-To-Ground Communication

3.1 Introduction

This chapter gives an overview of adaptive optics (AO) in the context of laser satellite-to ground link (SGL) communications. Adaptive optics was proposed by Babcock [47] in 1953 and independently by Linnik [73] in 1957, for improving astronomical images. Because of the prohibitive research and implementation costs, it was not possible at that time to build such a system. One of the first adaptive optics systems dates from 1977 [77]. It was not until 1989 for astronomical applications with the COMEON project [78]. Today, adaptive optics systems equip the majority of the world's major telescopes (VLT, Keck, Gemini, ...). Many other applications for adaptive optics are emerging, such as retina imaging or free space telecommunications. The first section introduces the typical components of an AO system and presents general concepts widely used in adaptive optics like Zernike polynomials and Strehl ratio. In the second section discusses the general requirements on an AO system based on the atmospheric characteristics presented in Chapter 3. The third introduces the concept of phase singularities, which also appear in the SGL scenarios at low elevation angles and which can severely disturb wavefront sensing and the correction of the wavefront. The forth section discusses multi kinds of simulations tools and how to improve the performance of various wavefront sensor types. And finally the conclusion of this chapter. A detailed discussion of the simulation tool, a specific algorithm and their application in SGL communications will be given in Chapter 4.

3.2 Adaptive Optics Systems

The adaptive optics (AO) system is a servo system which modifies in real time the emitted wave front in order to pre-compensate or post-compensate the wave front deformation due to atmospheric turbulence. In addition, due to the Earth’s rotation during the beam’s propagation, the point-ahead angle (PAA) between the downlink and the uplink has to be considered and make the turbulences effects slightly different for the two paths [79],[80],[81],[82].

The predominant development of AO has been for the use in astronomical applications at ground based observatories, therefore many of the components that are conventionally used in AO systems have a strong focus on low light levels [50],[38], incoherent light sources, only

moderate phase distortions and weak intensity fluctuations. The requirements for AO systems in the field of optical communications however differ from the requirements in astronomy. AO systems seem to be most suitable for the deployment on the ground (less on flight platforms), considering the complexity of these systems and taking into account, that most of the atmospheric phase distortions are generated close to the ground[83].

The basic principle of an AO system in a laser communication application is shown schematically in Figure 3-1 [78]. An incoming wavefront from a laser source that is corrugated after propagation through the atmosphere is collected at the receiver and reflected from a deformable mirror. The mirror is shaped to flatten the wavefront aberration using feedback from a wavefront sensor to give a corrected point-spread function at a detector, ideally close to that of a diffraction limited system. Usually such systems contain an additional element to correct angle-of-arrival errors, i.e. the Zernike modes 2 and 3, to relieve the deformable mirror, which is typically limited in its maximum stroke, from these modes. Here the element appears as a shiftable lens but is often a mirror on Piezo actuators.

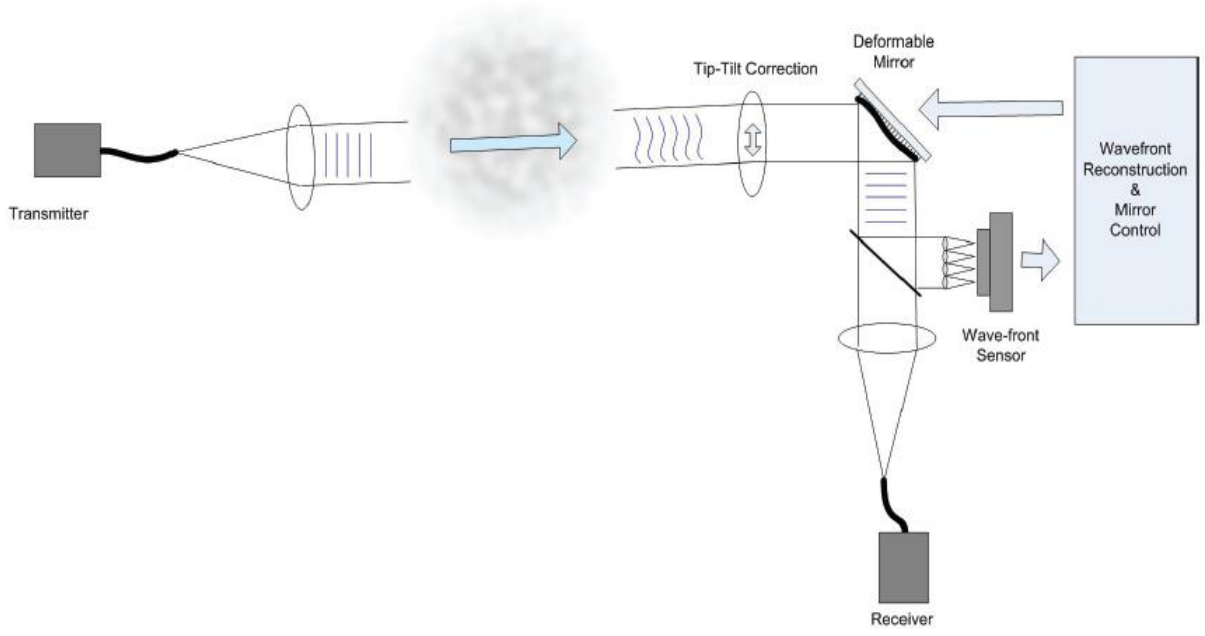

Figure 3-1: principle of an AO system in a laser communication application

The benefits of AO systems for the use in satellite-to ground communication scenario, this scenario is characterized by very strong scintillation and wavefront distortions, which increasingly become worse the lower the elevation angles are. Additionally, the fast transversal

movement of the communication beam through the atmosphere due to the satellite motion causes very fast fluctuations of the intensity and the phase [84].

As a result, these effects have to be taken into account for the AO system to ensure the right compensation for each case (uplink or downlink).

3.2.1 Principal components of adaptive optics

Adaptive Optics (AO) is a servo system whose objective is the real-time correction of wavefront distortions. The distortions are measured using a wavefront analyzer.The main components of an AO system are the correcting element to straighten the distorted wavefront, the wavefront sensor used to measure the residual wavefront error and the control computer, which is used to update the wavefront corrector with feedback from the wavefront sensor signal in real time.Two deformable mirrors with their actuator layout are depicted in Figure 3.2.

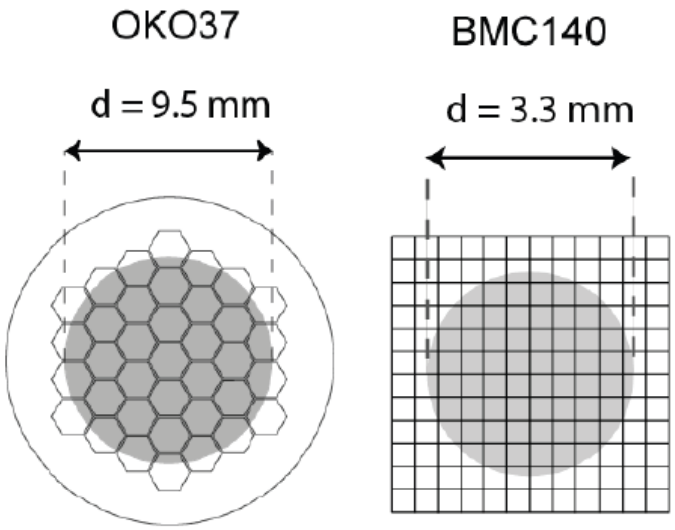

Figure 3-2: *Actuator layout of two deformable mirrors (left: BMC140 from Boston Micro machines, 140 actuators, segmented/continuous; right: OKO37 from Flexible Optical, 37actuators, continuous) with the typical optical pupil superimposed (from* [85]*).*

The wavefront corrector in most AO systems is typically a deformable mirror (DM), where a reflecting surface or membrane is moved by a number of actuators. A DM can be characterized by the surface type (continuous or segmented), the actuation type (piezoelectric, electrostatic, and magnetic), the stroke (i.e. the maximum surface deformation and the maximum inter-actuator stroke), the number and arrangement of the actuators and the response time of the mirror. A comparison of a selection of commercially available mirrors in terms of spatial correction can be found in [85],[86].The principal of AO is shown in Figure 3-3.

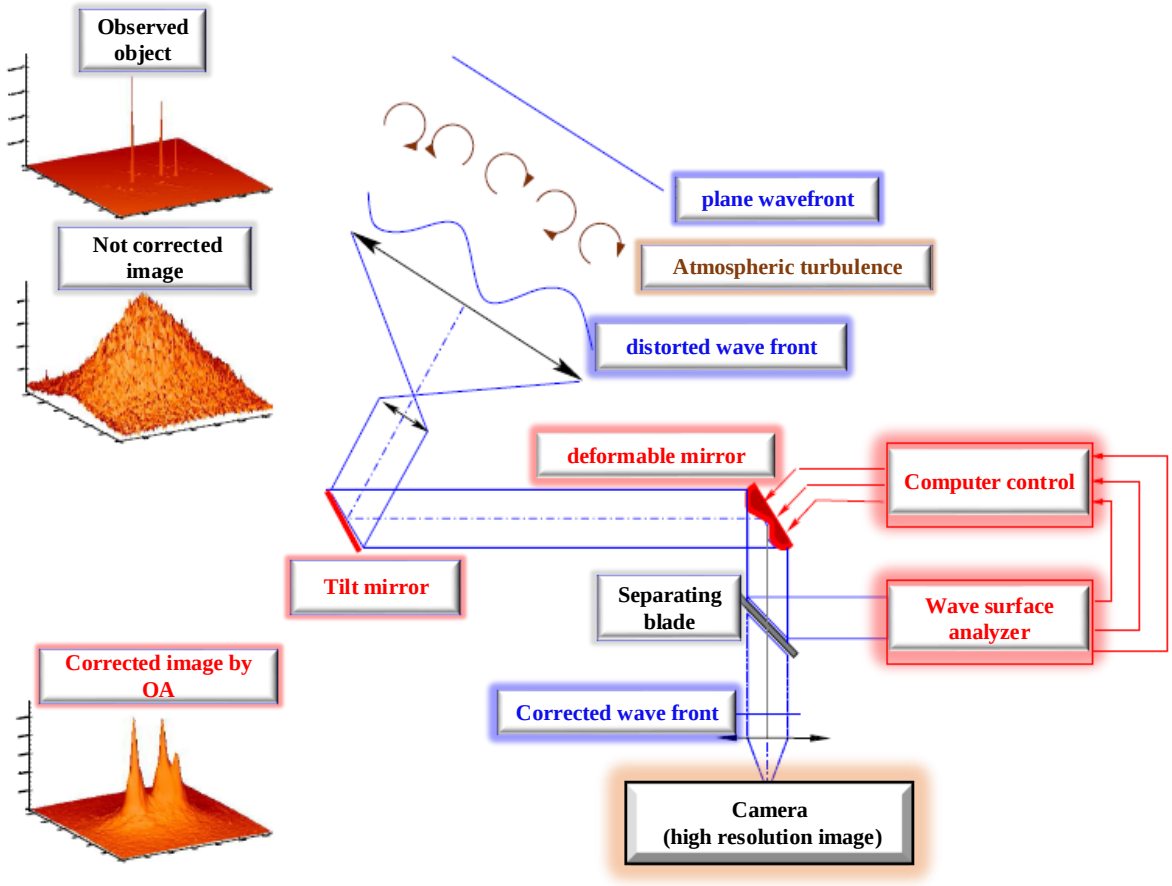

Figure 3-3: principle of an AO system in a laser communication application [38].

3.2.2 The wavefront analysis

There are some specific differences of LEO satellite-to-ground links, which distinguish the use of the wavefront sensor from that in astronomical applications. Atmospheric conditions are much more severe in SGL scenarios [87]:

- Very strong phase distortions due to the long path through the atmosphere at low elevation angles.
- Very strong intensity fluctuations due to the long path through the atmosphere at low elevation angles.
- Phase singularities, which impair the performance of wavefront sensors and might prohibit the use of continuous deformable mirrors.
- Challenging temporal requirements due to the fast motion of the beam through the atmosphere.
- Preferably deployment of the ground stations at non-astronomical sites at low altitudes and therefore at worse atmospheric turbulence conditions.

- Comparatively high received power levels, as the communication system at several Gbps requires a sufficient link budget.
- The communication laser is always a point source.
- Relatively small telescope apertures (<=1m) for near Earth scenarios will be used for communication, compared to several meters in Astronomy.
- The AO correction will be for a very small field-of-view, as a point source is observed. In the consequence no multi-conjugate system will be required even for strong turbulence.

It is not currently possible to measure the phase of the wavefront directly at optical wavelengths as is the case in the radio domain. This is because there is no optical detector capable of responding to temporal frequencies. Classically, one is free from of this problem by carrying out indirect measures, i.e. by analysing the impact of phase disturbances on the intensity distribution. Rousset [88], gave a very complete description of adaptive optics analyzers. We recall here only the properties of the Shack-Harmann analyzer. Indeed, it is on the one hand the most widely used analyzer for adaptive optics, and on the other hand, its limitations are representative of those of the of most pupil plane scanners.

3.2.2.1 Shack-Hartmann analyzer

The Shack-Hartmann analyzer (SH) type wave surface analyzer (WSA) is a pupil plane analyzer (figure 3-4), considered the most commonly used (WSA) in adaptive optics [89]. It is also the one used to carry out the work presented in this thesis.

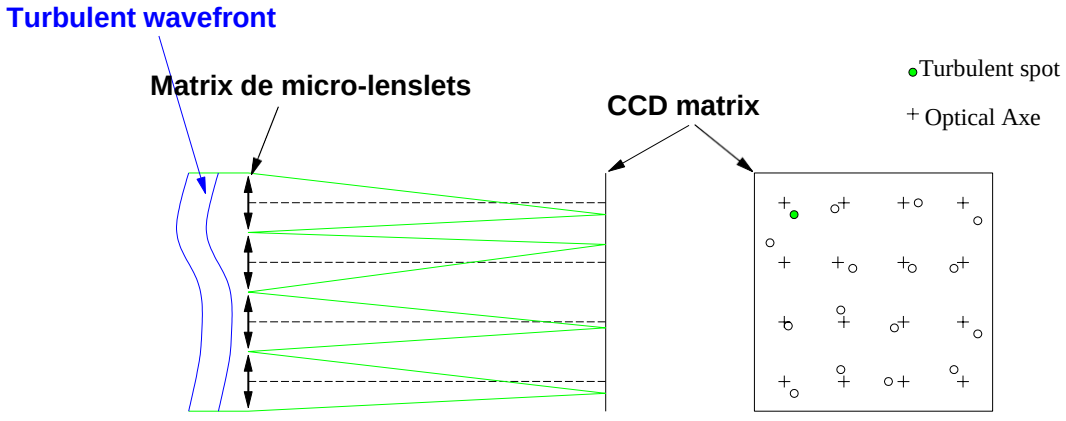

Figure 3-4: The Shack-Hartmann analyzer wave surface analyzer

a) Measurement

A micro-lens array samples the incident wavefront in the pupil plane. A measurement of the position of the image spot formed at the focus of each of the microlenses gives access to the local slope of the wavefront in the pupil plane of each microlens. The position measurement is most often performed by the center of gravity (COG), but other position estimators can also be used, such as correlation [89]. The slope measured by the COG in each sub-pupil k is for the x and y direction respectively:

$$P_x^k = \frac{\iint dr \frac{\delta \varphi_k(r)}{\delta x} |\psi_k(r)|^2}{\iint dr |\psi_k(r)|^2} \tag{3-1}$$

$$P_y^k = \frac{\iint dr \frac{\delta \varphi_k(r)}{\delta y} |\psi_k(r)|^2}{\iint dr |\psi_k(r)|^2} \tag{3-2}$$

Where the double integration is carried out on the surface of the sub-pupil k considered, φ_k the phase and $|\psi_k|$ the amplitude of the complex field. When the intensity is constant in each sub-pupil, the slope measurement is then an average on the surface of the sub-pupil. In the following, it is preferable to express the mean slope in radians of phase difference at the edge of the sub-pupil, such as:

$$\Delta\varphi_x = \frac{2\pi d}{\lambda f \mu_l} \times c_x \tag{3-3}$$

$$\Delta\varphi_y = \frac{2\pi d}{\lambda f \mu_l} \times c_y \tag{3-4}$$

Where d is the size of the sub-pupil.

The information collected on each of the sub-pupils is used to trace the shape of the wavefront. The position of the image can be measured in different ways. A center of gravity (COG) measurement is often performed, after having possibly threshold and/or windowed the image task. More complex algorithms exist, such as the weighted COG [90], using a weighting function for each pixel. There are also correlation methods [91], which correlate the image with a reference image and which are implemented within the framework of extended object wave surface analysis [92].

The SH can also provide a measure of the flux in the sub-pupil, by summing the Pixel intensities in the thumbnails formed on the detector. Thus, by measuring the intensity $i_{u,v}$ in the

sub-pupil identified by its coordinates (u, v) in the HS, and estimating its value average over time $\langle i_{u,v} \rangle$, it is possible to define a scintillation index $\delta i_{u,v}$ such as :

$$\delta i_{u,v} = \frac{i_{u,v} - \langle i_{u,v} \rangle}{\langle i_{u,v} \rangle} \tag{3-5}$$

b) Propagation of detection noise

Detection noises (photon and detector noise), present in the Shack-Hartmann thumbnails, propagate over the measurements provided by the HS. For slope measurements with a COG algorithm, the noise variances are given by [88] :

$$\sigma^2_{photon} = \frac{\pi^2}{2} \frac{1}{N_{ph}} \left(\frac{N_T}{N_D} \right)^2 \tag{3-6}$$

$$\sigma^2_{detector} = \frac{\pi^2}{3} \frac{1}{N_{ph}} \left(\frac{\sigma_{e^-}}{N_{ph}} \right)^2 \left(\frac{n^2_{pix}}{N_D} \right)^2 \tag{3-7}$$

Where N_T is the Full Width at Half Maximum (FWHM) of the source image, N_D is the FWHM at the diffraction limit, σ_{e^-} is the variance of the detector noise and n^2_{pix} is the number of pixels on the side of a square window, defining the COG computing area. N_{ph} is the number of photons contained in the window. In equation (3-6), σ^2_{photon} does not depend on the size of the GDC computation window, as the formula assumes a Gaussian-shaped task. For a task of cardinal sine shape, we can show that when $n_{pix} \geq 2N_D$ [93]:

$$\sigma^2_{photon} \simeq \frac{2}{N_{ph}} \left(\frac{n_{pix}}{N_D} \right) \tag{3-8}$$

The intensity in the sub-pupil is the sum of the intensities on each pixel:

$$i = \sum_{pixels} i_{pixel} \tag{3-9}$$

The noise variance is the sum of the variances of σ^2_{photon} photon noise and detector noise.

The photon noise is fishy in nature, therefore $\sigma^2_{photon} = \langle i \rangle$. So we have:

$$\sigma_i^2 = \langle i \rangle + \sum_{pixels} \sigma^2_{e^-} = \langle i \rangle + n^2_{pix} \sigma^2_{e^-} \tag{3-10}$$

The noise on the scintillation is then:

$$\sigma^2_{\delta i_{noise}} = \frac{\sigma_i^2}{\langle i \rangle^2} = \frac{1}{\langle i \rangle} + n^2_{pix} \frac{\sigma^2_{e^-}}{\langle i \rangle^2} \tag{3-11}$$

Where the term:

$$\sigma^2_{\delta i_{phot}} = \frac{1}{N_{ph}} \tag{3-12}$$

Represents the contribution of photon noise, and the term:

$$\sigma^2_{\delta i_{det}} = n^2_{pix} \frac{\sigma^2_{e^-}}{N^2_{pn}} \tag{3-13}$$

Represents the contribution of detector noise, noting $\langle i \rangle = N_{ph}$.

3.2.3 Modal analysis of the turbulent phase

3.2.3.1 The Zernike polynomials

Zernike polynomials are used to represent a wavefront over a circular aperture. These polynomials are expressed according to their radial orders n and their azimuthal frequencies m:

$$Z^{n,m}(r) = R^m_n(r)\Theta^m_n(\theta) \tag{3-14}$$

With

$$R^m_n(r) = \sum_{k=0}^{\frac{n-m}{2}} \frac{(-1)^k (n-k)!}{k!\left(\frac{n+m}{2}-k\right)!\left(\frac{n-m}{2}-k\right)!} r^{n-2k}, n \geq |m| \tag{3-15}$$

And

$$\Theta^m_n(\theta) = \begin{cases} \sqrt{n+1} & if\ m = 0 \\ \sqrt{2(n+1)cos(m\theta)} & if\ m \neq 0\ and\ i\ even \\ \sqrt{2(n+1)sin(m\theta)} & if\ m \neq 0\ and\ i\ odd \end{cases} \tag{3-16}$$

They are arranged according to the index i = n + m.

Originally the polynomials were used to describe aberrations of optical systems. Therefore the lower order polynomials give aberrations like tilt (i=2,3), defocus (i=4), astigmatism (i=5,6), and coma (i=7,8). Piston (i=1) is usually neglected for AO systems, as it does not influence the wavefront correction. The expressions of $R^m_n(r)$ and $\Theta^m_n(\theta)$ are given by Noll, Figure 3-5 shows the first 21 Zernike polynomials, the following formulas and the numbering for the polynomials are based on Noll's work [94].

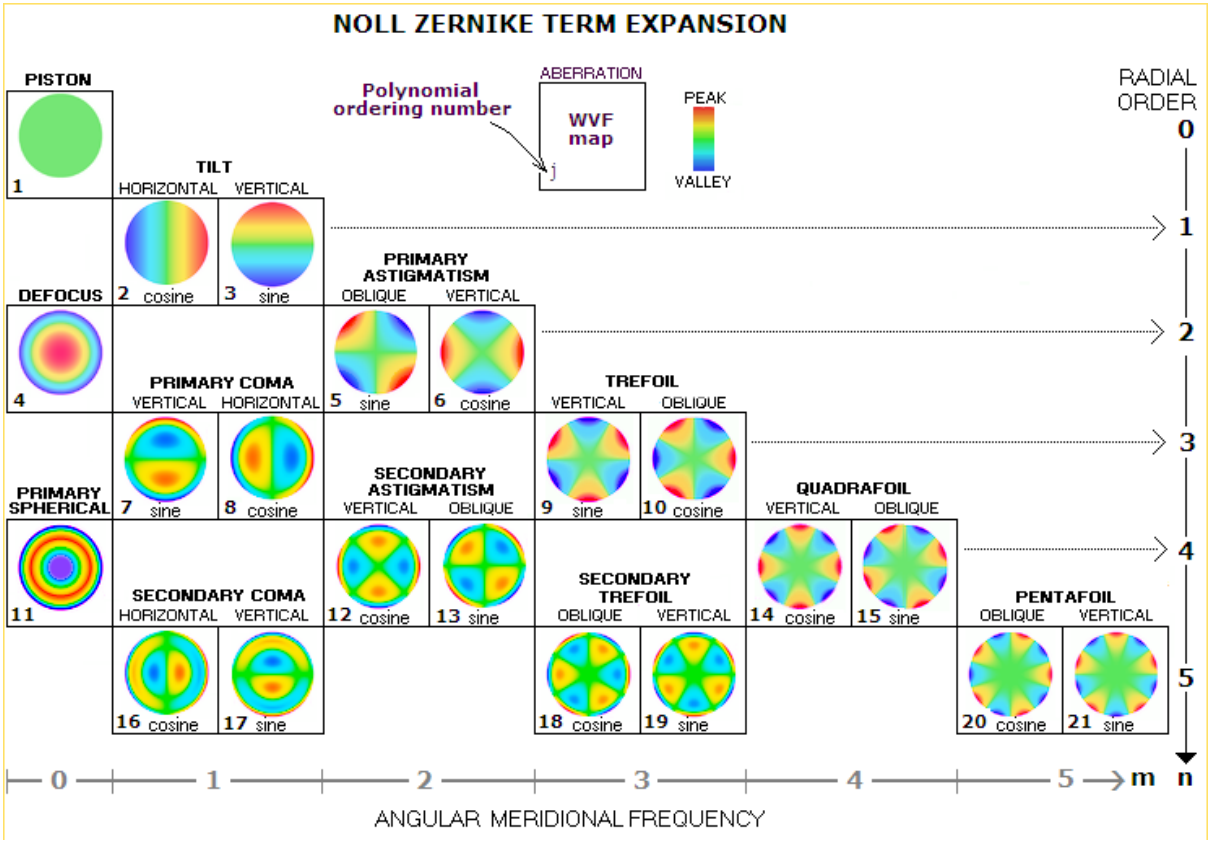

Figure 3-5: The first 21 Zernike polynomials ordered by increasing vertically by radial degree and horizontally by azimuthal degree [95].

3.2.3.2 Statistical properties of the phase and Zernike polynomials

To model the perturbed wavefront, the Zernike polynomials is complete and the perturbed phase can be decomposed using the Zernike polynomials:

$$\varphi(r) = \sum_{i=1}^{\infty} a_i Z_i(r) \tag{3-17}$$

Where a_i are coefficients corresponding to the orthonormal basis formed by $Z_i(r, \theta)$ and given by:

$$a_i = \frac{1}{\Sigma}\int_0^{\Sigma} \varphi(r')Z_i(r')dr' \tag{3-18}$$

Where Σ is the surface unit. These coefficients describe a total statistical characterization of the turbulent phase thanks to Zernike polynomials. Therefore, Noll's [94] provides the results

of the variances for the coefficients of each Zernike polynomials that is equal to the sum of the variances of every polynomial coefficient:

$$\sigma_{\varphi}^{2} = \frac{1}{\Sigma}\int_{0}^{\Sigma}\langle\varphi(r')\rangle dr' = \sum_{i=1}^{\infty}\langle a_i^2\rangle \tag{3-19}$$

Finally, an expression for the variance of the turbulent phase, over a circular pupil diameter D, without the variance of the piston term (the coefficient ak is associated only to the kth) is given by:

$$\sum_{i=1}^{\infty}\langle a_i^2\rangle \cong 1.03\left(\frac{D}{r_0}\right)^{\frac{5}{3}} \tag{3-20}$$

An empirical law gives the residual variance after perfect correction of the first j Zernike polynomials [94]:

$$\sigma_{\varphi,j}^{2} = 0.2944 j^{\frac{-\sqrt{3}}{2}}\left(\frac{D}{r_0}\right)^{\frac{5}{3}} \tag{3-21}$$

3.3 Optimization of adaptive optics system with a free wavefront sensor

The FWFS is technically more simple and do not rely on the use of complex WFS. Instead, they are based on the direct optimization of a system performance metric, like power in the bucket, coupled power, image sharpening, among others. Sensor-less systems perform the wave-front optimization with several iterations that require continuous sensing of the metric as feedback, it can be classified into stochastic, and sequential imagebased methods [96]. The stochastic approach is generally based on blind algorithms that start the optimization with a random set of variables, applying an iterative approximation of the best solution. An appropriate optimization control algorithm is the key to correcting distorted wavefronts successfully. The control algorithm must meet the following requirements: rapid convergence so that the AO system can keep up with changes of distorted wavefronts, high correction capability for wavefront aberrations, and be easy to implement. Some stochastic parallel algorithms, such as Stochastic Parallel Gradient Descent (SPGD) [9],[97], Genetic Algorithm (GA) [10], Simulated Annealing (SA) [8] and Algorithm Of Pattern Extraction (Alopex) [8] are often used as the control algorithms of AO system.

3.3.1 Sensor-less stochastic technique

The objective of a sensor-less iterative compensation system in FSOC, is to enhance the BER by increasing the mean coupled signal and reducing its variance. A sensor-less AO system has most of the required characteristics for free space optic communication (FSOC). Regarding turbulence compensation, it shows robustness facing phase singularities [87], [98], high power efficiency, and good tolerance to scintillation [87].

The stochastic approach therefore seems appropriate for propagation through turbulence when using as an objective function the optimization of the integrated intensity on the pupil. In addition, the proposed descent algorithm is parallel, i.e. each element of the vector subspace is optimized simultaneously. This increases the speed of convergence by the same amount compared to the previously studied cases where the optimization was sequential. Regarding technical aspects, these systems have a straight forward implementation and they are very simple to calibrate, making accessible the integration on existing systems. Its mechanical simplicity also implies robustness when it comes to portable optical ground stations. A significant plus comes with the cost reduction in the AO system, due to the absence of WFS.

3.3.2 Different stochastic parallel optimization algorithms

The first Adaptive optics metrics optimization methods were implemented in the Adaptive optics systems in the 1970s. Despite the simplicity of implementation (it does away with the complex optical element of the wave surface analyzer), practical implementation remains difficult. To correct the phase disturbances of atmospheric turbulence, phase disturbances of atmospheric turbulence can be corrected by using fast optimization techniques, e.g. GA type.in this these, we applied genetic algorithm has been successfully implemented on free space communications systems.

In this paragraph, we will briefly discuss the various types of several algorithms that correct the wavefront, and we will deal extensively with the algorithm used as a solution in this thesis.

3.3.2.1 The stochastic parallel gradient descent (SPGD) algorithm

The stochastic parallel gradient descent (SPGD) algorithm is a One of the most tested blind algorithms with potential uses in FSOC wavefront aberration correction algorithm

[9],[97], which can directly optimize the performance metric of the system and can be applied to the channel of medium or strong turbulence. But due to slow convergence the algorithm can not fully meet the wavefront correction real-time requirements of satellite-to-ground laser communication links. The control voltage gradient by using the variation of performance metric of the system ΔJ and the variation of the control voltages δu_i, searches and iterates in the gradient direction, in order to make the performance metric optimal. The perturbation producer generates random perturbation voltage vectors $\delta u^k = (\delta u_1^k, \delta u_2^k, \dots, \delta u_i^k,)$, independents and obeys the Bernoulli distribution, then calculate u^k by the formula $u^k = u^k + \gamma . \delta u^k . [J_+^k - J_-^k]$. Iterate like this until the performance metric meet the requirements.

3.3.2.2 Simulated Annealing (SA)

SA is based on the physical annealing process by which a solid is heated to a temperature close to its melting point, it can be used to approximate the global minimum for a function with many variables. Which it is allowed to cool slowly so as to relieve internal stresses and non-uniformities [99]. SA consists of three functional relationships per iteration: probability density of state-space of n actuators control para-meters to create perturbation vector$\Delta u^{(k)} = \{\Delta u_i\}^{(k)}$, acceptance probability $p^{(k)} = exp(\Delta J^{(k)}/T^{(k)})$ to adjudge whether the new solution is accepted, which is also called as the Metropolis criterion [100], and schedule of ‘‘annealing’’ in annealing-time steps $T^{(k)}$. We assumed that probability density of state-space has Gaussian distribution and $T^{(k)} = \lambda * T^{(k-1)}$, where l is the cooling rate. The control signals are updated with the rule $u^{(k+1)} = u^{(k)} + \delta \Delta u^{(k)}$ where δ is the adjustment coefficient, also called the step size.

3.3.2.3 Algorithm Of Pattern Extraction (Alopex)

Alopex is a stochastic correlative learning algorithm, has an inherent susceptibility to getting "stuck" in local minima or maxima of the response function. ALOPEX uses a cross-correlation of differences and a stochastic process to overcome this in an attempt to reach the absolute minimum (or maximum) of the response function. Which updates the control parameters by making use of correlation between the variations in control parameters and the variations in performance metric. Applied the Alopex in AO which will be control signals are in the following: $u^{(k+1)} = u^{(k)} + \eta \Delta u^{(k)}$, where $\Delta u^{(k)}$ has two probability 1 and -1 [8].

3.3.2.4 Genetic Algorithm (GA)

Genetic algorithms use Darwin's theory of the evolution of species. It is based on three principles: the principle of variation, the principle of adaptation and the principle of heredity [101],[102].

- **Variation:** Each individual within a population is unique. These differences, more or less important, will be decisive in the selection process.
- **Adaptation:** The individuals most suited to their environment more easily reach adulthood. Those with better survivability will therefore be able to reproduce more.
- **Heredity:** The characteristics of individuals must be hereditary in order to be able to be transmitted to their descendants. This mechanism will allow the species to evolve to share the characteristics advantageous to its survival.

a) The Principle

This paradigm, associated with the terminology of genetics, allows us to exploit genetic algorithms: We find the notions of Population, Individual, Chromosome and Gene [102].

The population is the whole of the possible solutions.

The individual represents a solution.

The Chromosome is part of the solution.

The Gene is a characteristic, a peculiarity.

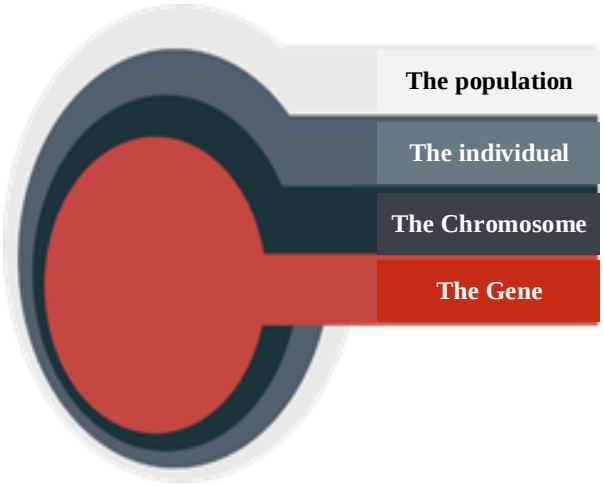

Figure 3-6: The notions of genetic algorithm

b) Evolution operators

- **Selection**: Selection of the most suitable individuals.
- **Crossbreeding**: Mixing by reproduction of the characteristics of the selected individuals.
- **Mutation**: Random alteration of an individual's characteristics.
- **Crossbreeding**: This is the result obtained when two chromosomes share their characteristics.

It allows the genetic mixing of the population and the application of the heredity principle of Darwin's theory [102].

There are two methods of crossing: single or double crossing [101].

- The single spanning consists in merging the particularities of two individuals from a pivot, in order to obtain one or two children:

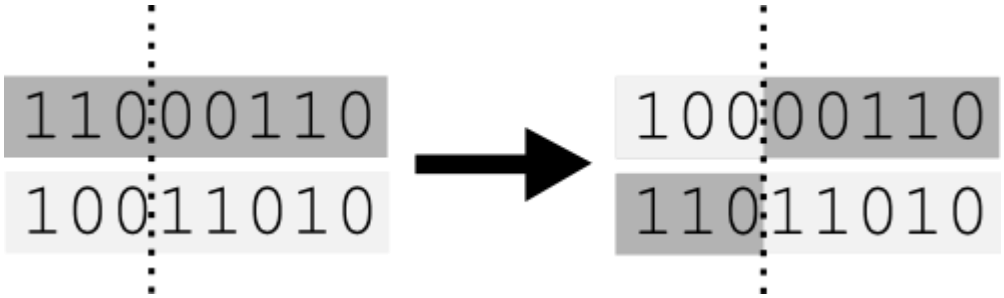

- Double spanning is based on the same principle, except that there are two pivots:

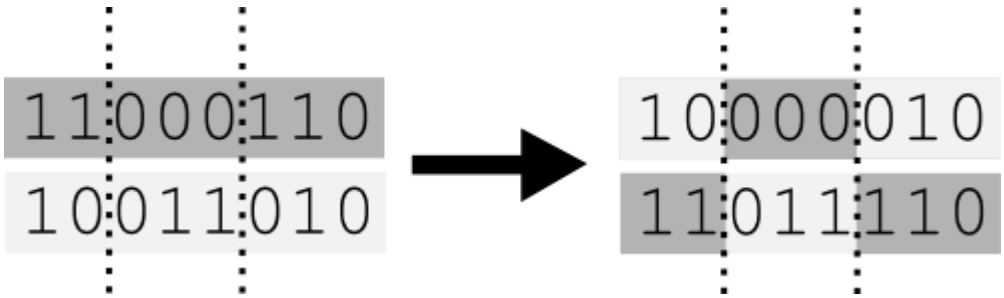

A mutation is then carried out on the children obtained during the crossing.

- **Mutation:** The mutation consists in altering a gene in a chromosome according to a mutation factor. This factor is the probability that a mutation will be made on an individual. This operator is the application of the principle of variation of Darwin's theory and allows, by the same occasion, to avoid a premature convergence of the algorithm towards a local extremes.

Here is an example of a mutation on an individual with only one chromosome:

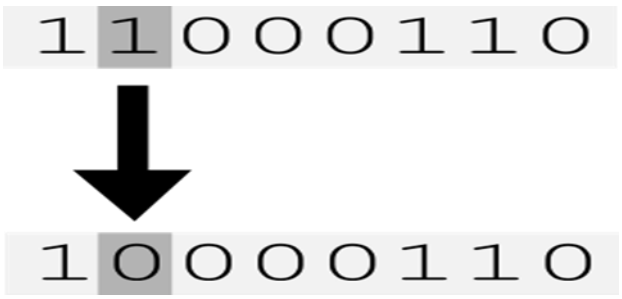

With these three evolutionary operators, we can apply genetic algorithms.

c) Algorithm

The basic principles being explained, here is how genetic algorithms work [101],[103]:

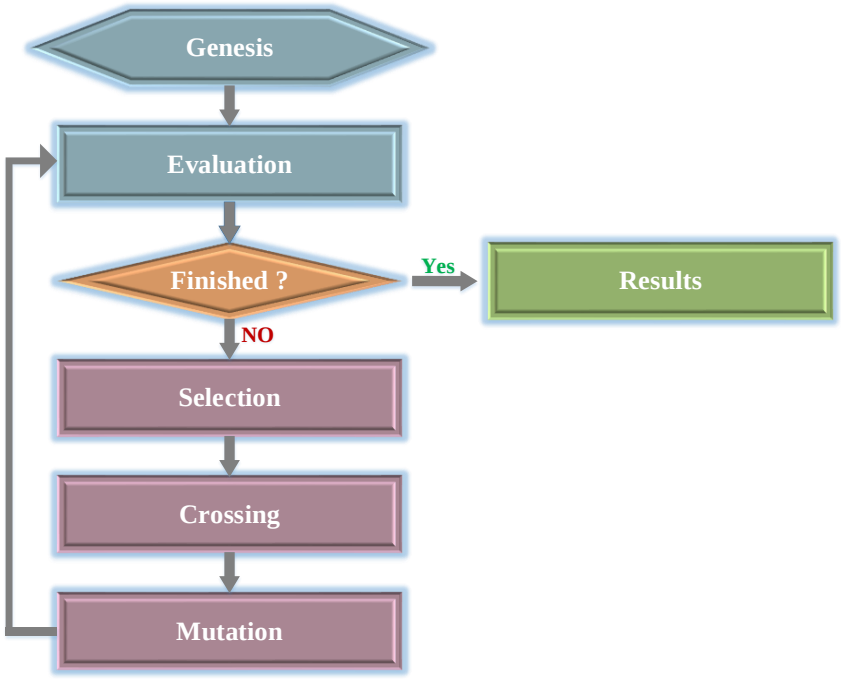

Figure 3-7: Principal of genetic algorithm work

Some explanations:

- Genesis is the stage of creating a random population. It is the starting point of our algorithm.
- Evaluation is the analysis of individuals to analyze if a solution is available. For this, we use a cost function, or error function, to define the adaptation score of the individuals during the selection process.
- We perform a loop as long as the evaluation considers that the solution is not optimal.

The proposed Genetic Algorithm and Modeling the problem and will be explained in the chapter 4.

3.4 Simulation tools for OA

There are many simulation tools implemented in Matlab, such as **OKOTECH, SCILAB, PILAB, and OOMAO**. We will review with detail in this thesis only the simulation tool **OOMAO** which used in this study [8],[10],[104].

3.4.1 OKOTECH

Flexible Optical B.V. (OKO Tech) is a small Dutch company operating in the field of application-oriented research and development of laser and high resolution optical imaging adaptation. Since its foundation in 1997, OKO has offered high quality deformable mirrors with an extremely smooth surface with HR metal and dielectric coatings suitable for the most demanding applications in imaging and laser [105].

OKO presents DLLs to facilitate the realistic simulation of optical systems including deformable mirrors produced by OKO. There are two separate libraries for two classes of mirrors: one for micromachined deformable mirrors (MMDM) and the other for piezoactive deformable mirrors (PDM).

3.4.2 SCILAB

There is a large number of software that can perform adaptive optics simulation. Most of them, such as WaveTrain and CAOS, are commercial or proprietary products, and their internal mechanism is not known to other researchers (Although CAOS is open source software, but it is implemented in the IDL, who is the owner). Some other simulation software (LightPipes, Arroyo, etc.) are open source, while these codes are almost all written in FORTRAN, or C /C++, and they do not have good interfaces for other users [106].

SciAO is an open source, multiplatform and user-friendly toolbox based on the Scilab / Scicos environment for modeling and simulation of wave optics [107], in particular the adaptive optics system. Although this toolkit is primarily designed to meet the requirements of AO simulations, we also consider moderately the needs of some other optical simulation systems (for example, simulation of Wave optics and imaging devices) and design modules software for them, which also makes it possible to simulate other optical problems beyond the AO field.

3.4.3 Object Oriented Matlab for Adaptive Optics (OOMAO):

OOMAO is a Matlab toolbox for the modeling and simulations of Adaptive Optics systems through using an object (oriented approach where there is a class for each AO component).Then Benefit of that to linking these components to each other to form the system optical path [108].

OOMAO is based on a small set of classes representing the source, atmosphere, telescope, wavefront sensor, Deformable Mirror (DM) and an imager of an AO system [109].

The aim of these systems is to increase the corrected field of view with respect to conventional adaptive optics .where the OOMAO optimizes the use of the computer resources by relying of special matrices like Sparse and Toeplitz matrices. The OOMAO consists of the main classes used during a simulation as shown in Fig [110]:

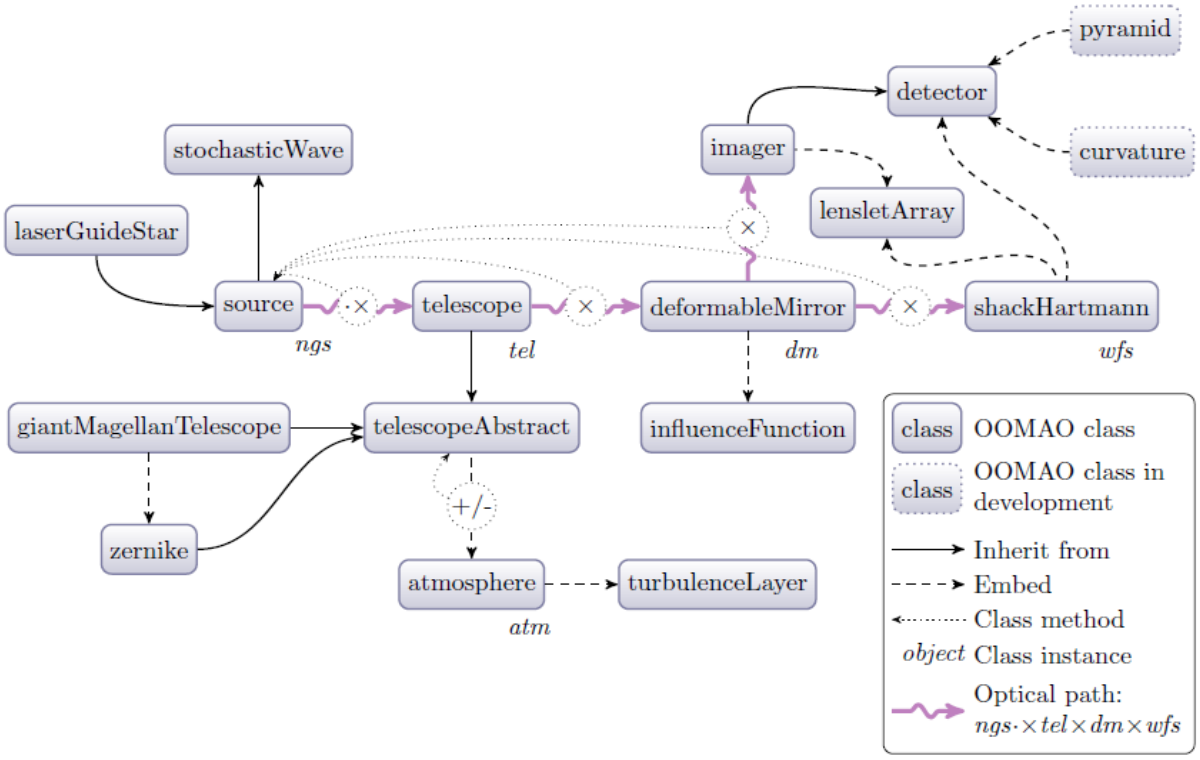

Figure 3-8: The main classes of OOMAO during a simulation

After that, we introduce the main steps in the construction and deployment of an AO system are as shown below:

3.4.3.1 The source

The source is an important metric in the OOMAO [108]. The importance of this metric lies in the fact that it plays a role in connecting between other classes. A source object carries a wavefront, both amplitude and phase, through different objects representing the atmosphere, the telescope, the wavefront sensor, …ect, both natural guide star and Laser guide star Adaptive Optics can be simulated. For a NGS, the source height is infinite. For a LGS, the source height is finite and can be set to a vector of heights depending on the thickness of the source. A simple

on {axis natural guide star object is created by calling the source constructor without parameters:

$$ngs = source;$$

For created an object from an OOMAO class in the first time The user is allowed to use the library of the OOMAO as well a summary of the object main parameters is also displayed. In this example, zenith and azimuth angle are both set to zero, the star height is infinite, the wavelength is 550nm and the magnitude is set to zero. Where a source object can be defined As follows [109],[110]:

```
>> src = source('zenith',30*constants.arcsec2radian,...
'wavelength',photometry.H,...
'magnitude',12);
@(source)> Created!
___ SOURCE ___
 Obj        zen[arcsec] azim[deg] height[m] lambda[micron] magnitude
 1          30.00       0.00      Inf       1.654          12.00
```

3.4.3.2 The Atmosphere

The atmosphere considered an important measure for OOMAO tools, after defined the source we will need to create the atmosphere, which the wave propagating in. we defined the all parameters including the turbulence profile by creating a single ground layer atmosphere with a, 15cm Fried parameter in the visible regime is created with [108],[111]:

```
<<atm = atmosphere(photometry.V,15e-2);
@(atmosphere)> Created!
___ATMOSPHERE___
Kolmogorov-Tatarski atmospheric turbulence:
 . Wavelength = 0.55micron,
. r0 = 15.00cm,
. Seeing = 0.74arcsec,

 Layer      Altitude[m]   fr0   wind([m/s] [deg])   D[m]      res[px]
      1     0.00          1.00  ( )
```

An outer scale of turbulence can be added to the constructor call:

```
<< atm = atmosphere(photometry.V,15e-2,30);
@ (atmosphere)> Created!
___ATMOSPHERE___
Von Karman atmospheric turbulence
.Wavelength = 0.55micron,
. r0 = 15.00cm,
. L0 = 30.00m,
. seeing = 0.74arcsec,

Layer          Altitude[m]    fr0   wind([m/s] [deg])    D[m]      res[px]
    1          0.00           1.00  ( )
```

@ (atmosphere)> Terminated!

3.4.3.3 The Telescope

The importance of the telescope comes from the need of the atmosphere to be coupled with a telescope object. The telescope aim can be identified in two roles, first, define the telescope parameters .Second, define the phase screens in the turbulence layers set by an atmosphere object. For this, we create a telescope of diameter D (8cm) with [108]:

```
<< tel = telescope;(8)
@ (telescope)> Created!
___TELESCOPE___
8.00cm diameter full aperture with 50.27m^2 of light collecting area;
```

A 14% central obscuration can be added with:

```
<<tel = telescope(8,'obstructionRatio',0.14);
@ (telescope)> Created!
___TELESCOPE___
8.00cm diameter with a 14.00% central obstruction with 49.28m^2 of
light collecting area;
---------------------------------------------------
@ (telescope) > Terminated!
```

This 8m diameter telescope has a two-arc minute field ─of ─view. The telescope pupil is sampled with 64 × 64 pixels and the motion of the phase screen in the telescope pupil is sampled at 500Hz. A 3 layers atmosphere is created.

```
<< atm = atmosphere(photometry.V,15e-2,30...,
'altitude',[0, 5,12]*1e3...,
'fractionnalR0...,[0.5,0.3,0.2],'
'windSpeed...,[10,5,15],'
'windDirection',[0,pi/3,pi];(
@ (atmosphere)> Created!
 ___ATMOSPHERE___
Von Karman atmospheric turbulence
 . Wavelength = 0.55micron,
 . r0 = 15.00cm,
 . L0 = 30.00m,
 . Seeing = 0.74arcsec,
 . theta0 (37%) = 3.22arcsec,
 . tau0 (37%) = 8.33millisec
-----------------------------------------------------
Layer Altitude[m]     fr0     wind ([m/s] [deg])     D[m]       res [px]
1          0.00       0.50      (0.00 10.00)
2       5000.00    0.30      (5.00 60.00)
3      12000.00   0.20      (15.00 180.00)

-----------------------------------------------------
@ (atmosphere)> Terminated!
```

And combined with the telescope object:

$$tel = tel + atm\,;$$

The phase screens size ***D*** at height ***h*** size for a field of view ***α*** is given by

$$d(h) = D(0) + 2h\tan(\alpha = 2) + atm\,; \qquad (3\text{-}22)$$

For display, the phase screens the Matlab R function imagesc can be called with the telescope object as argument as in the Figure 3-9 [109],[111]:

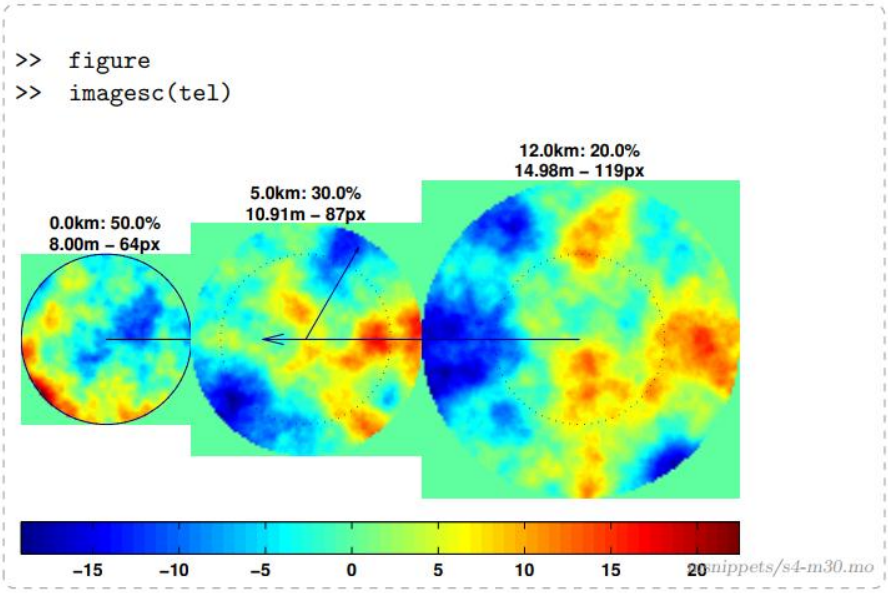

Figure 3-9: The telescope object of OOMAO in matlab

3.4.3.4 The Deformable Mirror

A numerical deformable mirror is made of a set of influence functions or modes. In OOMAO, a mode shape is derived from two cubic B´ezier curves As follows:

$$B1(t) = (1 - t_3)P_0 + (1 - t)2tp_1 + 3(1 - t)t_2P_2 + t_3P_3 \; ; t_2[0;1] \quad (3\text{-}23)$$

$$B2(t) = (1 - t_3)P_3 + (1 - t)2tp_4 + 3(1 - t)t_2P_5 + t_3P_6 \; ; t_2[0;1] \quad (3\text{-}24)$$

Where: $P_k = (x_k, zk)$ are point in the x − z plane. As t varies from 0 to 1, B1(t) will go from P_0 to P_3 and B2(t) will go from P_3 to P_6. P_0 will correspond to the highest point of the mode and is set to the coordinates ($x_0 = 0$, $z_0 = 1$). The derivative of the mode at P_0 must be zero, this is ensure by setting $z_1 = 0$. The mode is forced to zero at P6 by setting $z_6 = 0$. x_6 is set to 2. The derivative of the mode in P_6 is forced to zero by setting $z_5 = 0$. To ensure a smooth junction between both B´ezier curves, the following condition is imposed $P_3P_2 = -\alpha P_3P_4$ leading to $P_4 = -P_2/\alpha + (1 + 1/\alpha)\, P_3$ [110].

From the conditions stated above, a deformable mirror mode is set with the following parameters: x1, (x2, z2), (x3,z3), α and x5. The 1-D half plane mode is obtained by concatenated both B´ezier curves

$$B(t) = [B_1(t), B_2(t)] \tag{3-25}$$

Where: B(t) is a vector of x-z coordinates, B(t) = (B_x(t), B_z(t)). B_x(t) is normalized by B_x(tc); B_x(tc) is the x coordinate where B_z(t) = c, c is the mechanical coupling of the deformable mirror actuators.

The full 1-D mode M(t) is made by concatenating B(t) and its symmetric with respect to the z axis, i.e [108].

$$M_x(t) = ([B_{-x}(t); B_x(t)]; [B_{-z}(t); B_z(t)]) \tag{3-26}$$

The 2-D mode is the product of the 1-D modes in the x − z plane and in the y − z plane,

$$M(t) = M_x(t)M_y(t) \tag{3-28}$$

An influence function is created with two arguments passed to its constructor: the list of parameters in a cell and the mechanical coupling value. Instead of the list of parameters, the keywords 'monotonic' (0.2, [0.4; 0.7], [0.6; 0.4], 1, 1) and 'overshoot' (0.2, [0.4, 0.7], [0.5, 0.4], 0.3, 1) can be used to call predefined parameter lists, as shown in the next examples [108],[110]:

```
Bifa = influence Function ('monotonic', 0.75);
Figure, show (bifa, 'parent', subplot (1, 2, 1))
Title ('Monotonic influence function')
Bifb = influence Function ('overshoot', 0.75);
Show (bifb, 'parent', subplot (1, 2, 2))
Title ('Overshooted influence function')
```

The markers in the figures correspond to, from left to right, the points Pk from k = 0 to 6.

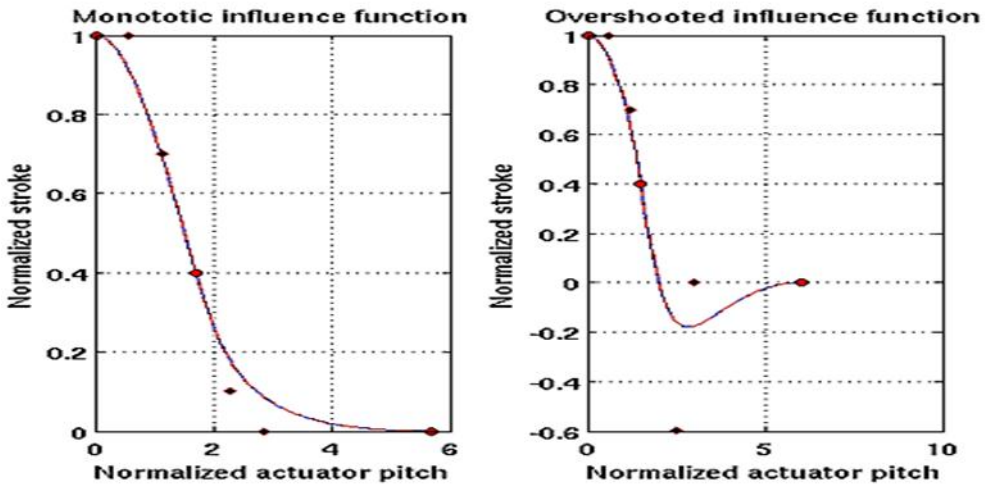

Figure 3-10: The influence function in two cases monotonic and overshooted [104].

3.5 Conclusion

In this chapter, we concluded it is not currently possible to measure the phase of the wavefront directly at optical wavelengths as is the case in the radio domain. This is because there is no optical detector capable of responding to temporal frequencies. Rousset gave a very complete description of adaptive optics analyzers. We recalled only the properties of the Shack-Harmann analyzer. Indeed, it is on the one hand the most widely used analyzer for adaptive optics, and on the other hand, its limitations are representative of the most pupil plane scanners.

We talked about some of the specific differences of the LEO satellite links, which distinguish the use of a wavefront sensor from those in astronomical applications. We concluded that atmospheric turbulence is more severe in SGL scenarios compared to astronomical applications.

To address the effect of atmospheric disturbance on the signal, especially in the phase, we use pre-compensation methods that mainly depend on metaheuristic algorithms. We mentioned several types of these algorithms, and these algorithms are applied in simulation tools in order to overcome the problem of phase distortion. We also concluded what is the algorithm used and what simulation tool we will use.

In the next chapter, we will apply the genetic algorithm within the simulation tool (OOMAO), and we will study and analyze the results.

CHAPTER IV:
Correction wavefront sensor based on stochastic technique for satellite-to-ground laser communication links

4 Correction wavefront sensor based on stochastic technique for satellite-to-ground laser communication links

4.1 Introduction

The communication satellite systems with optical laser links have become priority in communication fields for number of reasons. Compared to the radio communication which needs more than 1Gbps [112],[113], the communication satellite systems with optical laser links data rate is higher (more than 10 Gbps bit rate [41]), signal intensity (structure of fiber laser [114],[115]) and lower equipment size [115]. It has made a significant contribution in reducing the effects of atmospheric attenuation that is also determined by the geographic location especially in the tropical and equatorial regions where the rain effect plays an important role in the quality of communication [43],[45].as it leads to the instability in the intensity and the phase of the received signals [8].

In laser satellite communications, the elements of the atmosphere (wind, rain, dust…) can affect the quality of communication [115]. The problem occurs when the optical wave propagates in free space and is subjected to serious disturbances (wave-front sensor) which renders the system less effective and probably loses the information.

In adaptive optics (AO), the most important element is the deformable mirror. Which controlled by the approximation algorithms [8]. There are many algorithms that can correct wave front sensor such as: the stochastic parallel gradient descent (SPGD), Simulated Annealing (SA), and genetic algorithm (GA) [9],[10].This contribution provides a solution to correct wave front sensor based on a genetic algorithm. On the other hand, we suggest another solution called a hybrid solution, the provided solution consists of the combination of GA with AO solution. The hybrid solution gives positive results in correcting the wave front aberration in satellite laser communication.

This chapter is divided into four sections. A brief overview of the SHWF and the closed loop used in OOMAO, section two we discuss and modeling the technique used in the simulation . In section 3 improved our solution by suggest a new idea based on our results mentioned previously called Hybrid Genetic (HG and AO), we explained the principle of this method and we give a comparison between the solutions. Section 4 is dedicated to the

conclusion of this simulation, solutions and future work discussion of the obtained results. The last section is devoted to the overall results of our study and future works.

4.2 The SHWF and OOMAO closed-loop technique

In this section we talk about two techniques used in OOMAO, previously we explained the Shack Hartmann wavefront but in OOMAO, we will discuss in detail how to program the Shack Hartmann parameter and the initialization of the value of each parameter such as (lenslet, camera pixel,…). Also defined the closed loop of OOMAO and applique it and explain the figures.

4.2.1 The Shack Hartmann

To be complete an Adaptive Optics Systems needs a wavefront sensor. For this OOMPA uses a Shack-Hartmann wavefront sensor [108],[110]. That allows the wavefront distortion to be monitored by acquiring a single image, improving the bandwidth of the adaptive optics feedback loop. A Shack Hartmann wavefront sensor consists of a lenslet array and a charge coupled detector. The numerical model follows the physical model by embedding a lenslet array (lenslet Array) class and a detector (detector) class in the shackHartmann class. The lenslet Array class perform the numerical Fraunhoffer propagation of the wavefront to the detector. The detector class implements a CCD camera detection process including Poisson and read-out noise. The lenslet images are Nyquist sampled per default. A ShackHartmann object with a 9 × 9 lenslet array and a 54 × 54 resolution camera is created with [108],[111]:

```
 << wfs = shackHartmann;(9,54)
@ (lenslet array)> Created!
Clock rate is: 1.00Hz
@ (detector)> Created!
@ (lensletArray)> Setting the lenslet field stop size!
@ (lensletArray)> Set phasor (shift the intensity of half a pixel
for even intensity sampling(
 ___SHACK-HARTMANN___
Shack-Hartmann wavefront sensor:
 . 81 lenslets total on the pupil
 . 6 pixels per lenslet
 . Spot algorithm: centroiding, no thresholding!
-----------------------------------------------------
 ___LENSLET ARRAY___
9x9-lenslet array:
 .  2.0 pixels across the diffraction limited spot fwhm
 .  6 pixels across the square lenslet field stop size
 .  Optical throughput coefficient: 1.0
-----------------------------------------------------
 ___DETECTOR___
54x54 pixels camera
 . Quantum efficiency: 1.0
 . Photon noise disabled
 . 0.0 photo-events rms read-out noise
 . 1000.0 ms exposure time and 1.0Hz frame rate
-----------------------------------------------------
@ (shack-hartmann)> Created!
```

4.2.2 OOMAO closed-loop

Closed-loop Adaptive Optics Systems is an item important in the operation of AO systems. However, we can simulate AO systems in closed loop, open loop and in pseudo open loop [108],[110]. Closed loop has the advantage of a less dynamic range requirement in the sensor and of a good performance even in the presence of unmodeled nonlinearities or other error sources, mainly in the corrective elements, in order to simulate AO systems in OOMAO closed loop. The atmosphere is defined firstly; it is composed of three layers with a r_0 of 15cm and 30m outer scale.

```
 << atm = atmosphere( photometry.V,0.15,30...,
'altitude',[0,4,10]*1e3...,
'fractionnalR0...,[0.7,0.25,0.05],'
'windSpeed...,[5,10,20],'
'windDirection',[0,pi/4,pi] );
@ (atmosphere)> Created!
 ___ATMOSPHERE___
Von Karman atmospheric turbulence
 . Wavelength = 0.55micron,
 . r0 = 15.00cm,
 . L0 = 30.00m,
 . Seeing = 0.74arcsec,
 .theta0 (37%) = 7.01arcsec,
 . tau0 (37%) = 11.01millisec
 ----------------------------------------------------
Layer Altitude[m]     fr0     wind ([m/s] [deg])     D[m]       res [px]
1                  0.00     0.70     (5.00 10.00)
2            4000.00        0.25     (10.00 45.00)
3           10000.00        0.05     (20.00 180.00)
```

The closed-loop system will use one natural guide star on axis

```
 << ngs = source('wavelength',photometry.R);
@ (source)> Created!
 ___SOURCE___
Obj    zen[arcsec]   azim[deg] height[m]  lambda[micron] magnitude
 1        0.00          0.00          Inf          0.640              0.00
 ----------------------------------------------------
@ (source)> Terminated!
```

The wavefront sensing will be done at 700nm. The wavefront sensor will use a 92 lenslet array with a 542 pixels camera. Lenslets will less than 75% of the light of a fully illuminated lenslet with a flat wavefront are discarded [110].

```
<< wfs = shackHartmann;(9,54,0.75)
@ (lenslet array)> Created!
Clock rate is: 1.00Hz
@ (detector)> Created!
@ (lensletArray)> Setting the lenslet field stop size!
@ (lensletArray)> Set phasor (shift the intensity of half a pixel
for even intensity sampling)
 ___SHACK-HARTMANN___
Shack-Hartmann wavefront sensor:
 81 .lenslets total on the pupil
 6 .pixels per lenslet
 .spot algorithm: centroiding, no thresholding!
-----------------------------------------------------
 ___LENSLET ARRAY___
9x9 lenslet array:
 .  2.0 pixels across the diffraction limited spot fwhm
 . 6  pixels across the square lenslet field stop size
 . optical throughput coefficient: 1.0
-----------------------------------------------------
 ___DETECTOR___
54x54 pixels camera
 .quantum efficiency: 1.0
 .photon noise disabled
 .  0.0 photo-events rms read-out noise
 . 1000.0 ms exposure time and 1.0Hz frame rate
-----------------------------------------------------
@(shack-hartmann)> Created!
```

The telescope is an 8cm diameter with a 2.5 arc-minute field-of-view. The phase screens temporal evolution is sampled at 500Hz [108],[109].

```
<<tel = telescope(8,'resolution',54...,
'fieldOfViewInArcMin',2.5...,
'samplingTime',1/500);
@(telescope)> Created!
___TELESCOPE___
8.00cm diameter full aperture with 50.27m^2 of light collecting area;
the field-of-view is 2.50arcmin; the pupil is sampled with 54X54 pixels
                                                    ----------
```

The reference wavefront is propagated to set wavefront sensor valid lenslets and reference slopes.

```
ngs = ngs.*tel*wfs;
wfs.INIT;
figure
imagesc(wfs.camera,'parent',subplot(1,2,1))
slopesDisplay(wfs,'parent',subplot(1,2,2))
```

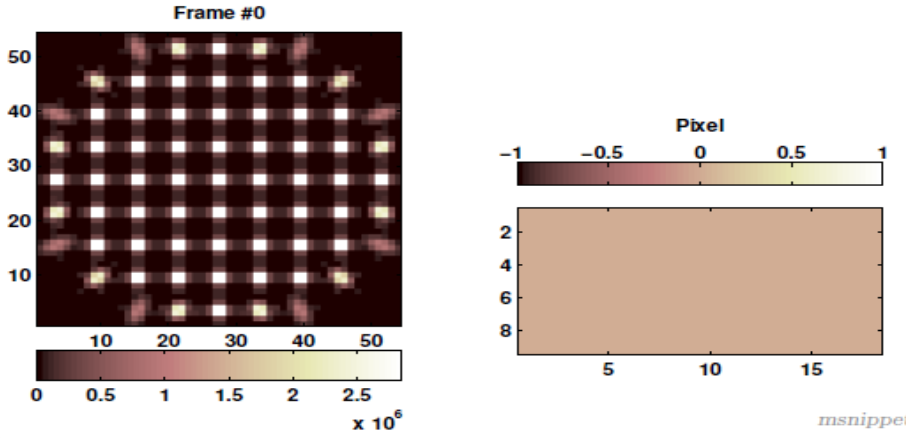

Figure 4-1: The reference of lenslets and reference slopes [104]

The deformable mirror will use 102 monotonic influence functions mechanically

Couple at 25% [108]:

```
>>  bif = influenceFunction('monotonic',25/100);
 @(bezier influence fun)> Created!
>>  figure, show(bif)
```

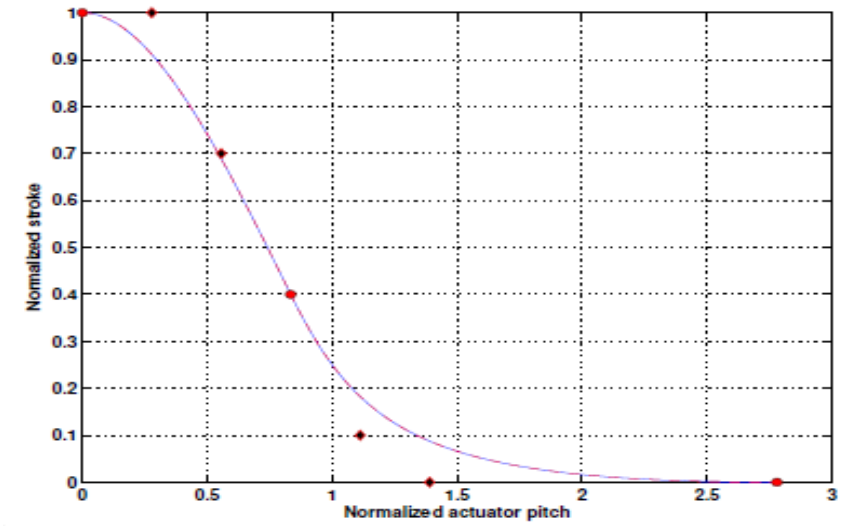

Figure 4-2: The influence function monotonic

4.3 Stochastic technique (genetic algorithm)

We have already talked about the principle and mechanism of the genetic algorithm work, for more information (see § 3.3.2.4)[38], of the previous chapter. In the present work, population refers to the possible collection of solutions. However, the individual represents a solution. Chromosome, in the other hand, is a component of the solution and Gene represents a characteristic (or a peculiarity).

4.3.1 Modeling the problem

I x J	Gene1	Gene2	….	Genej
Chrom1	0.08	0.0025	…	-0. 036
Chrom2			…	
...			…	
…			…	
Chromi			…	

Table 4-1: Population Coding

We consider **the population** as a matrix Pop(NxM) of real numbers contains the set of solutions generated in one iteration as shown in table1Where N is the number of chromosomes and M is the number of genes(or DM actuators). **The chromosome**: A chromosome Chromi is

a vector of real numbers contains the solution (i) in the population. **The Gene**: Genej is a real number, represents the value of the voltage assigned to an actuator (j) of the DM.

4.3.2 Algorithm flow-chart

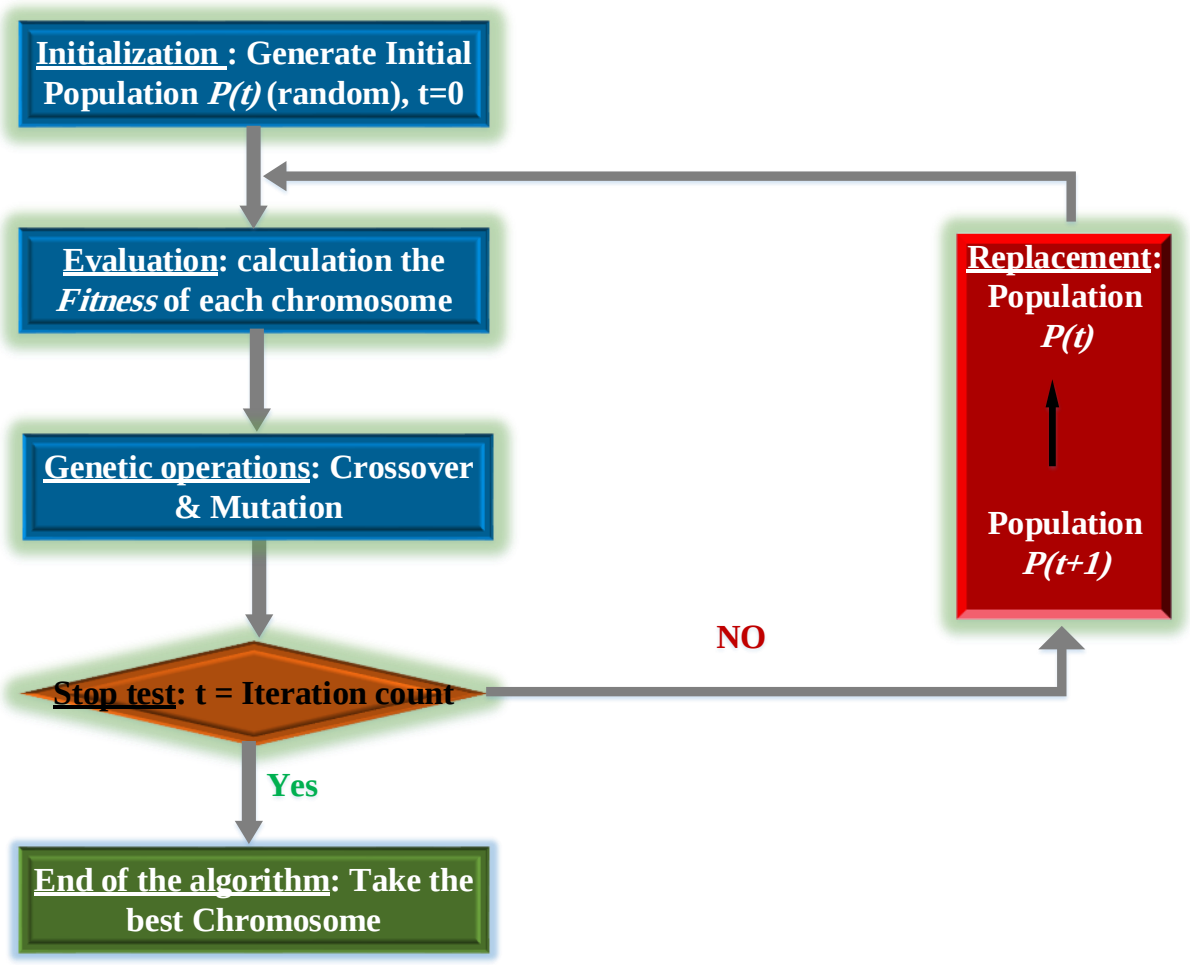

Figure 4-3: Algorithm flow-chart

We explain the main processes of our GA in the following:

- **Initialization:** In this step, we assign values to GA parameters (population size, iterations count,…), and generate the chromosomes by assigning random values to their genes.

- **Evaluation:** We use Fitness function to define the adaptation score of chromosomes during the selection process. We define the Fitness (i) for Chromi.

$$Fitness(i) = \frac{\sum_{j=1}^{M} \sigma_{ij}}{M} \quad (4\text{-}1)$$

Where **σ**ij is the standard deviation for Gaussian mutations of the sensor j, and M is the number of the actuators.

- **Selection:** According to the roulette method selection we select a set of best chromosomes, will be referred to as parents, in order to reproduce the next generation.

4.3.3 Experimental setup

In order to determine the effectiveness of the proposed solution, experiments were carried out on three different situations that allowed us to study the effect of the parameters of this algorithm on the fitness value. The values of the parameters presented in the tables below.

4.3.3.1 AO parameters settings:

The same AO parameter values were used in all situations. These parameters were proposed by the OOMAO Founders in [108],[111].

	Parameter	**Value**	
Atmosphere	Altitude	[0, 4000, 10000]	Atmosphere
	fractionnalR0	[0.7, 0.25, 0.05]	
	Wind speed	[5, 10, 20]	
	Wind Direction	[0, pi/4, pi]	
Source	Wavelength	60	Source
Shack Hartmann (wave sensor)	Wave front sensing	700nm	Shack Hartmann (wave sensor)
	lens let array	92	
	Camera	542 pixels	
Telescope	Diameter	8m	Telescope
	Resolution	54	
	Field Of View	2.5 arc minute	
	Sampling Time	500Hz	

Table 4-2: AO parameters.

4.3.3.2 GA parameters settings

We made more than 60 experiments divided into three situations according to three cases of study, wherein case (a) we fixed all GA parameters except population size, also with Iterations number in case (b), and with Min (and Max) value of voltage in case (c).

The values of the GA parameters, which all situations:

	Value			Description
	Situation (a)	**Situation (b)**	**Situation (c)**	
Min-coef	-7e-11	-7e-11	[-1e-12…-1e-6]	Minimum value of voltage to be applied on DM actuators
Max-coef	+7e-11	+7e-11	[+1e-12…+1e-6]	Maximum value of voltage to be applied on DM actuators
Pop Size	[30…3000]	800	800	Population size (Chromosomes number)
Chrom Size	80	80	80	Chromosome size (number of genes/actuator)
Iterations Count	500	[30…4000]	500	Genetic loops count
Cross Rate	60%	60%	60%	Crossover rate
Cross Points Count	40	40	40	Crossover points count
Mut Rate	70%	70%	70%	Mutation rate

Table 4-3: GA used parameters

4.3.4 Illustrative Example

For a single run of our algorithm Figure 1 represents Fitness as a function of the number of iterations when the population size is 800, the current applied to a lens is varied between -7e-11 and +7e-11, the crossover rate is 60%, the number of crossover points is 40, and the mutation rate is 70%.

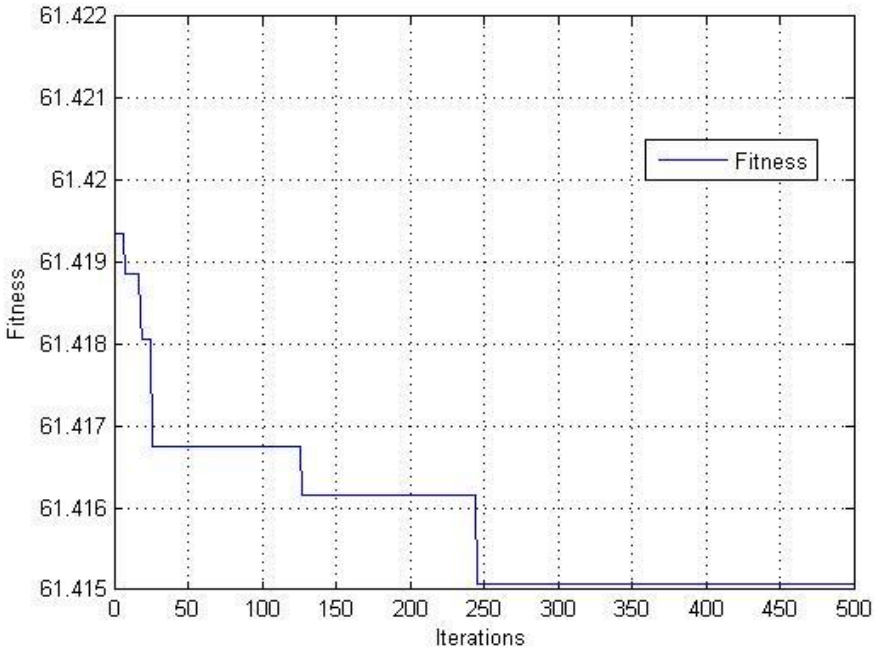

Figure 4-4: Illustrative Example

4.3.5 Results of simulation

We looked for the best configuration for genetic algorithm parameters (population size – iteration count- actuator current interval), in order to get the best performance of the genetic algorithm. The results of this simulation as shown in the figures below:

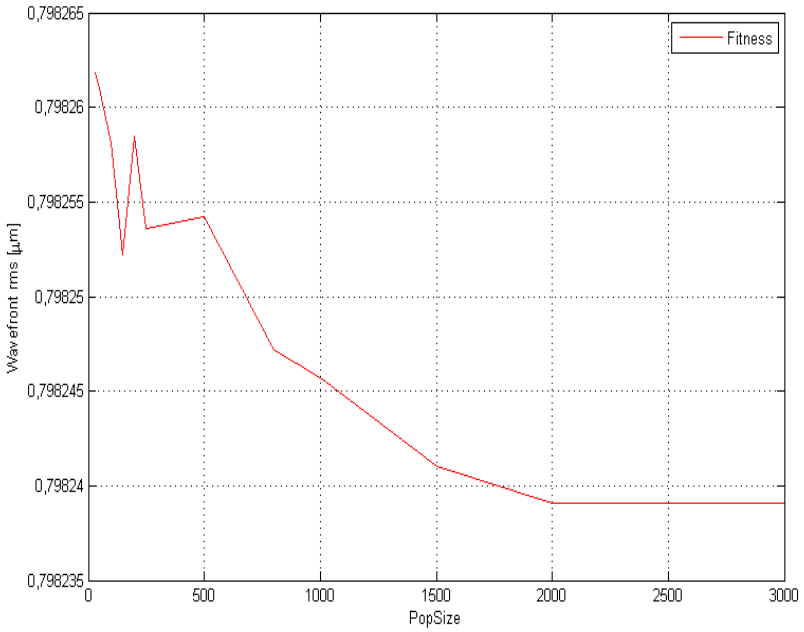

Figure 4-5: Situation (a) Fitness according to Popsize

Figure 4-5 represents the Fitness according to the size of population. It is noted that the Fitness varies inversely with the size of the population, as the figure shows; in this case, the reduction of Fitness is better for the number of the size of the population is increased and for greater number of population the Fitness remains constant.

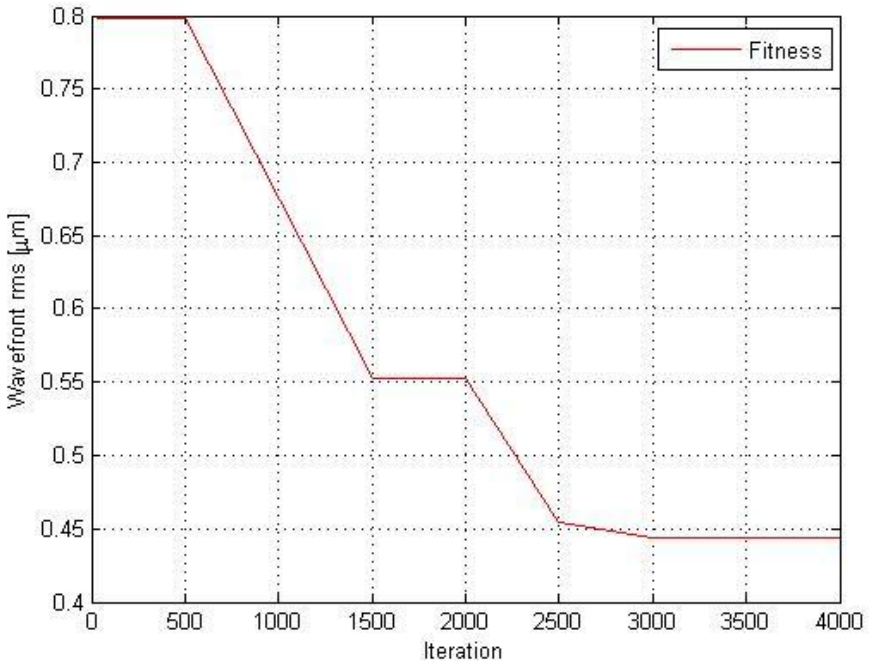

Figure 4-6: Situation (b) Fitness according to number of iteration

Figure 4-6 shows the variations of the Fitness according to the number of iterations. From this curve, we can see that fitness varies inversely with number of iterations. For variable iteration count values from 30 to 4000 iterations, Fitness ranges from 0.7983 to 0.4439.we notice in this case how the number of iteration is Significantly effect on fitness than the size of population.

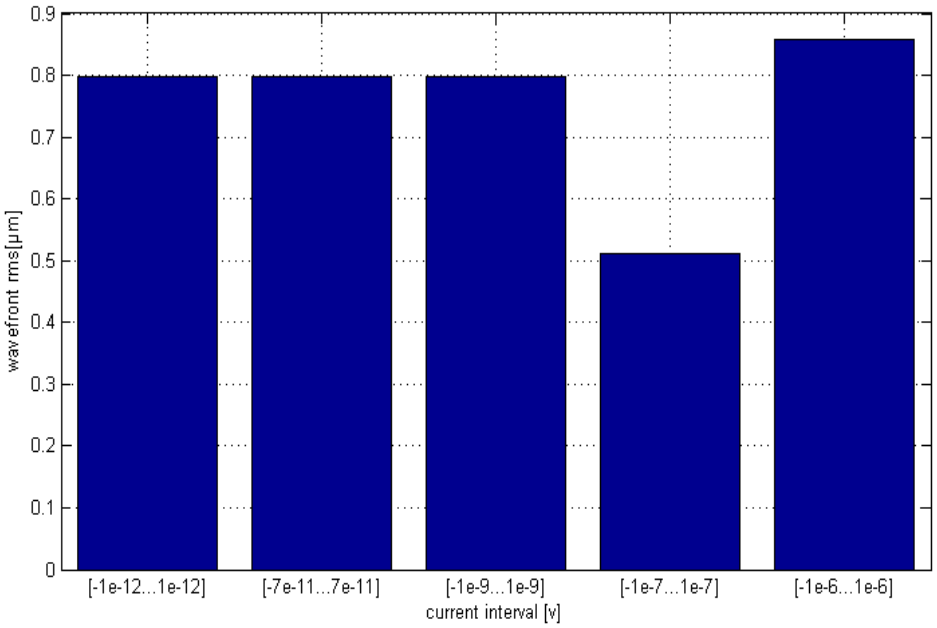

Figure 4-7: Situation (c) Fitness according to actuator current interval

Figure 4-7 shows the variations of the Fitness according to the current intervals of the actuators.

From this histogram, the best range (interval) of the current is variable from [$-1e^{-7}$ to $+1e^{-7}$] to obtain the best Fitness varies less than 0.51.

After the experimentally work, we have the best parameters to apply them in our genetic algorithm (population size >2000, iteration count >2500 and the actuator current [-1e-7…1e-7]), as shown in Table 4.

	Value	**Description**
Min-coef	-1e-7	Minimum value of voltage to be applied on DM actuators
Max-coef	+1e-7	Maximum value of voltage to be applied on DM actuators
popSize	2500	Population size (Chromosomes number)
Chrom Size	80	Chromosome size (number of genes/actuators)
Iterations Count	≥3000	Genetic loops count
Cross Rate	60%	Crossover rate
Cross Points Count	40	Crossover points count
mutRate	70%	Mutation rate

Table 4-4: Best parameters of genetic algorithm

4.4 Hybrid GA solution

In this paragraph, we discuss another solution called a hybrid solution explained in the followings

4.4.1 Principle of HGA solution

We execute the OOMAO closed loop and let the genetic algorithm use the obtained results in its initial population (as 50% of individuals), in other words the initial population of our GA is not totally random, we took some real solutions from the default OOMAO closed loop. Also, it uses the best parameters from the genetic algorithm.

4.4.2 The flow-chart of HGA solution

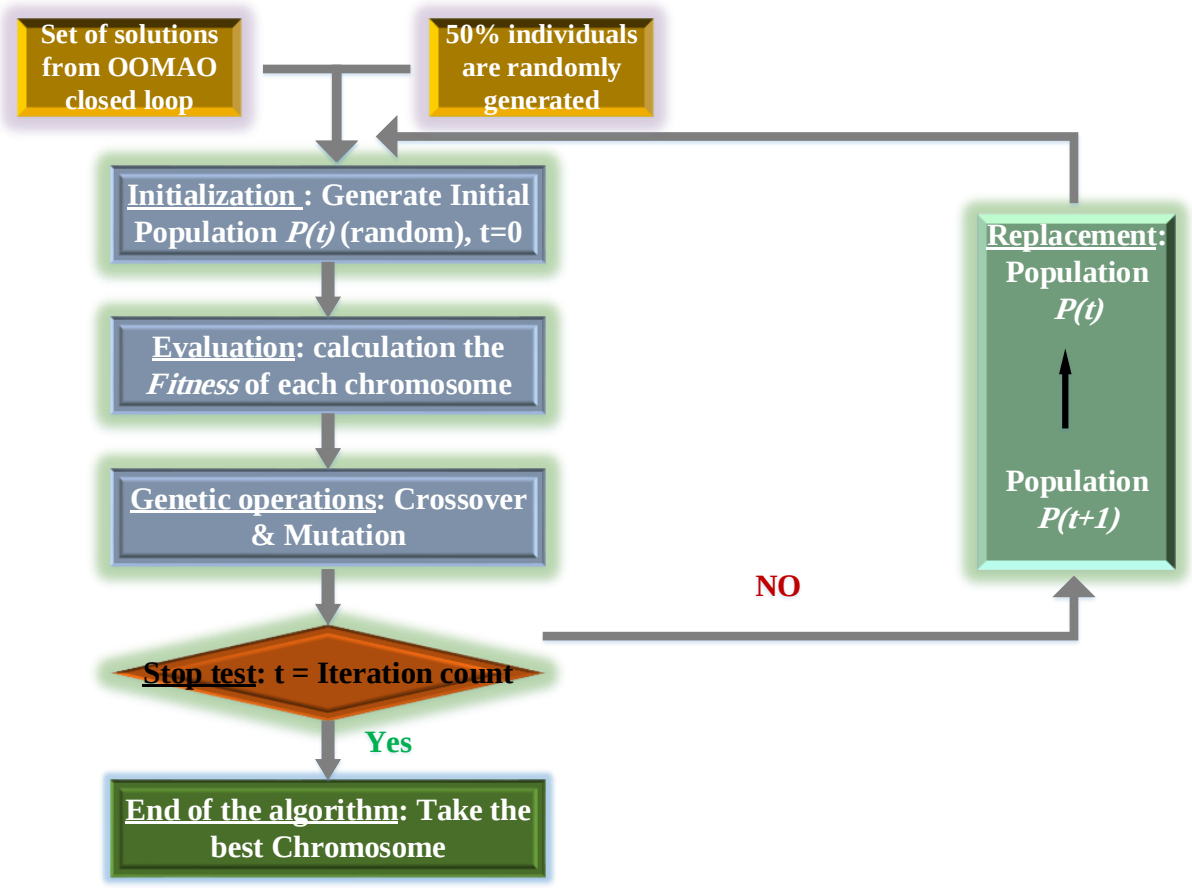

Figure 4-8: Our Genetic Algorithm with OOMAO

4.4.3 Comparison between OOMAO and Hybrid Algorithm

In order to obtain a more accurate wave interface correction, we make a comparison between two solutions. The first is the closed loop of OOMAO and the second is the hybrid solution for 4000 iterations and the best parameters of GA. We obtained results, draw the curves and compare it.

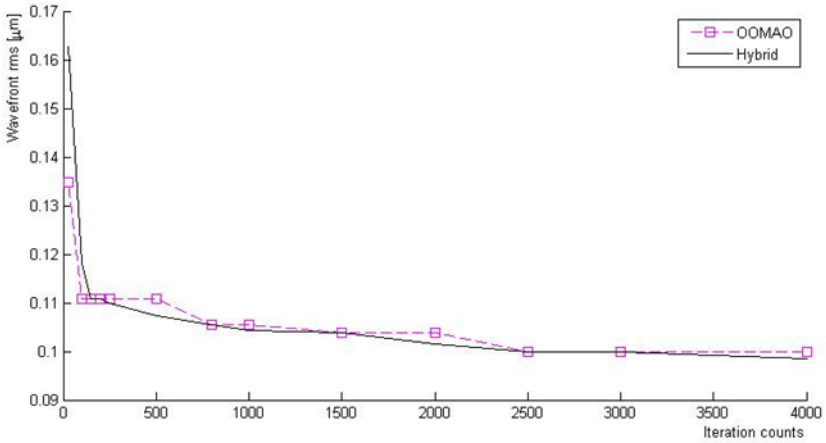

Figure 4-9: Comparison between OOMAO solution and the proposed hybrid solution

Figure 4-9 represents results obtained from the comparison between the OOMAO which proposed in [110],[111] and our hybrid solution. It can clearly be seen that there has been a sharp decrease in both graphs between 0 and 200 iteration because 50% of suggested solutions are random. After 300, hybrid solution has only shown a slight growth. This is because algorithm excludes the wrong solutions and start keeping only the correct ones. After 200, the graph has a horizontal pitch. Between (2500- 3000), there is a stability in hybrid solution graph which continues to drop making a better performance after 3000 iteration.

Overall, the graph illustrates the comparison between two solutions. Firstly, we notice that the values of hybrid solution is bigger than OA solution. That's because the number of iterations is small (less than 200) which leads to very weak result. Then, the number of iterations grows up making a better results because our GA is getting optimized by the time.

4.5 Conclusion

The genetic algorithm was applied in adaptive optical system to correct wave-front sensor in a disturbed atmosphere. Based on the OOMAO, we simulate the performance of an adaptive

optical system with telescope (resolution 54, diameter 8m) and deformable mirror containing 92 actuators. We used the best parameters of the previous simulation (Popsize 2500, Iterations count >3000, min-volt -1e-7, max-volt +1e-7) to create hybrid solution (AO and GA). By comparing the obtained results, it was found that using this hybrid solution leads to better enhancement of AO performance than those produced by applying the OOMAO with the difference of 0.0279μm.

General Conclusion

The work presented in this manuscript has focused on the study of laser satellites, which offer several advantages over standard satellites, but the main obstacle encountered in such satellites is that the latter continually suffer from the vibrations of the laser beam. Emitted because of the various surrounding internal and external sources, this is what degrades the quality of communication. In order to reduce the effects of these vibrations and improve the quality of communication, several measures have been taken.

We focused more on the external sources represented by the disturbances of the atmospheric, because of their significant impact on the level of intensity and phase of the received signal. Internal sources have been identified as disturbances within the telescope. The problem of atmospheric turbulence is evident in tropical and equatorial regions, where climate plays an important role in signal reception.

We are interested in this thesis for the study of the impact of atmospheric turbulence on free space optical links and on adaptive optical (OA) correction methods to reduce their influence.

In the first part we posed the problem and evaluated the effectiveness of the correction necessary to achieve the typical performances of atmospheric optical links (AOLs).

To quantify this efficiency, we studied most cases of atmospheric turbulence in order to reduce their effects on the propagation of the signal.

This demonstration was carried out on a simulation tool and not on a real system in order to get rid of ancillary problems, such as the temporal monitoring of the changes in turbulence. So I started by the same conditions of a real system at a propagation distance suitable for an optical communication, while keeping the parameters of interest that are the scintillation in the pupil and the diffractive effects.

In adaptive optics, we used already implemented pre-compensation techniques implementing only phase correction alone, this method requires an iterative algorithm to calculate the phase commands.

The algorithm developed in this thesis requires a convergence time too long to satisfy real time. A solution to accelerate this algorithm has however already been proposed, for applied a new algorithm called a hybrid, and could make the method valid for a real system.

From a completely different perspective, work on the coupling of measurement and formatting can be used in a broader field than that of optical telecommunications alone. The concept of controlled propagation in turbulent environments is currently experiencing a particular boom, especially in the field of biological imaging. The biological tissues observed are highly diffusing, which causes the same scintillation phenomenon as that observed during the propagation of a laser beam in turbulence. Phase correction alone is already applied in this area. The phase conjugation could constitute an improvement of the techniques already in place. In addition, in the context of microscopy, there is no longer any question of pupillary truncation, nor of temporal evolution of the disturbance and therefore of correction in real time. This case is particularly favorable to the concept of pre-compensation developed here.

In the last part of the manuscript, we present the results obtained when using genetic algorithm as a whole, namely the realization of the iterative phase conjugation. More than 60 experiments performed on an occurrence of turbulence are presented for reach to the best configuration of our algorithm. We demonstrate experimentally the convergence of the phase conjugation iterations. We have also confirmed the quality of the measurement and shaping techniques under realistic conditions of weak scintillation.

Finally, we integrate some of the solutions and the genetic algorithm previously identified, in order to improve the result performance of OOMAO and their impact on a real system. A method is proposed for analytically improving the consequences of each of the OOMAO and the genetic algorithm, it was found that using this hybrid solution leads to better enhancement of AO performance than those produced by applying the OOMAO.

Future work

In the field of communications with laser satellites, there are many ideas, but the difficulty lies in converting these ideas to reality, due to the lack of the means and finance those ideas.

We can divide our future work into two main parts, one concerned with simulation work and the other concerned with practical experiences or practical projects.

In our first section on simulation, I and a group of engineers are now working on applying a new idea from the results obtained from this work. The idea boils down to integrating more than one software techniques to solve a specific problem within the user system. The techniques that have been adopted up to the moment are Fuzzy Logic and data Mining, and Clustering method. Each technique, solves a specific problem within the simulation system. Initial results indicate that it will be an effective way to solve the problem of atmospheric turbulence that occur to the wave interface. But this method faces an important problem which is the lack of devices and other requirements to carry out the process of total data analysis, however there are good indicators where it is possible to reach a clear solution.

In the other side, there are many existing projects that pay attention to laser-satellite communications because of their importance, especially when natural disasters occur, such as earthquakes that may cause a partial or complete damage of the communications system.

Our idea is summarized about a project whose is based on Drones or airships that can measure the extent of air turbulence whenever we rise or move away from the surface of the earth, the idea also speaks about a group of Drones so every plane can controls to plane above it. The goal is to collect more a number of data in the different atmosphere. This idea collides with the financier of such a project as well. More than one engineering department must be involved to develop this idea.

In the end, I hope that my colleagues and I have presented an idea or ideas that may benefit others or may develop them for the better. I wish all colleagues working in the field of scientific research all the best and success.

Bibliography

[1] W. J. Larson and J. R. Wertz, "Space mission analysis and design," Torrance, CA (United States); Microcosm, Inc., 1992.

[2] A. E. Grant and J. H. Meadows, *Communication technology update and fundamentals*. Routledge, 2016.

[3] H. Potocnik, "The Problem of Space Travel: The Rocket Motor," *NASA Headquarters, Sept.*, 2007.

[4] M. L. Moss and A. M. Townsend, "How telecommunications systems are transforming urban spaces," *Cities Telecommun. Age*, pp. 31–41, 2000.

[5] M. Kermani, "Modélisation des vibrations dans la communication optique par les satellites lasers," 2001.

[6] D. L. Fried and H. T. Yura, "Telescope-performance reciprocity for propagation in a turbulent medium," *JOSA*, vol. 62, no. 4, pp. 600–602, 1972.

[7] R. L. Fante, "Electromagnetic beam propagation in turbulent media," *Proc. IEEE*, vol. 63, no. 12, pp. 1669–1692, 1975.

[8] H. Yang and X. Li, "Comparison of several stochastic parallel optimization algorithms for adaptive optics system without a wavefront sensor," *Opt. Laser Technol.*, vol. 43, no. 3, pp. 630–635, 2011.

[9] E. Chen, H. Cheng, Y. An, and X. Li, "The Improvement of SPGD Algorithm Convergence in Satellite-to-Ground Laser Communication Links," *Procedia Eng.*, vol. 29, pp. 409–414, 2012.

[10] M. R. N. Avanaki, S. A. Hojjatoleslami, H. Sarmadi, R. Ebrahimpour, and A. G. H. Podoleanu, "Genetic algorithm for optimization of optical systems," in *2010 18th Iranian Conference on Electrical Engineering*, 2010, pp. 172–176.

[11] P. A. Morreale and K. Terplan, *CRC handbook of modern telecommunications*. CRC press, 2018.

[12] S. Rageh and A.-G. Mohammed, “Etude et Modélisation de la Transmission dans les Satellites Lasers.” Université de Batna 2, 2011.

[13] M. OUACIFI, “Modélisation des vibrations au niveau des satellites lasers.” Université de Batna 2, 2009.

[14] M. Richharia, *Satellite communication systems: design principles*. Macmillan International Higher Education, 2017.

[15] H. Hemmati, *Near-earth laser communications*. CRC press, 2009.

[16] A. E. Roy, *Orbital motion*. CRC Press, 2004.

[17] A. Jamalipour, *Low earth orbital satellites for personal communication networks*. Artech House, Inc., 1997.

[18] S. Ohmori, H. Wakana, and S. Kawase, *Mobile satellite communications*. Artech House, Inc., 1997.

[19] P. Baran, “Satellite communications system and apparatus.” Google Patents, 19-Jun-1984.

[20] U. Scialom, “Optimization of satellite constellation reconfiguration.” Massachusetts Institute of Technology, 2003.

[21] A.-A. Kinane, “Optimisation de la mise à poste d’une constellation de satellites,” 2006.

[22] T. Tolker-Nielsen and G. Oppenhauser, “In-orbit test result of an operational optical intersatellite link between ARTEMIS and SPOT4, SILEX,” in *Free-Space Laser Communication Technologies XIV*, 2002, vol. 4635, pp. 1–15.

[23] E. Altman, “Les réseaux satellitaires de télécommunication,” 1999.

[24] C.-C. Chen and C. S. Gardner, “Impact of random pointing and tracking errors on the design of coherent and incoherent optical intersatellite communication links,” *IEEE Trans. Commun.*, vol. 37, no. 3, pp. 252–260, 1989.

[25] D. D. Otten, “Hybrid satellite communications system.” Google Patents, 18-Feb-2003.

[26] J. M. Dilhac, "The telegraph of claude chappe-an optical telecommunication network for the xviiith century," *Inst. Natl. des Sci. Appliquées Toulouse*, 2001.

[27] A. Breguet, "Sur les expériences photophoniques du Professeur Alexander Graham Bell et de M," *Sumner Tainter. comptes rendus l'Académie des Sci.*, vol. 91, pp. 595–598, 1880.

[28] D. Killinger, "Free space optics for laser communication through the air," *Opt. Photonics News*, vol. 13, no. 10, pp. 36–42, 2002.

[29] D. R. Winseck and R. M. Pike, *Communication and empire: Media, markets, and globalization, 1860–1930*. Duke University Press, 2007.

[30] L. B. Lucy, "The light curves of W Ursae majoris stars," *Astrophys. J.*, vol. 153, p. 877, 1968.

[31] M. Lipsett, C. McIntyre, and R. Liu, "Space instrumentation for laser communications," *IEEE J. Quantum Electron.*, vol. 5, no. 6, pp. 348–349, 1969.

[32] D. L. Begley, "Free-space laser communications: a historical perspective," in *The 15th Annual Meeting of the IEEE Lasers and Electro-Optics Society*, 2002, vol. 2, pp. 391–392.

[33] N. L. Himebaugh, L. N. Thibos, C. G. Begley, A. Bradley, and G. Wilson, "Predicting optical effects of tear film break up on retinal image quality using the Shack-Hartmann aberrometer and computational optical modeling," in *Lacrimal Gland, Tear Film, and Dry Eye Syndromes 3*, Springer, 2002, pp. 1141–1147.

[34] M. R. Garcia-Talavera, Z. Sodnik, P. Lopez, A. Alonso, T. Viera, and G. Oppenhauser, "Preliminary results of the in-orbit test of ARTEMIS with the optical ground station," in *Free-Space Laser Communication Technologies XIV*, 2002, vol. 4635, pp. 38–49.

[35] M. Toyoshima *et al.*, "Ground-to-OICETS laser communication experiments," in *Free-Space Laser Communications VI*, 2006, vol. 6304, p. 63040B.

[36] N. Perlot *et al.*, "Results of the optical downlink experiment KIODO from OICETS satellite to optical ground station Oberpfaffenhofen (OGS-OP)," in *Free-Space Laser Communication Technologies XIX and Atmospheric Propagation of Electromagnetic*

Waves, 2007, vol. 6457, p. 645704.

[37] V. Cazaubiel *et al.*, "LOLA: A 40.000 km optical link between an aircraft and a geostationary satellite," in *International Conference on Space Optics—ICSO 2006*, 2017, vol. 10567, p. 1056726.

[38] N. Schwartz, "Précompensation des effets de la turbulence par optique adaptative : application aux liaisons optiques en espace libre To cite this version : HAL Id : tel-00771276 Précompensation des effets de la turbulence par optique adaptative : application aux liaiso," 2013.

[39] M. W. Wright, J. E. Roberts, W. H. Farr, and K. E. Wilson, "Improved optical communications performance combining adaptive optics and pulse position modulation," *Opt. Eng.*, vol. 47, no. 1, p. 16003, 2008.

[40] S. G. Wilson, M. Brandt-Pearce, Q. Cao, and J. Leveque, "Optical MIMO transmission using Q-ary PPM for atmospheric channels," in *The Thrity-Seventh Asilomar Conference on Signals, Systems & Computers, 2003*, 2003, vol. 1, pp. 1090–1094.

[41] Y. Arimoto, Y. Hayano, and W. Klaus, "High-speed optical feeder-link system using adaptive optics," in *Free-Space Laser Communication Technologies IX*, 1997, vol. 2990, pp. 142–151.

[42] J. Voyez, "Mesures optiques de profils de turbulence atmosphérique pour les futurs systèmes d'optique adaptative." Université Nice Sophia Antipolis, 2013.

[43] K. Badron, A. F. Ismail, J. Din, and A. R. Tharek, "Rain induced attenuation studies for V-band satellite communication in tropical region," *J. Atmos. Solar-Terrestrial Phys.*, vol. 73, no. 5–6, pp. 601–610, 2011.

[44] M. Alhilali, H. Y. Lam, and J. Din, "Comparison of raindrop size distribution characteristics across the Southeast Asia region," *TELKOMNIKA Telecommun. Comput. Electron. Control*, vol. 16, no. 6, pp. 2522–2527, 2018.

[45] M. I. Abozeed, M. Alhilali, L. H. Yin, and J. Din, "Rain attenuation statistics for mobile satellite communications estimated from radar measurements in Malaysia," *Telkomnika*, vol. 17, no. 3, pp. 1110–1117, 2019.

[46] R. J. Sasiela, *Electromagnetic wave propagation in turbulence: evaluation and application of Mellin transforms*, vol. 18. Springer Science & Business Media, 2012.

[47] H. W. Babcock, "The possibility of compensating astronomical seeing," *Publ. Astron. Soc. Pacific*, vol. 65, no. 386, pp. 229–236, 1953.

[48] A. N. Kolmogorov, "The local structure of turbulence in incompressible viscous fluid for very large Reynolds numbers," *Cr Acad. Sci. URSS*, vol. 30, pp. 301–305, 1941.

[49] J. D. Jackson, *Classical electrodynamics*. John Wiley & Sons, 2007.

[50] K. Elayoubi, "Study of communications channels for optical links through the atmosphere," 2019.

[51] F. Martin, A. Tokovinin, A. Agabi, J. Borgnino, and A. Ziad, "GSM: a Grating Scale Monitor for atmospheric turbulence measurements. I. The instrument and first results of angle of arrival measurements.," *Astron. Astrophys. Suppl. Ser.*, vol. 108, pp. 173–180, 1994.

[52] A. Agabi, J. Borgnino, F. Martin, A. Tokovinin, and A. Ziad, "GSM: A Grating Scale Monitor for atmospheric turbulence measurements. II. First measurements of the wavefront outer scale at the OCA," *Astron. Astrophys. Suppl. Ser.*, vol. 109, pp. 557–562, 1995.

[53] A. Ziad *et al.*, "Comparison of measurements of the outer scale of turbulence by three different techniques," *Appl. Opt.*, vol. 43, no. 11, pp. 2316–2324, 2004.

[54] J. Borgnino, A. Berdja, A. Ziad, and J. Maire, "An Optical Turbulence Profiler for the terrestrial atmosphere boundary-layer," 2007.

[55] T. Fusco *et al.*, "NAOS on-line characterization of turbulence parameters and adaptive optics performance," *J. Opt. A Pure Appl. Opt.*, vol. 6, no. 6, p. 585, 2004.

[56] C. Amra, V. Michau, G. Chériaux, and M. Ferrari, "121128_Bierent_2599011271B_Th," 2012.

[57] P. Ciolli, A. Consortini, F. Pasqualetti, L. Ronchi, and R. Vanni, "Intensity fluctuations of an atmospherically degraded beam at the focus of a large collecting lens," *Appl.*

Opt., vol. 16, no. 5, pp. 1128_2-1130, 1977.

[58] A. Consortini, P. Pandolfini, C. Romanelli, and R. Vanni, "Turbulence investigation at small scale by angle-of-arrival fluctuations of a laser beam," *Opt. Acta Int. J. Opt.*, vol. 27, no. 8, pp. 1221–1228, 1980.

[59] P. S. Hill, A. R. M. Nowell, and P. A. Jumars, "Encounter rate by turbulent shear of particles similar in diameter to the Kolmogorov scale," *J. Mar. Res.*, vol. 50, no. 4, pp. 643–668, 1992.

[60] V. Thiermann and H. Grassl, "The measurement of turbulent surface-layer fluxes by use of bichromatic scintillation," *Boundary-Layer Meteorol.*, vol. 58, no. 4, pp. 367–389, 1992.

[61] A. Consortini and K. A. O'Donnell, "Measuring the inner scale of atmospheric turbulence by correlation of lateral displacements of thin parallel laser beams," *Waves in random media*, vol. 3, no. 2, pp. 85–92, 1993.

[62] A. Consortini, Y. Y. Sun, C. Innocenti, and Z. P. Li, "Measuring inner scale of atmospheric turbulence by angle of arrival and scintillation," *Opt. Commun.*, vol. 216, no. 1–3, pp. 19–23, 2003.

[63] A. M. Obukhov, "The local structure of atmospheric turbulence," in *Dokl. Akad. Nauk. SSSR*, 1949, vol. 67, no. 4, pp. 643–646.

[64] A. M. Yaglom, "On the local structure of a temperature field in a turbulent flow," in *Dokl. Akad. Nauk SSSR*, 1949, vol. 69, no. 6, pp. 743–746.

[65] V. I. Tatarski, *Wave propagation in a turbulent medium*. Courier Dover Publications, 2016.

[66] J. L. Walsh and P. B. Ulrich, "Laser beam propagation in the atmosphere," in *Topics in Applied Physics*, vol. 25, Springer Verlag Berlin, 1978, p. 223.

[67] O. Korotkova, T. D. Visser, and E. Wolf, "Polarization properties of stochastic electromagnetic beams," *Opt. Commun.*, vol. 281, no. 4, pp. 515–520, 2008.

[68] V. I. Tatarskii, "The effects of the turbulent atmosphere on wave propagation,"

Jerusalem Isr. Progr. Sci. Transl. 1971, 1971.

[69] J. W. Goodman, *Statistical optics*. John Wiley & Sons, 2015.

[70] M. J. Rycroft, "Atmospheric modelling and millimetre wave propagation: Brussard G. and Watson PA, Chapman & Hall, 1995, 329 pp.£ 60 hbk. ISBN 0-412-56230-8." Pergamon, 1995.

[71] F. Dios, J. A. Rubio, A. Rodríguez, and A. Comerón, "Scintillation and beam-wander analysis in an optical ground station-satellite uplink," *Appl. Opt.*, vol. 43, no. 19, pp. 3866–3873, 2004.

[72] J. H. Churnside and R. J. Lataitis, "Wander of an optical beam in the turbulent atmosphere," *Appl. Opt.*, vol. 29, no. 7, pp. 926–930, 1990.

[73] Y. V Linnik, "On the decomposition of the convolution of Gaussian and Poissonian laws," *Theory Probab. Its Appl.*, vol. 2, no. 1, pp. 31–57, 1957.

[74] R. Frehlich, "Simulation of laser propagation in a turbulent atmosphere," *Appl. Opt.*, vol. 39, no. 3, pp. 393–397, 2000.

[75] M.-T. Velluet, V. Michau, T. Fusco, and J.-M. Conan, "Coherent illumination for wavefront sensing and imaging through turbulence," in *Atmospheric Optics: Models, Measurements, and Target-in-the-Loop Propagation*, 2007, vol. 6708, p. 670808.

[76] A. K. Majumdar and J. C. Ricklin, *Free-space laser communications: principles and advances*, vol. 2. Springer Science & Business Media, 2010.

[77] J. W. Hardy, J. E. Lefebvre, and C. L. Koliopoulos, "Real-time atmospheric compensation," *JOSA*, vol. 67, no. 3, pp. 360–369, 1977.

[78] G. Rousset, J. C. Fontanella, P. Kern, P. Gigan, and F. Rigaut, "First diffraction-limited astronomical images with adaptive optics," *Astron. Astrophys.*, vol. 230, pp. L29–L32, 1990.

[79] C. Petit *et al.*, "Adaptive optics results with SOTA," in *2015 IEEE International Conference on Space Optical Systems and Applications (ICSOS)*, 2015, pp. 1–7.

[80] S. Dimitrov, B. Matuz, G. Liva, R. Barrios, R. Mata-Calvo, and D. Giggenbach,

"Digital modulation and coding for satellite optical feeder links," in *2014 7th Advanced Satellite Multimedia Systems Conference and the 13th Signal Processing for Space Communications Workshop (ASMS/SPSC)*, 2014, pp. 150–157.

[81] C. Lucien, L. Jérôme, V. Nicolas, R. Angélique, and G. Artaud, "Performance evaluation of coded transmission for adaptive-optics corrected satellite-to-ground laser links," in *2017 IEEE International Conference on Space Optical Systems and Applications (ICSOS)*, 2017, pp. 71–76.

[82] J. W. Hardy, *Adaptive optics for astronomical telescopes*, vol. 16. Oxford University Press on Demand, 1998.

[83] M. Knapek, "Adaptive Optics for the Mitigation of Atmospheric Effects in Laser Satellite-To-Ground Communications," 2010.

[84] H. M. Chulani and J. M. Rodríguez-Ramos, "Preliminary performance results of the weighted Fourier phase slope centroiding method for Shack–Hartmann wavefront sensors obtained with the OOMAO simulator," in *Adaptive Optics for Extremely Large Telescopes 5th Meeting (AO4ELT5)*, 2017.

[85] N. Devaney *et al.*, "Correction of ocular and atmospheric wavefronts: a comparison of the performance of various deformable mirrors," *Appl. Opt.*, vol. 47, no. 35, pp. 6550–6562, 2008.

[86] E. Dalimier and C. Dainty, "Comparative analysis of deformable mirrors for ocular adaptive optics," *Opt. Express*, vol. 13, no. 11, pp. 4275–4285, 2005.

[87] M. Knapek, "Adaptive optics for the mitigation of atmospheric effects in laser satellite-to-ground communications." Technische Universität München, 2011.

[88] G. Rousset, "Wave-front sensors," *Adapt. Opt. Astron.*, vol. 1, p. 91, 1999.

[89] L. A. Poyneer, "Scene-based Shack-Hartmann wave-front sensing: analysis and simulation," *Appl. Opt.*, vol. 42, no. 29, pp. 5807–5815, 2003.

[90] M. Nicolle, T. Fusco, G. Rousset, and V. Michau, "Improvement of Shack–Hartmann wave-front sensor measurement for extreme adaptive optics," *Opt. Lett.*, vol. 29, no. 23, pp. 2743–2745, 2004.

[91] V. Michau, G. Rousset, and J. Fontanella, "Wavefront sensing from extended sources," in *Real Time and Post Facto Solar Image Correction*, 1993, p. 124.

[92] C. Robert, V. Michau, B. Fleury, S. Magli, and L. Vial, "Mid-infrared Shack-Hartmann wavefront sensor fully cryogenic using extended source for endoatmospheric applications," *Opt. Express*, vol. 20, no. 14, pp. 15636–15653, 2012.

[93] S. Thomas, T. Fusco, A. Tokovinin, M. Nicolle, V. Michau, and G. Rousset, "Comparison of centroid computation algorithms in a Shack–Hartmann sensor," *Mon. Not. R. Astron. Soc.*, vol. 371, no. 1, pp. 323–336, 2006.

[94] R. J. Noll, "Zernike polynomials and atmospheric turbulence," *JOsA*, vol. 66, no. 3, pp. 207–211, 1976.

[95] V. Sacek, "https://www.telescope-optics.net/zernike_expansion_schemes.htm." [Online]. Available: https://www.google.com/search?q=add+website+reference+to+mendeley&oq=add+website+to+mendely&aqs=chrome.2.69i57j0l2.39675j0j7&sourceid=chrome&ie=UTF-8. [Accessed: 07-Feb-2020].

[96] S. Bonora, R. Zawadzki, G. Naletto, U. Bortolozzo, and S. Residori, "Devices and techniques for sensorless adaptive optics," *Adapt. Opt. Prog.*, 2012.

[97] T. Weyrauch, M. A. Vorontsov, T. G. Bifano, J. A. Hammer, M. Cohen, and G. Cauwenberghs, "Microscale adaptive optics: wave-front control with a μ-mirror array and a VLSI stochastic gradient descent controller," *Appl. Opt.*, vol. 40, no. 24, pp. 4243–4253, 2001.

[98] A. K. Majumdar, "Free-space optical (FSO) platforms: Unmanned aerial vehicle (UAV) and mobile," in *Advanced free space optics (FSO)*, Springer, 2015, pp. 203–225.

[99] S. Kirkpatrick, "Optimization by simulated annealing: Quantitative studies," *J. Stat. Phys.*, vol. 34, no. 5–6, pp. 975–986, 1984.

[100] N. Metropolis, A. W. Rosenbluth, M. N. Rosenbluth, A. H. Teller, and E. Teller, "Equation of state calculations by fast computing machines," *J. Chem. Phys.*, vol. 21,

no. 6, pp. 1087–1092, 1953.

[101] L. D. Chambers, *Practical Handbook of Genetic Algorithms: Complex Coding Systems, Volume III*. CRC press, 2019.

[102] M. Gen and L. Lin, "Genetic algorithms," *Wiley Encycl. Comput. Sci. Eng.*, pp. 1–15, 2007.

[103] J. J. Grefenstette, *Genetic algorithms and their applications: proceedings of the second international conference on genetic algorithms*. Psychology Press, 2013.

[104] H. Nosato, T. Itatani, M. Murakawa, T. Higuchi, and H. Noguchi, "Automatic wave-front correction of a femtosecond laser using genetic algorithm," *Conf. Proc. - IEEE Int. Conf. Syst. Man Cybern.*, vol. 4, pp. 3675–3679, 2004, doi: 10.1109/icsmc.2004.1400914.

[105] G. Vdovin, O. Soloviev, M. Loktev, and V. Patlan, "OKO technologies Guide to adaptive optics," 2013.

[106] S. L. Campbell, J.-P. Chancelier, and R. Nikoukhah, *Modeling and Simulation in SCILAB*. Springer, 2006.

[107] J.-P. Chancelier, F. Delebecque, C. Gomez, M. Goursat, R. Nikoukhah, and S. Steer, *Introduction à SCILAB*. Springer Science & Business Media, 2007.

[108] R. Conan, "Object – Oriented Matlab Adaptive Optics User Guide," pp. 1–35, 2010.

[109] M. Sciences, "Giant Magellan Telescope Laser Tomography Adaptive Optics Simulation Documentation," 2011.

[110] R. Conan and C. Correia, "Object-oriented Matlab adaptive optics toolbox," in *Adaptive optics systems IV*, 2014, vol. 9148, p. 91486C.

[111] "GitHub - rconan/OOMAO: Object-Oriented, Matlab & Adaptive Optics." [Online]. Available: https://github.com/rconan/OOMAO. [Accessed: 07-Feb-2020].

[112] X. Zhu and J. M. Kahn, "Free-space optical communication through atmospheric turbulence channels," *IEEE Trans. Commun.*, vol. 50, no. 8, pp. 1293–1300, 2002.

[113] L. J. Ippolito, *Radiowave propagation in satellite communications*. Springer Science & Business Media, 2012.

[114] G. A. Siles, J. M. Riera, and P. Garcia-del-Pino, "Atmospheric attenuation in wireless communication systems at millimeter and THz frequencies [wireless corner]," *IEEE Antennas Propag. Mag.*, vol. 57, no. 1, pp. 48–61, 2015.

[115] J. D. Barchers and D. L. Fried, "Optimal control of laser beams for propagation through a turbulent medium," *JOSA A*, vol. 19, no. 9, pp. 1779–1793, 2002.

Abstract

Communication is one of the most important things that has received human attention throughout history. The oldest method of communication used by the ancient person to sending smoke signals, beating drums or blowing the trumpet. The first use of signal systems was in Germany and France by telegraph. The first optical communication methods used in the war between France and Austria, by the French engineer “Claude Chabi” and his brothers in 1792.

In 1945, the scientist Arthur C. Clarke published an article on the setting of communication satellites in fixed orbits. The idea was applied decades later by the Soviet Union by launching the first Sputnik 1 satellite that was working on radio transmission, after which NASA launched the first communications satellite in the sixties of the last century. Because of the tremendous development in the transmission of information, communication was adopted through the laser satellites, where these are available Technology is a massive flow of information within one second. The biggest problem facing this technique is the atmospheric turbulences that occur when the visual signal passes through the layers of the Earth's atmosphere. This problem appears clearly in the equatorial and tropical regions. To address this problem we use several methods, including the method of adaptive optics. Adaptive optics mainly rely on iterative algorithms in order to build a distorted wavefront in order to modify it and try to return the wave to its natural form. We suggest a solution that allows to reduce the effects of scintillation on phase measurements. Finally, we suggest a stage pre-compensation method especially for measurement and control, which would enable optimal correction implementation. This method has proven effective for improving the wavefront of a laser signal.

Résumé

La communication est l'une des choses les plus importantes qui ait retenu l'attention humaine tout au long de l'histoire. La méthode de communication la plus ancienne utilisée par la personne âgée pour envoyer des signaux de fumée, battre des tambours ou sonner de la trompette. La première utilisation des systèmes de signalisation a eu lieu en Allemagne et en France par télégraphe. Les premières méthodes de communication optique utilisées dans la guerre entre la France et l'Autriche, par l'ingénieur français «Claude Chabi» et ses frères en 1792.

En 1945, le scientifique Arthur C. Clarke a publié un article sur la mise en place de satellites de communication sur des orbites fixes. L'idée a été appliquée des décennies plus tard par l'Union soviétique en lançant le premier satellite Spoutnik 1 qui travaillait sur la transmission radio, après quoi la NASA a lancé le premier satellite de communication dans les années soixante du siècle dernier. En raison de l'énorme développement de la transmission de l'information, la communication a été adoptée par les satellites laser, où ils sont disponibles. La technologie est un flux massif d'informations en une seconde. Le plus gros problème auquel est confrontée cette technique est les turbulences atmosphériques qui se produisent lorsque le signal visuel traverse les couches de l'atmosphère terrestre. Ce problème apparaît clairement dans les régions équatoriales et tropicales. Pour résoudre ce problème, nous utilisons plusieurs méthodes, y compris la méthode de l'optique adaptative. L'optique adaptative s'appuie principalement sur des algorithmes itératifs pour construire un front d'onde déformé afin de le modifier et essayer de remettre l'onde dans sa forme naturelle. Nous proposons une solution qui permet de réduire les effets de la scintillation sur les mesures de phase. Enfin, nous proposons une méthode de pré compensation d'étape en particulier pour la mesure et le contrôle, qui permettrait une mise en œuvre optimale de la correction. Cette méthode s'est avérée efficace pour améliorer le front d'onde d'un signal laser.

ملخص

الاتصال من أهم الأمور التي حظيت باهتمام الإنسان عبر التاريخ، اقدم طرق الاتصال التي استعملها الانسان القديم كانت عن طريق ارسال اشارات دخانية او قرع الطبول اونفخ البوق. اول استعمال لانظمة الاشارة كان في المانيا وفرنسا عن طريق التليغراف.استعملت اول طرق الاتصال البصري خلال الحرب بين فرنسا والنمسا عن طريق المهندس الفرنسي «كلود شابي» وإخوانه عام 1792.

في العام 1945نشر العالم آرثر سي كلارك مقالا يتحدث عن وضع اقمارصناعية خاصة بالاتصالات في مدارات ثابتة. تم تطبيق الفكرة بعد عقود من قبل الاتحاد السوفيتي باطلاق اول قمر صناعي سبوتنيك1 كان يعمل بارسال راديوي، بعدها قامت ناسا باطلاق اول قمر صناعي خاص بالاتصالات في ستينيات القرن الماضي.وبسبب التطور الهائل في نقل المعلومات تم اعتماد الاتصال عن طريق الاقمار الصناعية الليزرية حيث توفر هذة التقنية تدفق هائل من المعلومات خلال الثانية الواحدة. المشكلة الاكبر التي تعترض هذه التقنية هي الاضطرابات الجوية التي تحدث للاشارة البصرية عند مرورها بطبقات الغلاف الجوي للارض، تظهر هذه الاشكالية بوضوح في المناطق الاستوائية والمدارية. لعلاج هذه الاشكالية نستعمل عدة طرق منها طريقة البصريات التكيفية.تعتمد البصريات التكيفية اساسا على خوارزميات تكراريه وذلك لبناء واجهة موجة مشوهه وذلك لتعديلها ومحاولة اعادة الموجة لشكلها الطبيعي.نقتراح حل يتيح تقليل آثار التلألؤ على قياسات الطور. أخيرًا ، نقترح طريقة للتعويض المسبق للمرحلة خاصةً للقياس والتحكم ، والتي من شأنها أن تمكن من تنفيذ التصحيح الأمثل. اثبتت هذه الطريقة فعاليتها لتحسين واجهة الموجة لاشارة ليزرية.